Effect of Nonplastic Silt Content on Liquefaction Behavior of Fine Sand

by

Mohammad Emdadul Karim

A thesis submitted to the Department of Civil Engineering,
Bangladesh University of Engineering and Technology,
Dhaka, in partial fulfillment of the degree of
Master of Science in Civil Engineering (Geotechnical)

25th February, 2014

The thesis titled **"Effect of Nonplastic Silt Content on Liquefaction Behavior of Fine Sand"** Submitted by **Mohammad Emdadul Karim,** Roll No. **0411042207(F)**, Session **April-2011**, has been accepted as satisfactory in partial fulfillment of the requirement for the degree of **Master of Science in Civil Engineering (Geotechnical)** on **25th February, 2014**.

BOARD OF EXAMINERS

Dr. Md. Jahangir Alam — Chairman (Supervisor)
Associate Professor
Department of Civil Engineering
BUET, Dhaka-1000.

Dr. A. M. M. Taufiqul Anwar — Member (Ex-Officio)
Professor and Head
Department of Civil Engineering
BUET, Dhaka - 1000.

Dr. Mehedi Ahmed Ansary — Member
Professor
Department of Civil Engineering,
BUET, Dhaka-1000.

Dr. Md. Abu Taiyab — Member (External)
Associate Professor
Department of Civil Engineering
DUET, Dhaka.

CANDIDATE'S DECLARATION

It is hereby declared that this thesis or any part of it has not been submitted elsewhere for the award of any degree or diploma.

Signature of the Candidate

_____

Mohammad Emdadul Karim

Contents

List of Figures

List of Tables

Notations

CSR	cyclic stress ratio
CRR	cyclic resistance ratio
C_c	coefficient of curvature
C_u	uniformity coefficient
D_r	or RD_c relative density
D_{50}	mean particle diameter
e	gross void ratio
e_f	maximum index void ratio of fine
e_s	maximum index of void ratio of sand
e_{max}	maximum void ratio
e_{min}	minimum void ratio
f	frequency
FC	fines content
G_s	specific gravity of soil
G_{sec}	secant shear modulus
G_{sf}	specific gravity of fines
G_{ss}	specific gravity of sand
LFC	limiting fines content
N	cycle of loading
N_L	cycle at ±3% axial strain or initial liquefaction
N/N_L	cycle ratio
NP	non-plastic

ND	not determined
R_u	excess pore water pressure ratio
SEM	scanning electro microscope
u	excess pore water pressure
u_{excess}	excess pore water pressure
USCS	unified soil classification system
V_v	volume of void
V_s	volume of soil
V	total volume
W_d	dry weight of soil
W_{fines}	weight of fines
W_{sand}	weight of sand
XRD	x-ray diffraction
σ	total stress
σ'	effective stress
$\sigma'_{3c}\ or\ \sigma'_3$	horizontal effective stresses
P'	mean effective stress = $(\sigma'_1 + \sigma'_3)/2$
q	shear stress = $(\sigma'_1 - \sigma'_3)$
q_{max}	peak shear stress
γ_w	unit weight of water
τ	shear stress
$\emptyset'$	effective friction angle

ACKNOWLEDGMENTS

The author wishes to express his deepest gratitude to his supervisor Dr. Md. Jahangir Alam, Associate Professor of Civil Engineering, Bangladesh University of Engineering and Technology (BUET), Dhaka for his kind and continuous guidance, valuable suggestions and constant inspiration throughout the research.

The author also expresses her profound gratitude to Dr. A. M. M. Taufiqul Anwar, Professor and Head, Department of Civil Engineering, BUET, Dhaka, for his co-operation. The author gratefully acknowledges the constructive criticisms and valuable suggestions made by Prof. Dr. Mehedi Ahmed Ansary of Department of Civil Engineering, BUET, Dhaka and Associate Prof. Dr. Md. Abu Taiyab of Department of Civil Engineering, DUET, Gazipur.

The triaxial testing machine used in the research was trained by Dr. Md. Jahangir Alam, Associate Professor of Department of Civil Engineering, BUET, Dhaka and Dr. Rachid Hankour (late), Vice President and Director of Lab Systems, Geocomp Corporation, U.S.A. The author expresses sincere gratitude to both of them. The author is very much grateful to the technicians of Geotechnical Engineering.

Last but not the least, the author gratefully remembers his family members, especially his parents who have always been supportive and never forgotten their son in supplications to Almighty.

ABSTRACT

To identify the effect of non-plastic silt on the cyclic and monotonic behavior of sand-silt mixtures, total 49 stress-controlled cyclic and 13 strain-controlled triaxial tests have been done on sand-silt mixtures. These tests have been done on specimens of size 71 mm diameter and 142 mm height with frequency of 1 Hz for cyclic test and with a rate of 0.05 percent axial strain per minute for monotonic test. All tests were conducted at isotropic (consolidated) effective confining pressure of 100 kPa. Specimens were prepared at a constant relative density, constant gross void ratio and constant density approach by moist tamping method. Concept of Limiting Fines Content (*LFC*) was verified by these cyclic triaxial tests and undrained monotonic triaxial tests.

The rate of generation of excess pore water pressure with respect to cycles of loading was found to increase initially with increase in silt content till the limiting fines content (30%) and thereafter it reverses its trend when the specimens were tested at a constant dry density. The cyclic resistance was observed to be opposite to the pore pressure response. Cyclic Resistance Ratio (*CRR*) and Secant Shear Modulus decreased till *LFC*; after that they became constant with increasing silt content.

In monotonic test, peak shear strength of sand-silt mixture decreases with increase of silt content up to *LFC*. Peak shear strength remains almost constant at silt content greater than *LFC*. At constant gross void ratio approach the undrained peak shear strength decreases with increase in silt content till *LFC* and for further increment of silt content the peak shear strength increases with increase in silt.

The *CRR,* Secant Shear Modulus and undrained peak shear strength of sand-silt mixtures remain reasonably equal after *LFC* because of equal inner void among the silt particles, is verified by equal permeability test results (by Falling head method) after *LFC* till pure silt.

CHAPTER 1

INTRODUCTION

1.1 General

As it was originally derived from the Latin verb liquefacere, which means to weaken, to melt, or to dissolve. Liquefaction is an engineering phenomenon referring to the loss of soil shear strength due to rapid pore water pressure build up during cycling loading. Seismic soil liquefaction occurs when the structure of a loose and saturated soil breaks down due to rapidly applied loading. As the soil structure breaks down, the loosely-packed individual soil particles attempt to move into a denser and more stable configuration. During an earthquake event, however, there is not enough time for the water within the pores of the soil to be squeezed out or dissipate. So water is trapped in the soil pores and prevents the soil particles moving to a denser state. Simultaneously, this is accompanied by an increase in pore water pressure which reduces the contact forces between the individual soil particles, and consequently resulting in softening and weakening of the soil deposit to a considerable extent. Because of this high pore water pressure, the contact forces become very small or almost zero, and in an extreme case, the excess pore water pressure may increase to a level that may break the particle-to-particle contact. In such cases, the soil will have very little or no resistance to shearing, and will exhibit a behavior more like a viscous liquid than a solid body. While most frequently associated with saturated cohesionless soil deposits under dynamic loadings, liquefaction phenomenon has also been reported in both mixtures of cohesive and cohesionless soils under both dynamic and static loading.

1.2 Background and Present State of the Problem

Most liquefaction research was carried out on clean sands with the assumption that the behavior of silty sand is similar to that of clean sands. Recent researches made by [1, 2, 3, 4, 5, 6, 7, 8] indicate that sand deposited with silt content is much more liquefiable than clean sand. Also, stress-strain characteristics and pore pressure generation in silty sand samples are quite different from clean sand [9]. These new findings emphasize the importance of deposits with mixture of sand and silt. Moreover, the behavior of silty sand soils such as hydraulic fills is not clearly known

during earthquake. Therefore, a deep understanding of silty sand behavior is needed for liquefaction assessment of silty sandy soils. Several laboratory studies have reported that increasing the fines content in a sand will improve the liquefaction resistance of the sand [10, 6], decrease the liquefaction resistance of the sand [11, 12, 13, 14, 15, 16, 17], or decrease the liquefaction resistance until some limiting fines content is reached, and then increase its resistance [18, 19, 20].

However, now-a-days, plasticity behavior of fines becomes one of the most important parameter, which influences the cyclic shear strength of sand. Literature review shows that there is still on consensus on the influence of silt content on cyclic shear strength of sand. In the southeast region of Bangladesh, nonplastic-silt exists in upper layers soil strata. Therefore further study is necessary to understand the behavior of sand with nonplastic-silt.

1.3 Objectives

The objectives of the study are as follows:

i. To identify the effect of nonplastic silt content on the cyclic behavior of fine sand.
ii. To identify the effect of nonplastic silt content on the monotonic behavior of fine sand.
iii. To identify the effect of nonplastic silt content on the permeability of fine sand.

1.4 Outline of Methodology

i. Soil samples (sand and silt) have collected from the Bank of Padma River at Mawa, Munsiganj.
ii. 11 samples have prepared by mixing silt with fine sand at different percentages.
iii. Atterberg limits and grain size analysis have done on collected soil samples.
iv. Modified Proctor Test has done for determining the maximum dry density. Minimum dry density will be determined by Minimum Density in Water method.
v. Triaxial soil specimens have prepared by moist tamping method with trial method at 10 percent moisture content.
vi. Cyclic, monotonic and permeability tests have performed on each sand-silt mixtures.

CHAPTER 2

LITERATURE REVIEW

2.1 Introduction

During earthquake, major destruction of various types of structures occurs due to the creation of fissures, abnormal and/or unequal movement, and loss of strength or stiffness of the ground. The loss of strength or stiffness of the ground results in the settlement of buildings, failure of earth dams, landslides and other hazards. The process by which loss of strength occurs in soil is called soil liquefaction [20]. Before the 1964 Niigata earth quake caused dramatic damage due to liquefaction, and thus led to a significant acceleration in liquefaction research [22]. Initial research effort [23, 24, 25, 26, 27, 28], focused mostly on investigation of clean sands and the factors that most affect the liquefaction resistance of these soils. Fine soil such as silts, clayey silts and sand with fines and silty soils were considered non-liquefiable (till 1969). After same case study [29, 30, 31], the concept of liquefaction of fine grain soil has changed. Now-a-days it is said that fine grain soils are also venerable for liquefaction behavior of fine sand (Figure 2-1) [32].

2.2 Case Studies on Liquefaction of Fine Grained Soil

Comprehensive laboratory investigation program on liquefaction on sands was initiated at University of California Berkely in 1960 by Seed and his group. Seed and Lee [33] reported the first comprehensive data on liquefaction of sand. Fine soils such as silts, clayey silts and sands with fines and silty soils were considered non-liquefiable as before 1969. After same field studies the concept of fine grain was changed. The observations following the Haicheng (1975) and Tangshan (1976) earthquakes indicate that many cohesive soils had liquefied [34]. These cohesive soils had clay fraction less than 20%, liquid limit between 21-35%, plasticity index between 4% and 14% and water content more than 90% of their liquid limit. Kishida [29] reported liquefaction of soils with up to70% fines and 10% clay fraction during Mino-Owar, Tohankai and Fukui earthquakes. Tohno and Yasuda [30] reported that soils with fines up to 90% and clay content of 18% exhibited liquefaction during Tokachi -Oki earthquake of 1968. Soils with up to 48% fines and 18 % clay content were found to have liquefied during the Hokkaido Nansai-Oki earthquake of 1993.

Gold mine tailings liquefied during the Oshima-Kinkai earthquake in Japan [31]. These tailings had silt sized particles and liquid limit of 31%, plasticity index of 10 % and water content of 37 %. Litchfield [35] reported that, during the Darfield earthquake of 2010, the shaking turned some of the layers of sand and silt is liquid mush as in Figure 2-2.

2.3 Laboratory Studies on the Effect of Nonplastic Silt on Fine Sand

The effect of nonplastic silt on fine sand has been extensively studied in the laboratory. There is a considerable amount of published data concerning laboratory liquefaction of sand and nonplastic silt mixtures. This section presents the results of laboratory investigation on sand silt mixtures from Amini and Qi, Polito and Martin II, Sitharam et al., Belkhatir el at., Dash and Sitharam and Baziar et al. [36, 37, 38, 22, 39, 40].

Amini and Qi [36] performed a comprehensive experimental program, in which total of 150 stress-controlled undrained cyclic triaxial tests were performed by silty sandy soils, were prepared by mixing appropriate amounts of Ottawa 20-30 sands with low plasticity silt. The grain size distribution curves of the soils are shown in Figure 2-3. The properties for the soils used during this study are shown in Table 2-1. The silts had a liquid limit of approximately 20 and a plasticity index of about 3. Two methods of sample preparation used for each soil type. These included most tamping (representing uniform soil conditions) and sedimentation (representing layered soil conditions). The silt content range from 0% to 50%, and confining pressure in the range of 50 to 250 kPa were considered. The term “liquefaction,” as used in their study, refers to the state in soils where the effective pressure has decreased and reached zero, shifting all of the confining pressure to the pore water.

The comparison is shown in Figure 2-4 to Figure 2-6 as a function of silt content. The results indicated that the liquefaction resistance of layered and uniform soils was not significantly different, despite the fact that the sand fabric produced by the two methods of sample preparation was totally different. However the main identification of this result is the increasing in silt content caused the liquefaction resistance of silty sands to increase for both uniform and layered soil conditions.

Polito and Martin II [37] used first sand in their testing program was Monterey No. 0/30 sand, commercially available sand from California. Monterey No. 0/30 sand is a medium to fine sand, having over 98% retained between the No. 20 (0.84 mm) and No. 100 (0.15 mm) sieves. It has a mean grain size D_{50} of 0.43 mm and its grains are subangular to subrounded in shape.

The second sand used in the study was Yatesville sand. It consists of the coarse fraction of Yatesville sand, which was obtained from a dam site in Louisa County, Kentucky. It is a medium to fine sand, having approximately 99% passing the No. 20 (0.84 mm), 45% passing the No. 100 (0.15 mm) sieves, and a mean grain size D_{50} of 0.18 mm. Its grains are subangular to subrounded in shape.

The silt used in the study was derived from the fine-grained portion of the Yatesville silt. It has a maximum grain size of 0.074 mm, a minimum grain size of 0.004 mm, and a mean grain size D_{50} of 0.03 mm. The silt is nonplastic, with no discernible liquid or plastic limit. Grain size distributions for both of the sands and the silt are presented in Figure 2-7.

Eight combinations of sand and silt were created using each sand, with silt contents varying from 4 to 75%. Additional tests were performed using each of the clean sands and the pure silt.

The effect of altering silt content while holding the void ratio of the specimens constant was initially examined. For the Monterey sand, a void ratio of 0.68 was used. For the Yatesville sand, a void ratio of 0.76 was used. These void ratios were chosen because they produced densities that allowed specimens to be formed over the entire range of silt contents investigated. The results of these constant void ratio tests on Monterey sand are presented in Figure 2-8. As may be seen in Figure 2-8, the cyclic resistance of the Monterey sand and silt mixtures decreases as the silt content increases until a minimum cyclic resistance of 0.11 is reached at a silt content of 35%. As the silt content continues to increase above 35%, the cyclic resistance increases.

The variation in cyclic resistance with increasing silt content for the Yatesville sand and silt follows a similar pattern to that shown in Figure 2-9. The cyclic resistance

first decreases with increasing silt content until a minimum cyclic resistance of 0.09is reached between a silt content of 37 and 50%. As the silt content continues to increase, the cyclic resistance begins to increase, reaching a value of 0.31 at a silt content of 100%.

The change in cyclic resistance that occurs when the soil changes from a sand-controlled matrix to a silt-controlled matrix can be clearly seen in Figure 2-10, which presents a plot of cyclic resistance versus silt content for specimens of Yatesville sand and silt adjusted to 30% relative density. The marked drop in cyclic resistance occurs as the silt content exceeds the limiting silts content.

In summary, the study has shown that for silty sands below the limiting silts content the cyclic resistance is a function of the specimen's relative density. The study has also shown that for soils above the limiting silts content the cyclic resistance is again controlled by the relative density of the soil, but is lower than it is for soils below the limiting silts content at similar relative densities. Additionally, the increase in cyclic resistance that occurs with an increase in relative density occurs at a slower rate.

Sitharam et al. [38] did laboratory experiments, were carried out on representative natural sand samples (base sand) collected from earthquake-affected area of Ahmedabad City Gujarat state in India. The base sand of Ahmedebad city consists of medium to fine sand with non-plastic fines of 9.2%. The index properties were determined and presented in the Table 2-2. Figure 2-11 shows the ranges of grain size distribution for liquefaction susceptible soils as proposed by Tsuchida and Xenaki and Athanasopoulos [41, 42], along with grain size distribution plot of sand samples considered for the current investigation. Figure 2-11 clearly high lights that sand samples falls within the range of most liquefiable soils.

The clean sand (particle size >0.075mm) was prepared by removing the silt portion by washing from the base sand using 75-micron sieve. The sand samples with non-plastic fines were prepared by adding the non-plastic fines derived from the base sand in different percentage (15%, 30% and 45%) by weight to the clean sand. Tests were conducted on sand samples of size 50mm diameter and 100mm height which were prepared by dry deposition method. A series of strain controlled cyclic triaxial tests

were carried out on isotropically compressed ($\sigma'_3 = 100$ kPa) samples at 1Hz frequency up to initial liquefaction.

Figure 2-12 illustrates the liquefaction susceptibility of sands with varying percentage of non-plastic fines at a constant dry density method. As may be seen, the liquefaction potential is influenced by the nonplastic fines. This clearly indicates that the percentage of non-plastic fines in the sand samples has a significant effect on the liquefaction potential. It is seen that the liquefaction potential of the sand sample increases with increase in the addition of non-plastic fines up to 30%. However, with further increase in non-plastic fines (FC>30%) the liquefaction potential is found to be decreasing. This may be attributed due to the change in the sand matrix from sand controlled matrix to silt controlled matrix.

Figure 2-13 shows the liquefaction potential of sand in the form of cyclic shear strain required for 20 numbers of loading cycles for clean sand samples mixed with varying percentage of non-plastic fines at constant dry density under of 1.694 g/cm^3. It is indicated in this figure that the cyclic shear strain at 20 numbers of cycle decreases with increase in the percentage of non-plastic fine content up to 30% and thereafter the shear strain amplitudes corresponding to 20 number of cycle is increasing with increase in the non-plastic fine content. The experimental results from the current study indicate that the threshold value (limiting value) of fine content is, approximately, equal to 30%.

To study the behavior sand-silt mixtures M. Belkhatir. et al. [22] collected sand samples from the liquefied layer of the deposit areas close to the epicenter of Chlef earthquake (October 10, 1980). Chlef sand has been used for all tests presented in this research. Individual sand particles are subrounded and the predominant minerals are feldspar and quartz. The tests were conducted on the mixtures of Chlef sand and silt. The liquid limit and plastic limit of the silt are 27% and 22% respectively. Chlef sand was mixed with 0 to 50% silt to get different silt content. The dry pluviation method was employed in the present study to prepare the soil samples for the monotonic and cyclic testing. The index properties of the soils used during this study are summarized in Table 2-5. The grain size distribution curves for the soils are shown in Figure 2-14.

Figure 2-15 and Figure 2-16 show the results of the undrained monotonic compression triaxial tests carried out for different fines content ranging from 0 to 50% at 100 kPa mean confining pressure within two separate density ranges (D_r = 12, 90%). We notice in general that an increase in the amount of fines leads to a decrease in the deviatoric stress. This decrease results from the role of the fines in reducing the soil dilatancy and amplifying the phase of contractancy of the sand-silt mixtures, leading to a reduction of the confining effective pressure and consequently to a decrease in the peak strength of the mixtures as is illustrated by Figure 2-15(a) and Figure 2-16 (a). The stress path in the (p', q) plane shows clearly the role of the fines in the decrease in the average effective pressure and the maximum deviatoric stress (Figure 2-15 (b) and Figure 2-16 (b)). In this case, the effect of fines on the undrained behaviour of the mixtures is observed for the lower fines contents (0% and 10%), and becomes very marked beyond 20%.

Figure 2-17 and Figure 2-17(b) illustrate the variation of the cyclic stress ratio ($CSR = q_m / 2\sigma_3'$) and the cyclic liquefaction resistance (CLR) with the number of cycles (N_c) and fines content respectively. The cyclic liquefaction resistance (CLR) is defined as the cyclic stress ratio leading to liquefaction for 15 cycles according to [43]. The test results show that the liquefaction resistance of the sand-silt mixture decreases with increase in the fines content. These results confirm those found during monotonic tests showing that the increase in the fines content reduces the dilatancy phase and amplifies the phase of contractancy. Consequently, the increase of the contractancy phase induced a reduction in the liquefaction potential with the increase in the fines content. For the mixtures of Chlef sand-silt, the presence of fine-grained soils increases the phase of contractancy resulting in a significant decrease in the liquefaction potential particularly, for the fines contents less than 10%. It should be noted that for the studied amplitude ($q_m = 30\ kPa$), the increase in fines content accelerates the liquefaction processes of the Chle sand-silt mixtures. Figure 2-17(c) presents the loading cycles till the liquefaction versus the fines content. We notice that the liquefaction resistance decreases with the increase in the fines content and loading amplitudes. The soil samples sheared with higher level loading (CSR = 0.25) are more vulnerable to liquefaction than those sheared with smaller loading level (CSR = 0.15).

Clean sand, clean sand and silt mixtures and pure silt were used by Dash and Sitharam [39] in their study. Clean sand was obtained by wet sieving the original Ahmedabad (India) sand through 75 micron IS sieve which had around 9.8% of nonplastic silt. Clean sand was identified as poorly graded sand with symbol SP as per IS 1498 (1970) [44].

Quarry dust (<75 microns) was used in this study as a substitute for silt. It is a byproduct of rubble crusher units in and around Bangalore (India). The grain size distribution as per IS 2720 (Part 4) [44] of the clean sand and the quarry dust (<75 microns) are presented in Figure 2-18. As per IS classification system the quarry dust was identified as inorganic silt with symbol ML. The index properties of sand and silt are shown in Table 2-3.

Sand-silt mixtures were prepared by adding quarry dust (silt) in various percentages (by weight) to the clean sand. Fourteen combinations of sand and silt were created using Ahmedabad clean sand with varying silt contents from 5 to 75% for carrying out undrained triaxial tests. Clean sand and silt were also used for the testing program. A series of stress controlled cyclic triaxial test with 0.1Hz frequency and strain controlled monotonic triaxial tests was carried out on sand-silt mixture specimens of 50 mm diameter and 100 mm height with varying silt content.

In view of these conflicting conclusions, a total of 88 cyclic tests and 25 monotonic tests were carried out at two different constant post-consolidation gross void ratios to study the effect of nonplastic fines on undrained cyclic and monotonic peak strength of sandy soils. Specimens up to 60 and 75% silt content were tested at constant gross void ratios of 0.44 and 0.54 respectively, as it was difficult to prepare specimens beyond these silt contents at respective gross void ratios as the corresponding relative densities were more than 100%. The cyclic and monotonic peak strengths of the specimens are plotted in Figure 2-19 and Figure 2-20 as a function of silt content. It can be seen that both the strength parameters initially decrease and reaches a minimum value at the limiting silts content and thereafter the trend is reversed with further increase in silt content. A similar behaviour was observed in both cases of constant gross void ratio. Again to reinforce this finding another series of cyclic triaxial tests were conducted at a post consolidation gross void ratio of 0.4 over a silt

content range of 10–35% (close to limiting silts content) and the results thus obtained are reported in Table 2-4. As seen in Table 2-4, similar cyclic strength behaviour as reported in other two cases is also seen in this case. This variation in both the strength parameters at constant gross void ratio is attributed to a corresponding decreasing and then increasing trend in relative density with increase in silt content at constant gross void ratio as presented in Figure 2-21. The relative density rather than the silt content of a specimen is found to be the major player in this approach.

A total of 48 undrained cyclic and 14 undrained monotonic tests were conducted on isotropically consolidated specimens at a post consolidation average relative density of 53% with silt content varying from 0 to 100%. The undrained cyclic and monotonic strength response of these specimens is presented in Figure 2-22 and Figure 2-23 as a function of silt content where it can be seen that with a little increase at 5% silt content, both the strength parameters fall drastically to around the limiting silts content and thereafter they remain relatively constant with further increase in silt content even up to pure silt. The little increase in these strength parameters at 5% silt content at a constant relative density may be due to more weight contained in the same volume (i.e. more dry density) as compared to clean sand and also the presence of up to 5% fines has little or no influence on these strengths as reported in the literature by many researchers in the past [45]. The effect of fines in reducing these strength parameters after 5% silt content can well be observed in this figure despite the fact that the dry density continues to increase with increase in silt content till the point of limiting silts content as is seen in Figure 2-24. Again the stability in these strength parameters after around the limiting silts content despite a continuous decrease in dry density (Figure 2-24) is also attributed to the influence of fines in constant relative density approach. It can also be seen that both cyclic and monotonic strength of specimens below the limiting silts content (21%) is at much higher level than of specimens with silt contents beyond the limiting silts content.

The natural soil used in a experimental investigation was taken from city of Firouzkooh north of Iran by Baziar et al. [40]. To accomplish the objectives of this study, sands with varying silt content ranged from 0 to 100% (percent passing No. 200 sieve) were used. The soil properties, used for this study are presented in Table 2-6 and the grain size distribution curves for the soil samples are also shown in Figure

2-25. Specimens with five different silt contents were prepared for the hollow torsional tests. A series of 60 tests were conducted on samples with the same relative density of 60% and the confining pressures of 60, 120 and 240 kPa and silt content of 15%, 30%, 60%, and 100%. The hollow cylindrical samples had external and internal diameters of 100 and 50mm respectively and the height of 100mm. The under compaction method was implemented to prepare uniform samples [43]. The required parameters for specimen preparation, such as water content and percentage of under compaction values were selected as 9% and 4%, respectively. All the specimens were isotropically consolidated under three effective confining pressures (σ'_3) of 60, 120, 240 kPa. Frequency of cyclic loading was 0.1 Hz and the numbers of cycles varied in the range of 0.17 to 900 cycles.

Figure 2-26 shows the effect of silt content on liquefaction resistance ratio (*CRR*) in a constant relative density of 60%. This Figure is similar to the modified liquefaction resistance diagrams presented by Polito and Martin [37]. Figure 2-26 also reveals the relation of *CRR* with silt content at the different confining pressures with the same relative density (60%). It can be seen in this Figures that, for low value of silt content ($SC<SC_{th}$, where SC_{th} is threshold fines content for change of behavior in silty sand) an increase in silt content causes decrease of liquefaction resistance. However with the amount of silt content more than the SC_{th} till the silt content of about 60% liquefaction resistance tend to be increased and then decreased again. Value of silt contents which are reported as limits for change of behavior (30% and 60%), are based on the results of test performed in this research. However the determination of exact values of these limits needs more tests results. Figure 2-26 also shows that the change of confining pressure from 60 kPa to 240 kPa causes an approximately 40% decrease in the cyclic resistance.

Baziar et al. [40] proposed a simple model to predict pore water pressure generation in non-plastic silty soil during cyclic loading (see Figure 2-29). They used stress-controlled cyclic hollow torsional tests at relative density 60 percent and with three different confining pressures 60, 120 and 240 kPa.

Dash and Sitharam [47] proposed two reconstituted pore pressure boundaries, first is in Figure 2-27 (Excess pore pressure ratio (R_u) verses cyclic ratio (N/N_L)) and the second one is in Figure 2-28 (Excess pore pressure ratio (R_u) verses shear strain).

On the basis of the results of sieve analyses on soils that did or did not liquefy during past earthquakes, Tsuchida [41] proposed the grain-size distribution boundary curves in Figure 2-30 (a). The lower boundary reflects the influence of plastic fines in decreasing the ability of sand to contract during shaking. The zone between the upper boundaries corresponds to coarse soils with coefficients of permeability greater than 10^{-3} to 10^{-2} m/s. Sands most susceptible to liquefaction have coefficients of permeability in the range of 10^{-5} to 10^{-3} m/s.

According to Figure 2-30 (a) the natural soil deposits with D_{50} less than 0.02 mm or larger than 2.0 mm do not liquefy. On the other hand, mine tailing of crushed rock and other wastes are highly susceptible to liquefaction, even though they contain significant amount of silt and clay size particles, because these fines are composed of nonplastic solids. Grain size distribution curve for the fine-grained tailings obtained from several disposal ponds and their susceptibility to liquefaction are shown in Figure 2-30 (b).

The nature of empirical field data is also well illustrated by the recent results obtained in Adapazari, Turkey by Bray et al. [48]. They plotted the characteristics of fine-grained soils that were identified as having "liquefied" at 12 building sites during the 1999 Kocaeli earthquake, as shown in Figure 2-31. Recognizing that every bullet in these plots is considered a soil that "liquefied," Bray et al concluded that gradational characteristics are not a reliable indicator of liquefaction susceptibility.

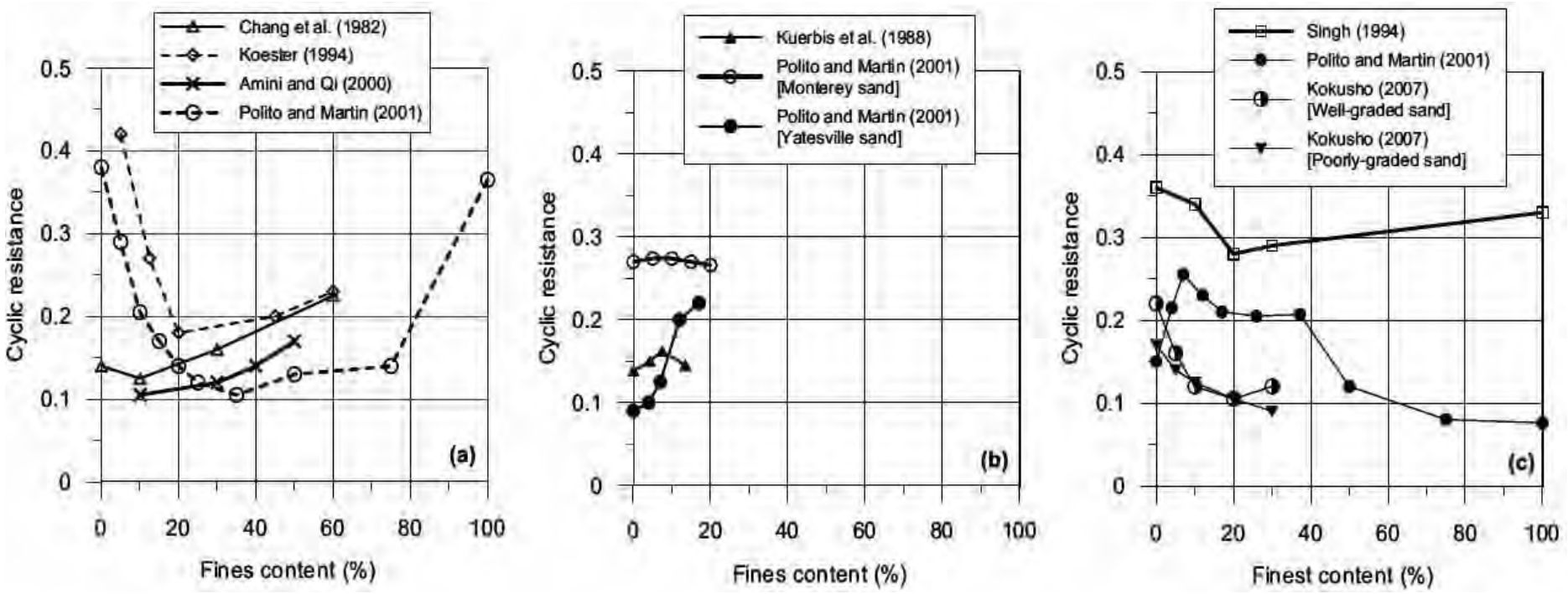

Figure 2-1. Results from previous studies on the effect of fine content (*FC*) on cyclic resistance: (a) studies at constant overall void ratio; (b) studies at constant sand skeleton void ratio; and (c) studies at constant relative density [32].

Figure 2-2. Liquid silt has gushed up through cracks in the surface [35].

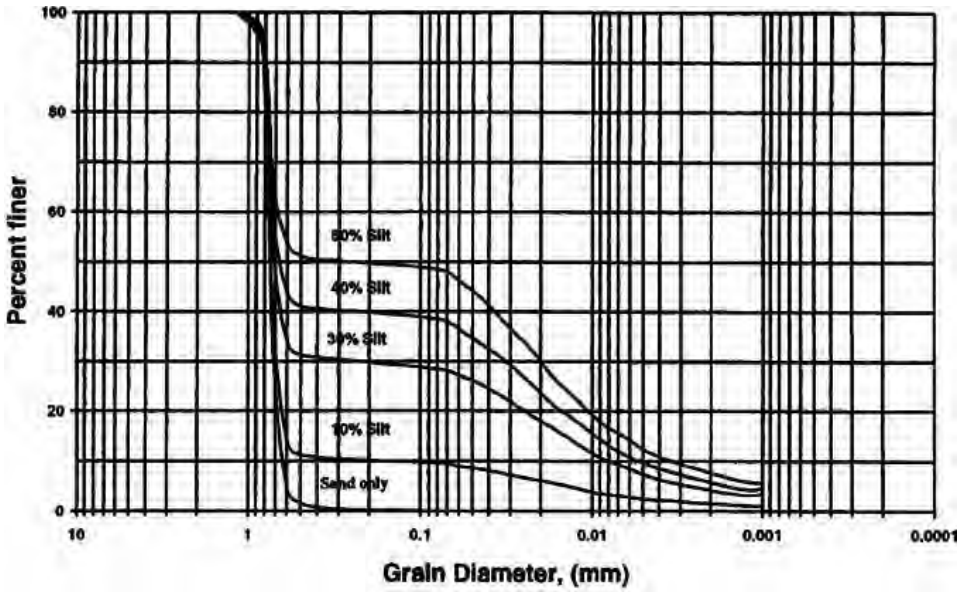

Figure 2-3. Grain size distribution curve [36].

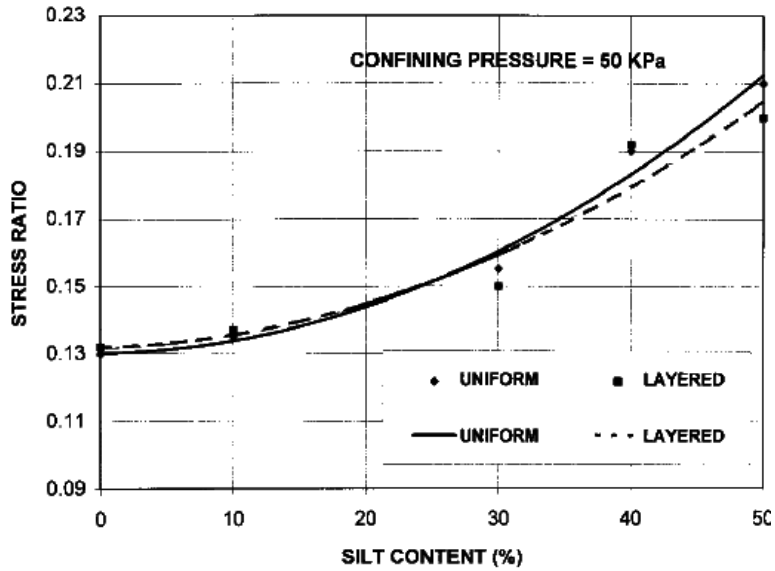

Figure 2-4. Comparison between liquefaction behavior of layered and uniform soils as function of silt content for stress ratios to cause liquefaction at ten cycles [36].

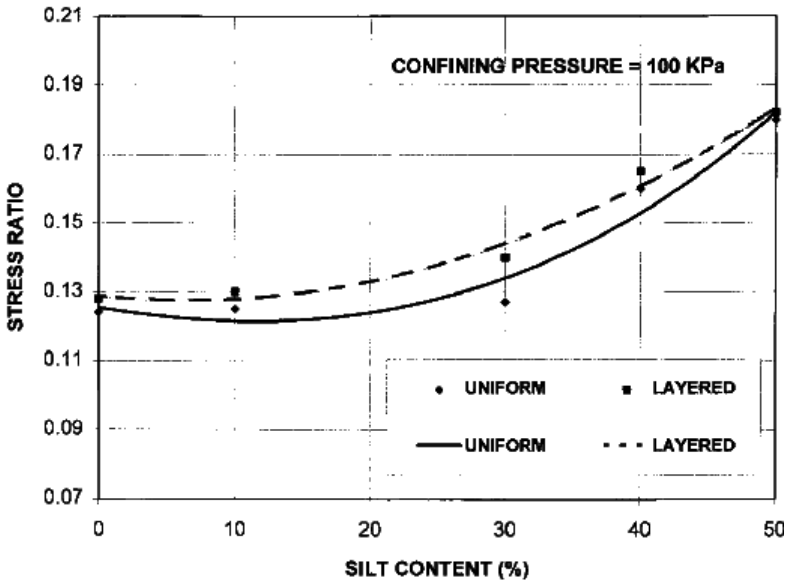

Figure 2-5. Comparison between liquefaction behavior of layered and uniform soils as function of silt content for stress ratios to cause liquefaction at ten cycles [36].

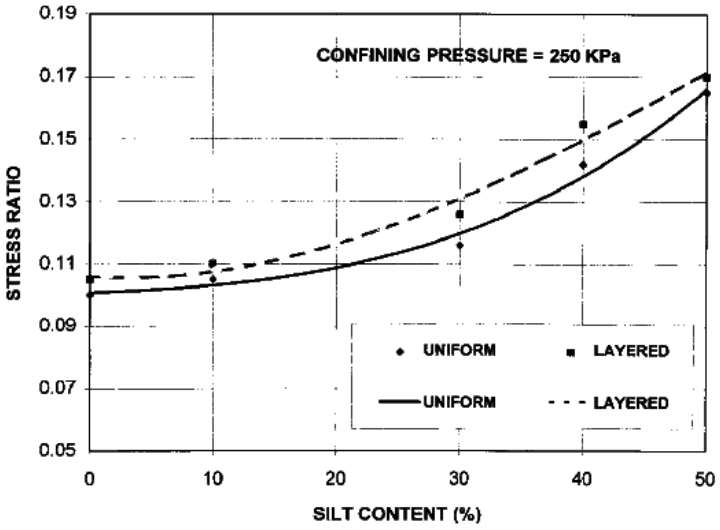

Figure 2-6. Comparison between liquefaction behavior of layered and uniform soils as confining pressure for stress ratios to cause liquefaction at ten cycles [36].

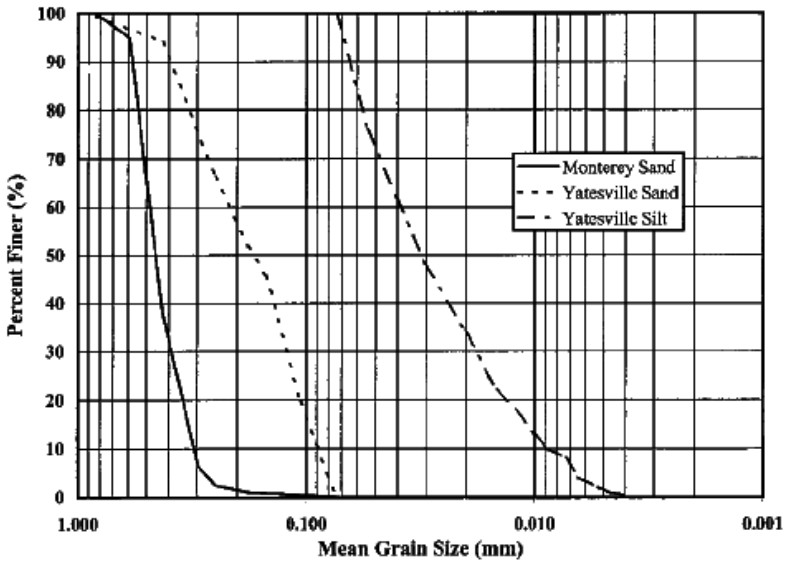

Figure 2-7. Grain size distributions of soils used [37].

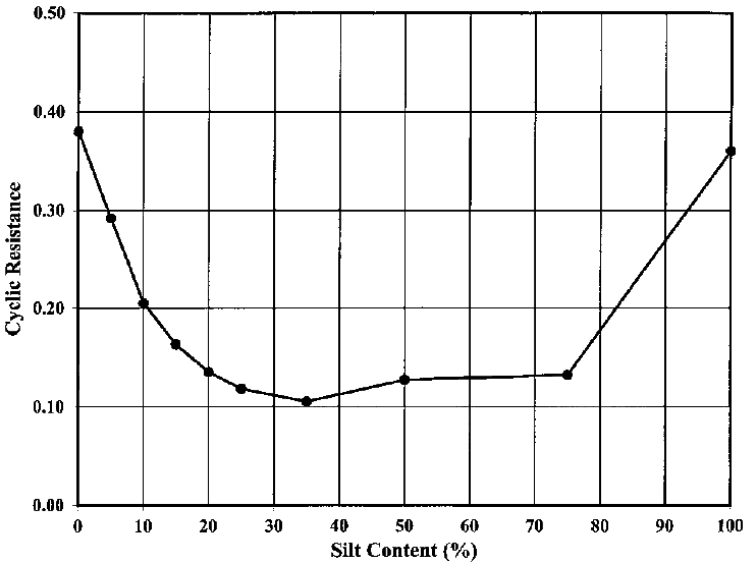

Figure 2-8. Cyclic resistance of Monterey sand at constant void ratio with variation in silt content [37].

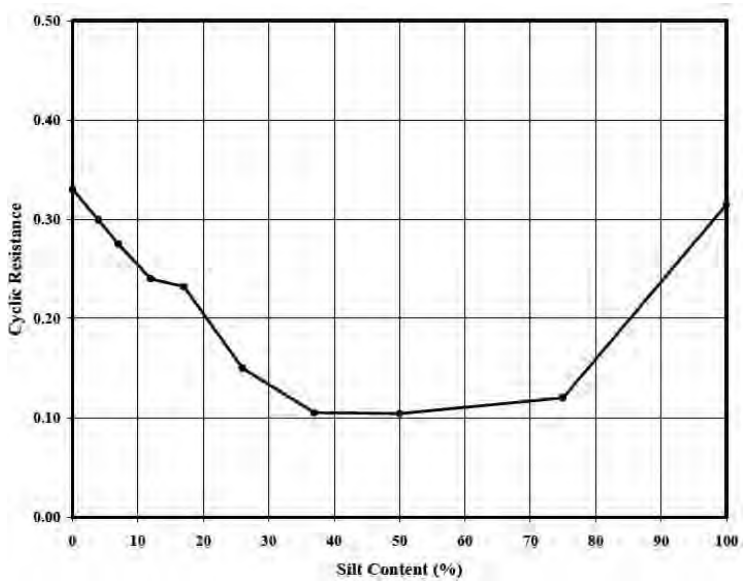

Figure 2-9. Cyclic resistance of Monterey sand at constant void ratio with variation in silt content [37].

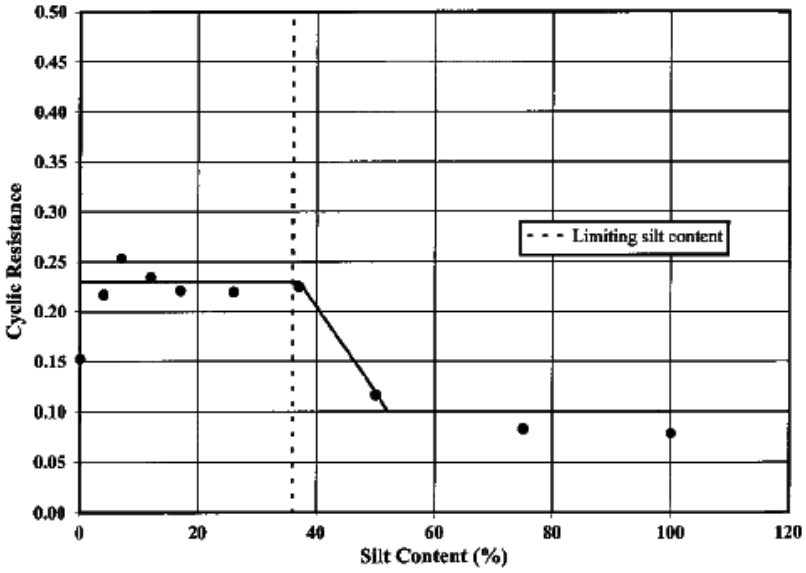

Figure 2-10. Variation in cyclic resistance with silt content for Yatesville sand specimens prepared by moist tamping adjusted to 30% relative density [37].

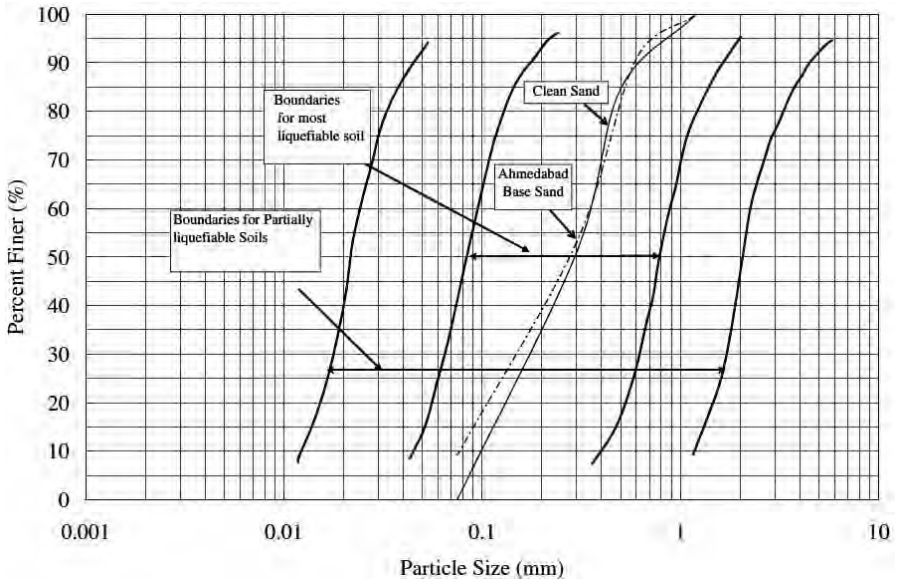

Figure 2-11. Grain size of distribution of soils susceptible to liquefaction [38].

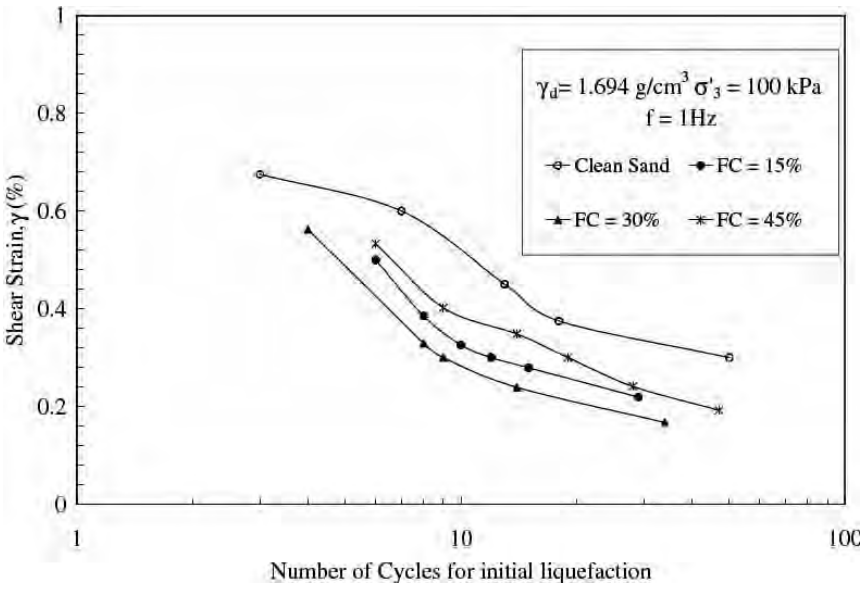

Figure 2-12. Relationship between shear strain and number of cycles for initial liquefaction for clean sand with different percentage of non-plastic fines [38].

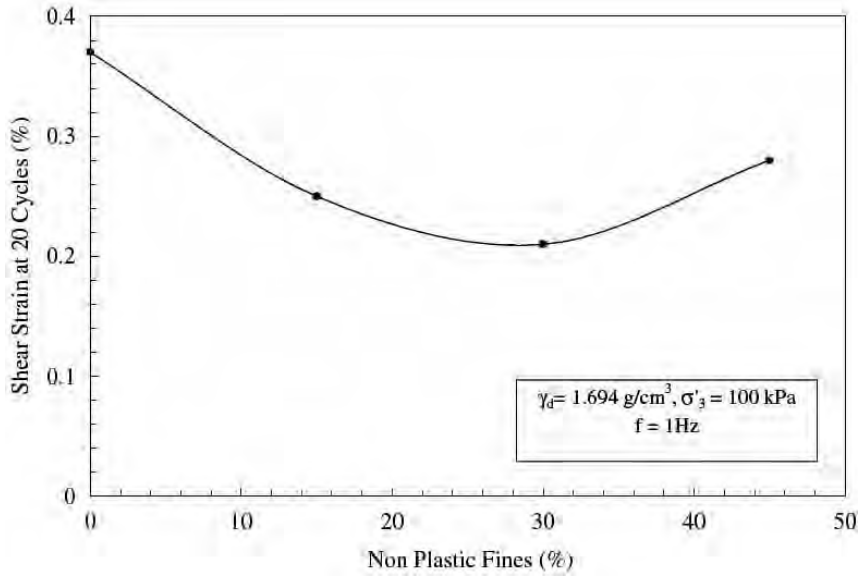

Figure 2-13. Cyclic strength in terms of cyclic shear strain at 20 numbers of cycles with different percentage of non-plastic fines [38].

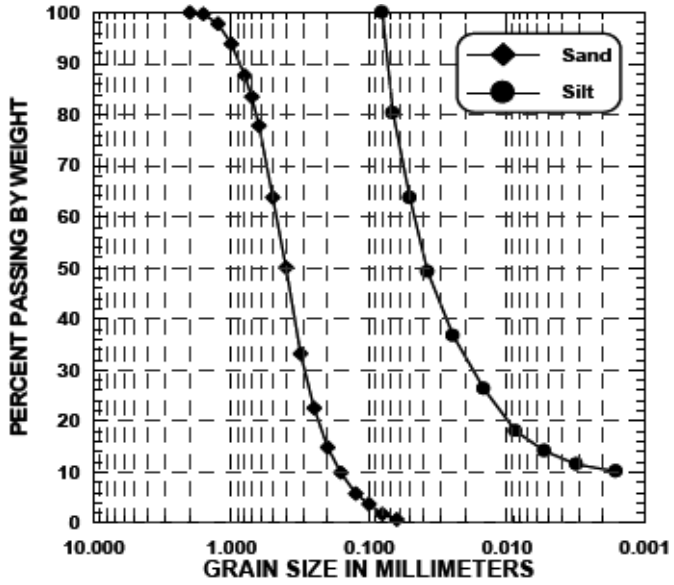

Figure 2-14. Grain size distribution curves [22].

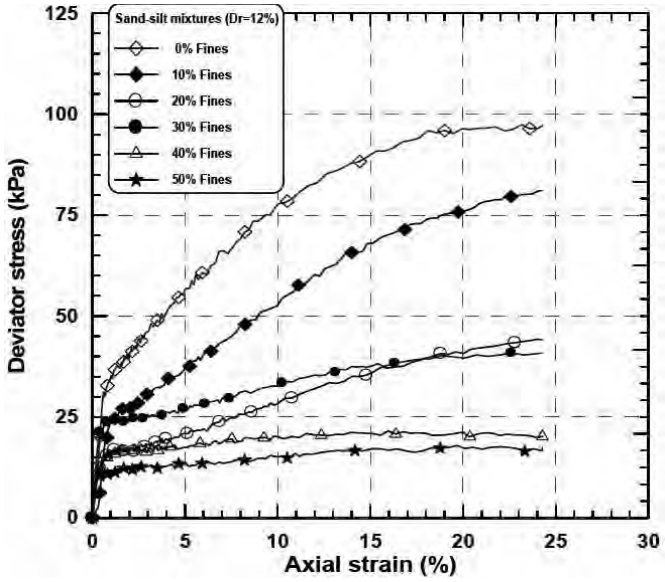

(a)

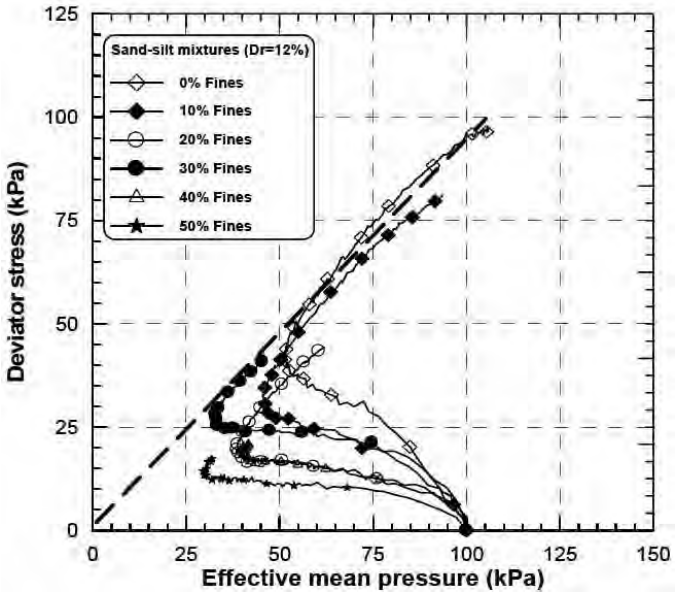

(b)

Figure 2-15. Undrained monotonic response of the sand-silt mixtures (σ_3'=100 kPa, D_r = 12%) [22].

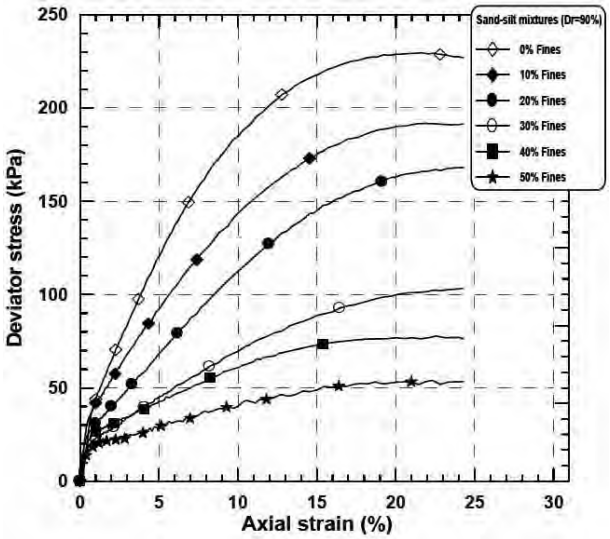

(a)

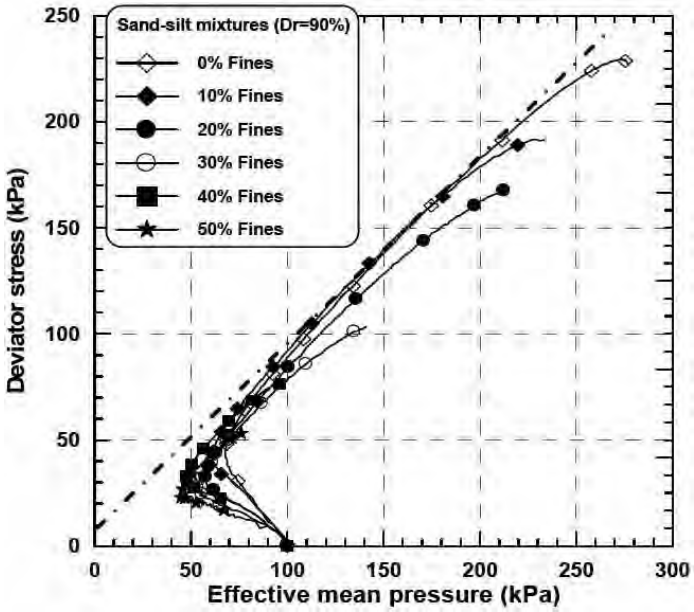

(b)

Figure 2-16. Undrained monotonic response of the sand-silt mixtures (σ_3'=100 kPa, D_r = 90%) [22].

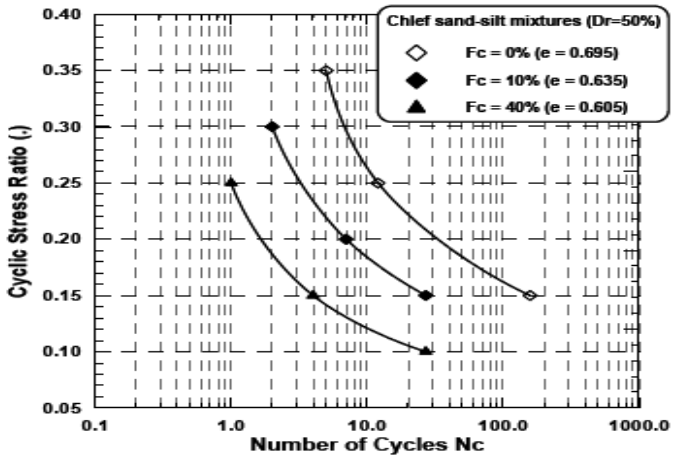

(a)

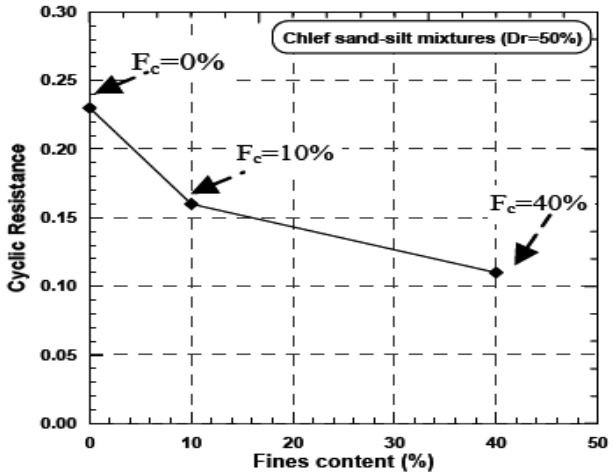

(b)

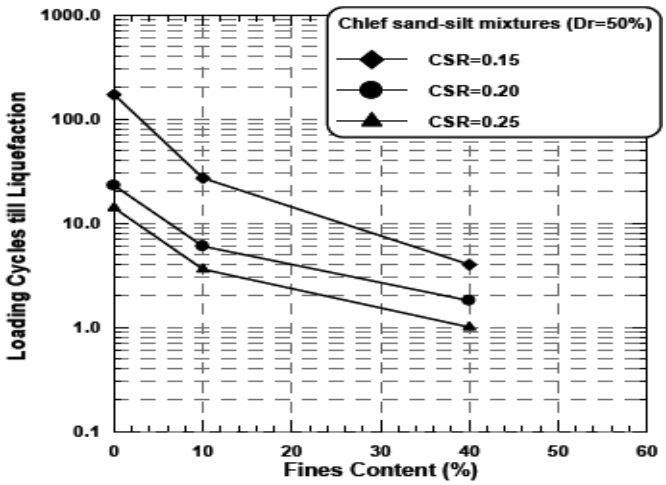

(c)

Figure 2-17. Effect of fines on the liquefaction potential of the Chlef sand-silt mixtures (σ_3'=100 kPa, D_r=50%) [22].

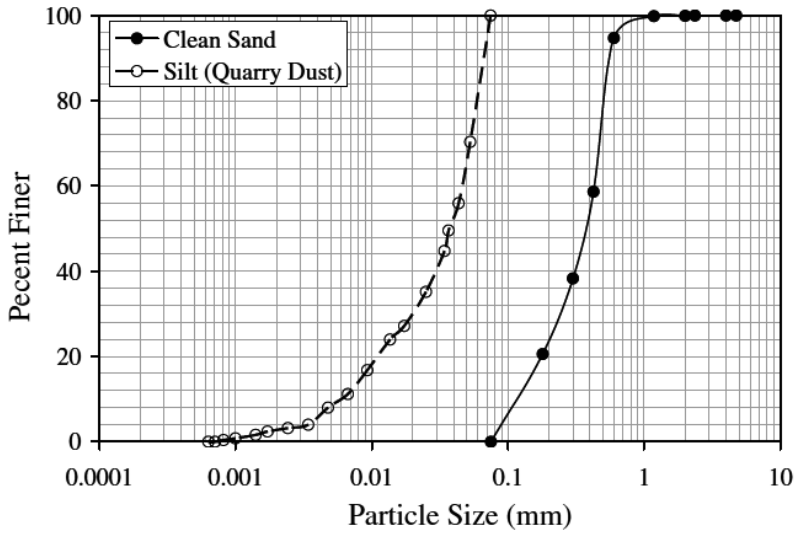

Figure 2-18. Grain size distribution of materials used [39].

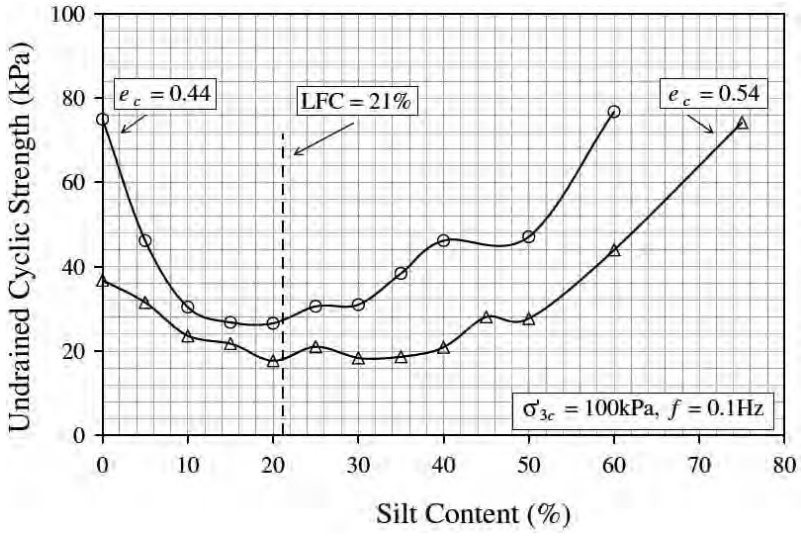

Figure 2-19. Variation in cyclic strength with silt content at e_c = 0.44 and e_c = 0.54 [39].

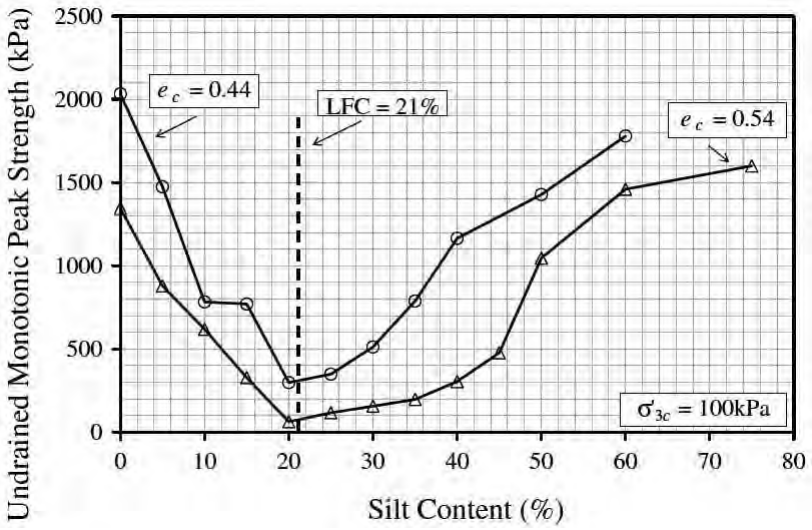

Figure 2-20. Variation in monotonic peak strength with silt content at e_c = 0.44 and e_c = 0.54 [39].

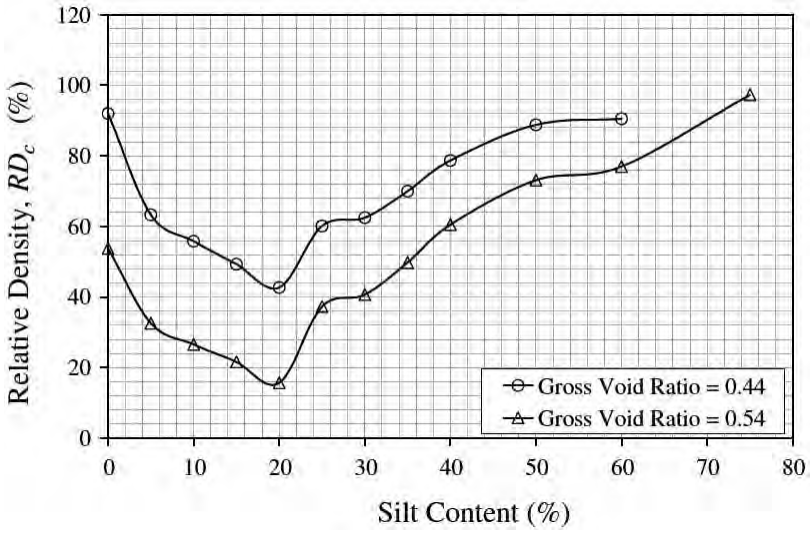

Figure 2-21. Variation in relative density with silt content at e_c = 0.44 and e_c = 0.54 [39].

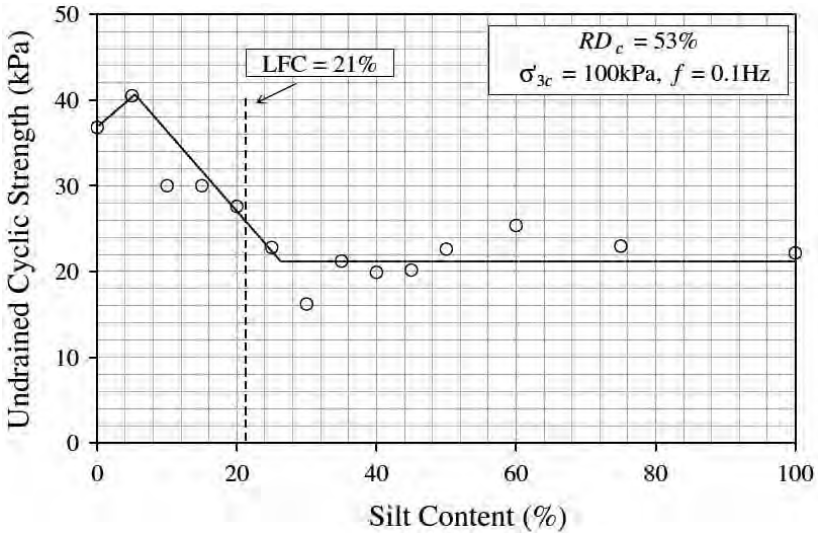

Figure 2-22. Variation in cyclic strength with silt content at RD_c = 53% [39].

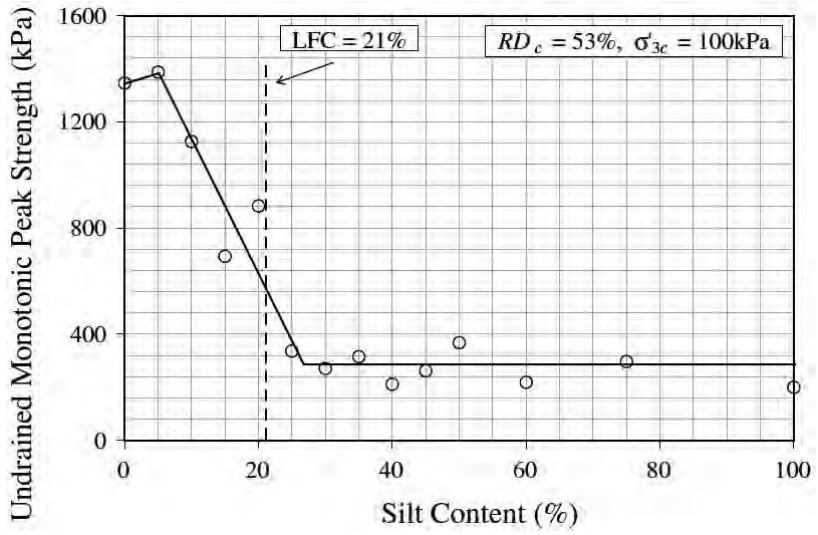

Figure 2-23.Variation in monotonic peak strength with silt content at RD_c = 53% [39].

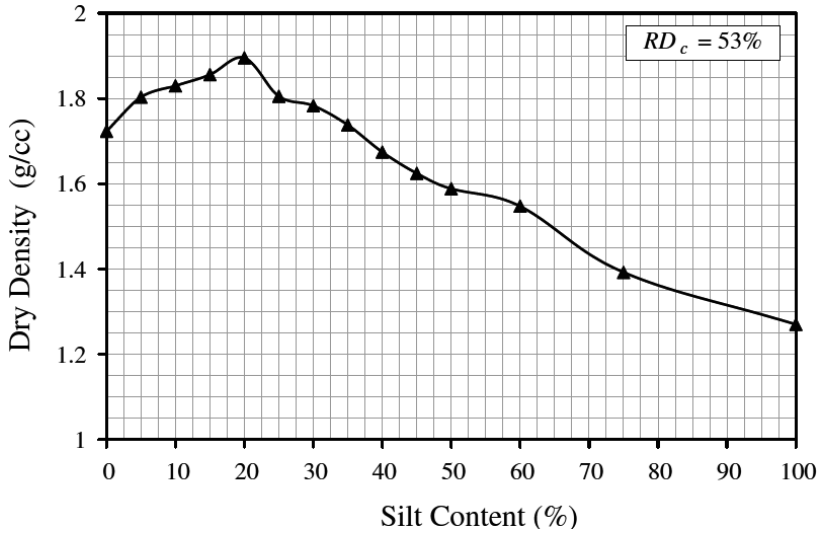

Figure 2-24. Variation in dry density with silt content at RD_c = 53% [39].

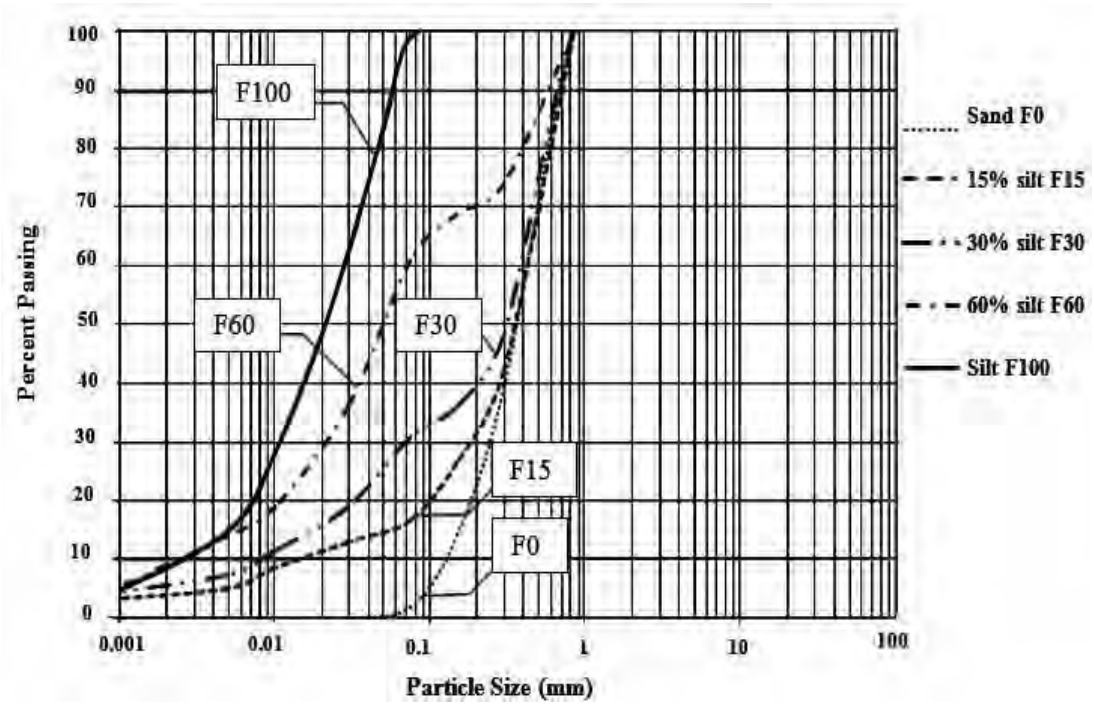

Figure 2-25. Grain size distribution of natural soils samples used in the present study [40].

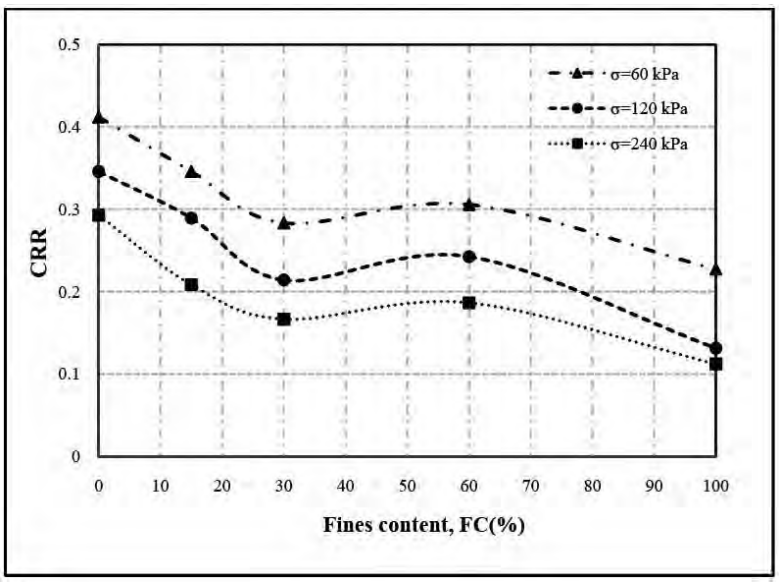

Figure 2-26. Effect of fines content on the liquefaction resistance ratio (*CRR*) for constant relative density (D_r= 60%) [40].

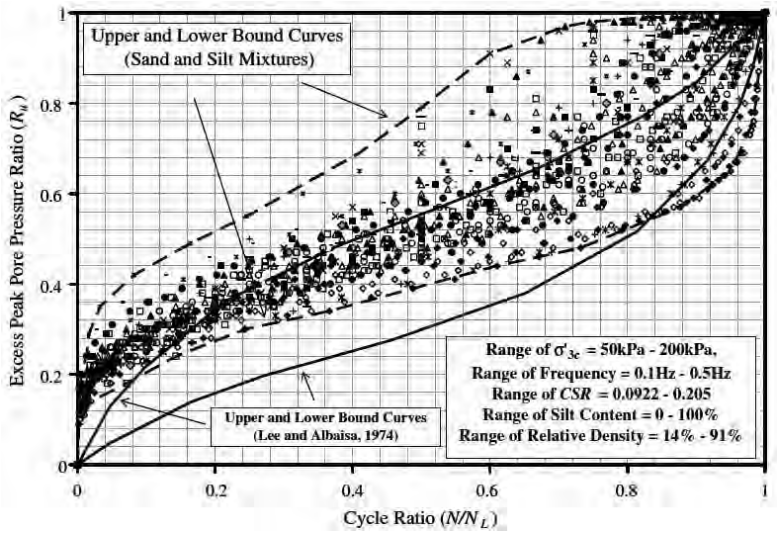

Figure 2-27. Maximum and minimum peak pore pressure generation in sand and silt mixture specimens over a wide range of parameters and compared with Lee and Albaisa [47].

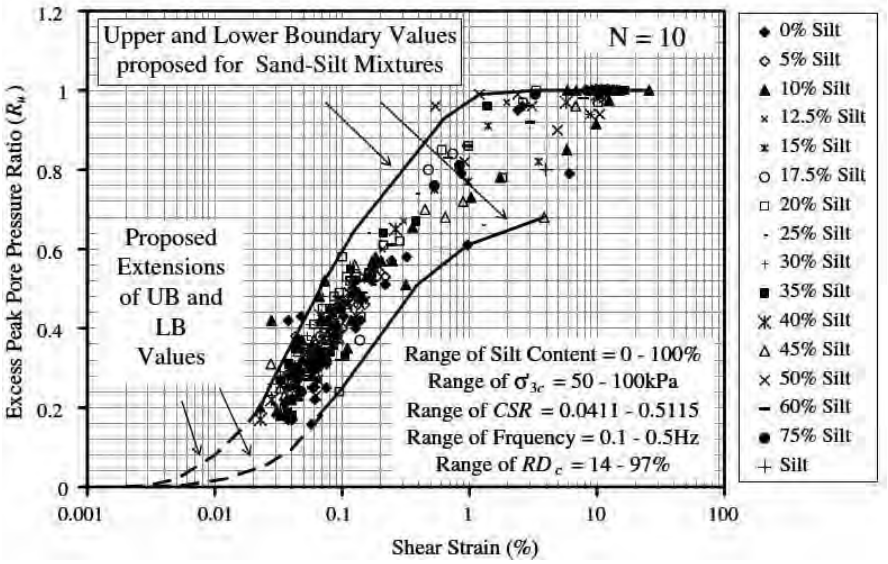

Figure 2-28. Peak pore water pressure generation in sand and silt mixture specimens @10th cycle over a wide range of parameters and proposed new narrow band [47].

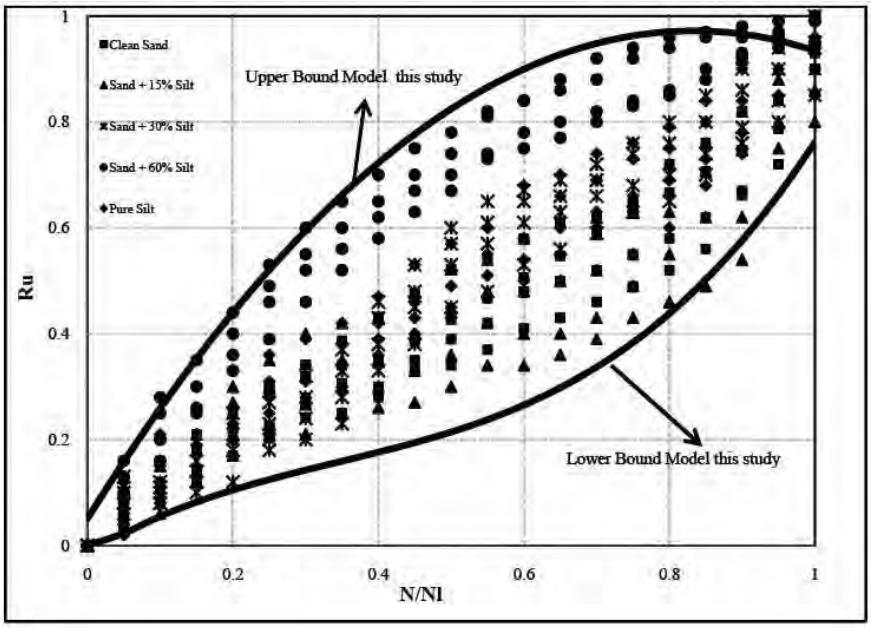

Figure 2-29. Excess pore water pressure generation data for all specimens and comparison with model presented in this study [40].

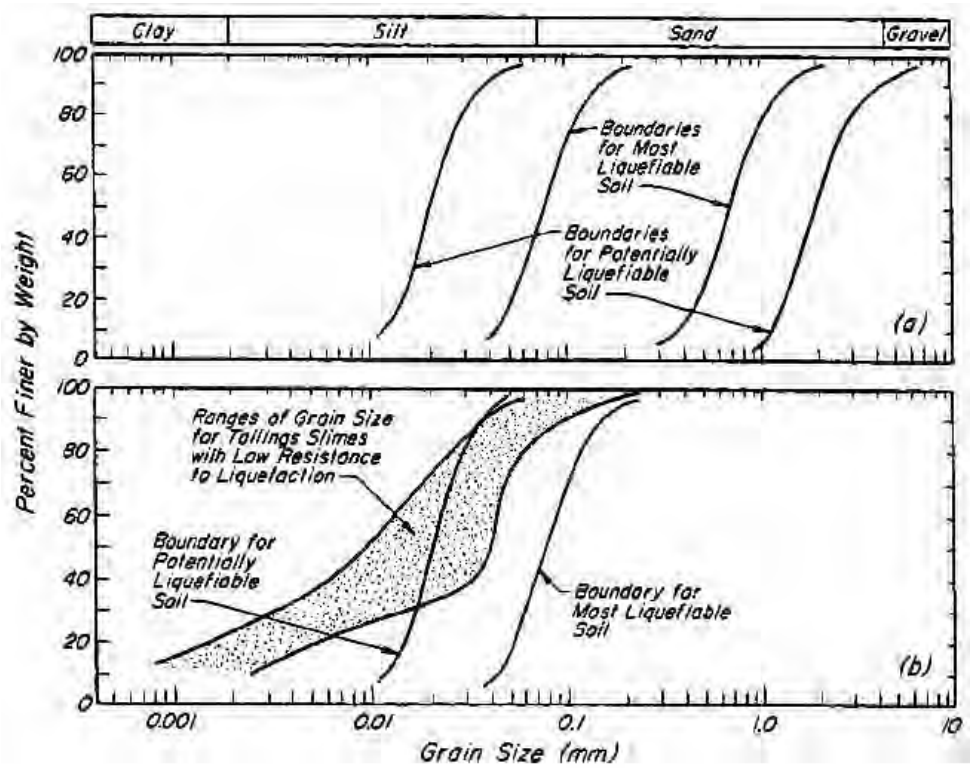

Figure 2-30. (a) Gradation curves defining limits of liquefaction and nonliquefaction soils (after Tsuchida) [41], (b) Range of grain sizes for tailing dams with low resistance to liquefaction (after Ishihara, 1985) [49].

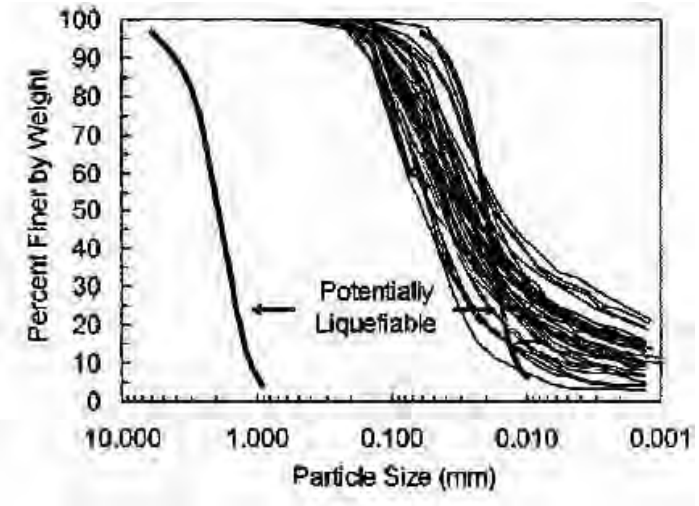

Figure 2-31. Characteristics of fine-grained soils that were reported by Bray et al. to have "liquefied" at 12 building sites in Adapazari, Turkey during the 1999 Kocaeli earthquake (Bray et al.) [48]: comparison of grain size distributions to the criteria by Tsuchida [41].

Table 2-1. Properties of soils tested [36].

Series (1)	Fines content (%) (2)	G_s (3)	D_{50} (mm) (4)	C_u (5)	e_{max} (6)	e_{min} (7)	Particle shape (8)
A	10	2.64	0.67	7.5	0.87	0.49	Subrounded to subangular
B	30	2.65	0.66	93.0	0.87	0.44	Subrounded to subangular
C	40	2.66	0.65	137.0	0.88	0.40	Subrounded to subangular
D	50	2.68	0.25	200.0	0.90	0.37	Subrounded to subangular

Table 2-2. Index properties of the sand samples [38].

Properties	Values	
	Base Sand	Clean Sand
Specific gravity	2.65	2.65
Liquid limit (%)	—	—
Plasticity index (%)	—	—
Coefficient of curvature C_c	0.82	0.944
Coefficient of uniformity C_u	4.48	3.57
Median grain size D_{50} (mm)	0.28	0.3
Maximum void ratio (e_{max})	0.67	0.69
Minimum void ratio (e_{min})	0.38	0.44

Table 2-3. Index properties of component soils used in this study [39].

Soil types	Clean sand	Quarry dust (Silt)
IS classification symbol	SP	ML
Maximum grain size (mm)	2	0.0747
Mean grain size D_{50} (mm)	0.375	0.037
Minimum grain size (mm)	0.075	0.00063
Uniformity coefficient (C_u)	3.58	7.83
Coefficient of gradation (C_z)	1.163	1.418
Specific gravity (G_s)	2.65	2.67
Minimum index density (kN/m^3)	15.77	10.14
Maximum index density (kN/m^3)	18.66	16.16
Minimum index void ration (e_{min})	0.42	0.652
Maximum index void ration (e_{max})	0.68	1.632
Liquid limit (%)	NP	33.75
Plastic limit (%)	ND	32.18
Plasticity index (%)	NP	1.57 (NP)

NP nonplastic, *ND* not determinable

Table 2-4. Cyclic resistance ratio at $e_c = 0.4$ [39].

Silt content (%)	Undrained cyclic strength (kPa) at $e_c = 0.4$
10	38
15	30
20	27.6
25	20.2
35	23.7

Table 2-5. Index properties of Chlef sand-silt mixtures [22].

Material	Fines Content (%)	G_S	D_{50} (mm)	C_u	e_{min}	e_{max}	I_p(%)
Clean Sand	0	2.680	0.40	2.90	0.535	0.854	-
Silty Sand	10	2.682	-	-	0.472	0.798	-
Silty Sand	20	2.684	-	-	0.431	0.748	-
Silty Sand	30	2.686	-	-	0.412	0.718	-
Silty Sand	40	2.688	-	-	0.478	0.732	-
Silty Sand	50	2.69	-	-	0.600	0.874	-
Silt	100	2.70	0.004	29.4	0.72	1.420	5.0

Table 2-6. Physical property of tested material [40].

No.	Name	(USCS)	G_s	γ_d(gm/c^3)	e_{max}	e_{min}	e	D_{50}	C_c	C_u
1	F0	SP	2.67	1.574	0.870	0.580	0.696	0.371	0.899	2.44
2	F15	SM	2.67	1.692	0.830	0.410	0.578	0.351	9.093	30.46
3	F30	SM	2.67	1.740	0.854	0.319	0.533	0.308	1.522	48.92
4	F60	SM	2.68	1.560	1.259	0.370	0.720	0.050	0.033	30.43
5	F100	ML	2.68	1.321	1.880	0.460	1.028	0.021	1.650	11.54

CHAPTER 3

TESTING PROGRAM

3.1 Introduction

Total 49 cyclic stress-control tests and 13 undrained strain-control static or monotonic triaxial tests have been done on sand-silt mixtures at 100 kPa effective confining pressure. These tests have been done on specimens of size 71 mm diameter and 142 mm height with frequency of 1 Hz for cyclic loading and 0.05% axial strain per minute for monotonic loading. Specimens were prepared at a constant relative density and constant density approach by moist tamping method. On the other hand for determination of index property specific gravity, liquid limit, plastic limit, sieve analysis, hydrometer analysis, modified proctor test (maximum density) and minimum density in water method (minimum density) test have done. Else electro microscopic view, stereo microscopic view as well as X-ray diffraction (*XRD*) were carried on sand and silt sample to identify the feature of their grains and minerals. To explain the description of sand-silt mixtures behavior permeability test were done on each mixture. In this chapter geology, mineralogy, index property of samples and testing programs are explained.

3.2 Geology of Studied Soils

From the Geological Map of Bangladesh (Figure 3-1) [50], in the both side of river bed of Jamuna River and north side of the Padma River (Mawa) same types of soil is found, which is colored orange and identified as Alluvial silt (*asl*), as in the map. *Alluvial silt (asl)* is defined as Light to medium grey, fine sandy to clayey silt in the map. Commonly poorly stratified; average grain size decreases away from main channels. Chiefly deposited in flood basins and inter stream areas. Unit includes small back swamp deposited during episodic and unusually large floods. Illite is the most abundant clay mineral. Most areas are flooded annually. Included in this unit are thin veneers of sand spread by episodic large floods over flood-plain silts. Historic pottery, artifacts, and charcoal (radiocarbon 500-6000 yrs. B.P. (Before Present)) found in upper 4 m.

3.3 Properties of Sand and Silt

3.3.1 Index properties

Fine sand and silt were collected from sandbars of Padma River, Mawa, Munshiganj, Bangladesh, near proposed Padma Bridge site (Figure 3-2). The sample was washed through 75μm sieve to obtain clean sand and silt. Two methods are used to find the particle-size distribution of soil, are sieve analysis (sand) and analysis (silt). The grain size analysis reports are shown in Figure 3-4. Fine sand and silt specimen were viewed under Scanning Electron Microscope (*SEM*) (Figure 3-5) to see the shape of particles. Figure 3-5 (a) shows the image of fine sand with 50 times magnification and Figure 3-5 (b) shows the image of silt with 150 times magnification. From these two images from *SEM* it is clearly seen that the fine sand and silt particles are angular and rough. That means fine sand and silt; both are same granular material with different particle sizes. It was tried to determine Plastic Limit (*PL*) of silt and observed that the silt was non-plastic. But it should be noted that 8.11 percent of clay mineral (Illite) is found in silt sample. Index properties of sand and silt are shown in Table 3-2.

Sand–silt mixtures were prepared by adding non-plastic silt in various percentages (silt = 0% to 100%, by weight of total soil) to the clean sand. Maximum and minimum index densities of sand-silt mixtures were determined and shown in Table 3-3 and Figure 3-6(a). Maximum and minimum void ratios of sand-silt mixtures are shown in Figure 3-6(b). Maximum density was determined by modified proctor test and minimum density was determined by minimum density test in water method [51].

3.3.2 Limiting Fines Content

As fines (silt) are added to a sand, it passes from one phase to the other through a transition point called as the Limiting Fines (silt) Content (*LFC*). Below this point the soil structure is generally a sand dominated one with silt contained in a sand-skeleton whereas beyond this point there are enough fines such that the sand grains loose contact with each other and the soil structure becomes predominantly a silt dominated one. The *LFC* is generally calculated using the following expression [52]:

$$LFC = \frac{W_{fines}}{W_{sand} + W_{fines}} = \frac{G_{sf} e_s}{G_{sf} e_s + G_{ss}(1 + e_f)} \ldots\ldots\ldots\ldots\ldots\ldots\ldots\ldots (3.1)$$

Where, W_{fines} is the weight of fines and W_{sand} is the weight of sand in a sand–silt mixture. Similarly, G_{sf}, G_{ss}, e_f and e_s stand for specific gravity and maximum index void ratio of fines and sand, respectively. Using the Eq. 3.1, the limiting silts content for sand–silt mixtures used in this study was found to be 30%. For clearance of concept of *LFC* more explanation is given below.

In Figure 3-7 (a) and Figure 3-7 (b), where the inner void is decreasing with increasing the fines content, the fine particles fill the inner void spaces between the large grains until point (b) is reached (*LFC* phase). At this point the inner void spaces are almost completely filled by the fines. From point (b) the large particles start to separate from each other, where from the silt dominant part start. Between point (b) and (c) the large particles become significantly displaced from each other by the large quantity of smaller particles until it reaches (d). From the *LFC* phase the inner void of the fines become equal. So it behaves same as silt which will be proved later.

3.3.3 Mineralogy

Hight et al. [53] reported that soil of the Jamuna River contains several percent of mica (see in Figure 3-8) which is highly vulnerable to triggering failure and consequent flowage of soil (as in Figure 3-9). The ratio of the mica plate as high as approximately 50:1 compared to the rotund sand particles, the presence of even 1% mica by weights is approximately equivalent to that of 25% of mica by number of grains. Therefore some tests have been done to identify the percent of mica content in the sand and silt samples which are explained below.

3.3.3.1 Stereo microscopic test

Samples were oven dried for visual inspection of mineral, the stereo microscope was used with 40 times magnification. The stereo microscopic views are shown in Figure 3-10. It is clear that the silt particles are too much smaller than that of sand particles. It is very difficult to identify mineral with visual inspection at 40 time magnification. So, we go for X-ray diffraction (*XRD*) test which is the best method to determine mineral percent of different minerals content, is explained in section 3.3.3.2.

3.3.3.2 X-Ray Diffraction Test

X-ray diffraction (*XRD*) is a mature x-ray technology that is widely used in the minerals industry for mineral identification and quantification. The sample preparation procedure is that, first of all sampling plate was cleaned by Ethanol for removing dust. There is a space of 15 mm length, 10 mm width and 2 mm deep in the sampling plate for placing the sample in the space (Figure 3-11). Later the plate was placed into the *XRD* box (*X' Part PRO XRD System*). Randomly oriented mounts of the sand and silt were x-rayed at a scanning speed of 0.02° (2θ) sec^{-1} by using a *CuKα* (1.542 Å) radiation range of 5 to 65 degrees. Figure 3-12 shows the counts verses position graph of sand and silt mixture. The peak counts are used to calculate the percent of minerals content in the specimens. The percent of minerals content are given in Table 3-1. In here 8.11 percent of Illite mineral (one kinds of clay mineral) is present, which match with the report of geological map of Bangladesh (section 3.2, *als*). On the other hand 4.28 percent of muscovite (mica) is found in the silt specimen. Quartz and Albite is the common mineral found in sand and silt.

3.4 Specimen Preparation

Soil specimens used in this study were of 71 mm in diameter and 142 mm in height. The specimens were formed by using wet tamping method in a split mold. The inner-diameter of the mold is 71 mm and height 142 mm (Figure 3-13). The dry soil is mixed with 10 percent water and then compacted in several equal layers by a tamping road that delivers some blows to each layer to achieve the target relative density. Number of layers and number of blows per layer were determined by trial to achieve target relative density. The tamping road weighs 1kg, and has a drop of 6 inches. In order to obtain a uniform density throughout the specimen, the compaction method of specimen preparation suggested by Ladd [46] was used. After preparing the specimen, was encased by a thin rubber membrane and griped top and bottom with o-ring after that placed inside a plastic cylindrical chamber that was filled with water (Figure 3-14).

3.5 Saturation and Consolidation

When the preparation of the specimen was complete and the specimen was formed, initial saturation of the specimen was done by passing carbon dioxide (CO_2) (Figure

3-15(a)) about one hour through the specimen. After that the distilled water was passed through the specimen by gravity pressure of 5 kPa for 3 to 5 hours (Figure 3-15(b)). It is mentionable that, at the initial time 20 kPa confining pressure was ensured by compression of the fluid in the chamber. At the end of this process the machine was switched on. The machine is capable of applying sufficient back pressure till it was ensured that the Skempton's B parameter equal to 95%. The specimens were then isotropically consolidated to a desired effective confining stress by compression of the fluid in the chamber. The duration for the process of consolidation was varied from about 2 hours (for clean sands) to about 3 hours (for pure silt). All relative densities reported here are post consolidation relative densities. Same sample preparation, saturation, and consolidation techniques were adopted for both cyclic and monotonic triaxial test.

3.6 Cyclic Triaxial and Monotonic Triaxial Testing

The testing apparatus used in the current study is capable of conducting static as well as cyclic loadings. The triaxial system used is shown in Figure 3-16, which consists of the following components: Triaxial cell, loading frame with computer-control platen that applies cyclic axial load on top of soil specimen, two computer-control flow pumps to control the chamber pressure and back pressure, high performance linear servo control electro actuator for cyclic loading with update rates of 500 times per second, micro-processor for controlling cyclic loading, PC with a Pentium processor to control the test and a data logger and a pump to make a void space on the cell chamber for cyclic loading (the pressure of the void space will be equal to the pressure of the water in the cell chamber). Various transducers are mounted in the system for measuring the axial load, confining pressure, pore-water pressure and axial strain. The excess pore water pressures were measured at the bottom of each specimen both for cyclic and monotonic triaxial test.

All cyclic triaxial tests were conducted at a cyclic loading frequency of 1 Hz and before starting the cyclic deviator load the triaxial cell was needed to make quarter inch air cushion using pump (Figure 3-17). The specimen was then loaded with a sinusoidal deviator stress until liquefied or 6% double amplitude axial strain (± 3% axial strain) occurred.

The procedure of monotonic triaxial test is as like as cyclic triaxial test only the different is in the last phase the monotonic test the actuator gives a static axial stress which is called deviatory stress. All tests were conducted at an axial strain rate 0.05 % per minutes, maximum axial strain 15% (ASTM 4258-09) [54].

3.7 Permeability Test Apparatus and Procedures

The permeability tests have done by Falling Head method. Though it is not a standard method, my aim is to see the effect of fines in permeability. In this method the diameter of the specimen was 63.5 mm and height 80 mm. The soil is mixed with 10 percent of water amounts of the total sample and then compacted in three equal layers by a tamping road to obtain 60% relative density (Figure 3-18).

3.8 Experimental Program

In Padma bank pure fine sand, pure silt and sand-silt mixture at different percents of deposit were found by a Japanese consulting company in different layers (some samples were extruded in BUET Geotechnical Lab for some investigation). They collected undisturbed soil samples for investigation, based on Padma Bridge construction. Some pictures of the undisturbed sand and silt are shown in Figure 3-3 as evident. Here the silt specimen was collected from 10 m depth and the sand at 27 m. Pure fine sand was also found within 10 m in another bore hole. Mainly in rainy season sandy soil deposit occurs and in winter season silty soil deposit occurs for the change of stream flow rate with season. The deposits of sand, sand-silt mixture at different percent and pure silt sample found naturally in different layers. Therefore the target is to investigate the behavior of sand-silt mixtures.

The relative density at the Jamuna Bridge (Figure 3-1) site was estimated based on the data of *SPT* and *CPT*. One of the typical data by Hight et al. [53] is shown in Figure 3-19, where it may be seen that the relative density takes values around 50 percent, but the majority data indicate values less than 65 percent. In the top 10 m the relative density near about 60 percent as in Figure 3-19. The studied sand and silt was collected from the top surface of Padma bank (see Figure 3-1). In the Geological Map of Bangladesh same type of soil is identify as in the both side of riverbed of Jamuna River (Jamuna Bridge site) and north side of the Padma River (Mawa, collected studied samples) (as in Section 3.2 and Figure 3-1). Based on Figure 3-1 and Figure

3-19 all tests have been done at 60 percent relative density of sand-silt mixtures with effective confining pressure 100 kPa.

The detailed program of experiments corresponding to all the approaches and parameter effects are presented in Table 3-4 and Table 3-5. The results of around 49 stress-controlled cyclic triaxial tests on specimens with different silt contents and over a wide range of parameters have been utilized in this study to check pore pressure bands prepared by Lee and Albaisa, Dash and Sitharam [55, 47] the pore pressure generation characteristics of sand–silt mixtures. Total 13 strain-controlled monotonic triaxial tests have been done on different percent of silt content on sand. The results of cyclic and monotonic triaxial tests have been used to see the cyclic and monotonic strength at increasing rate of silt content.

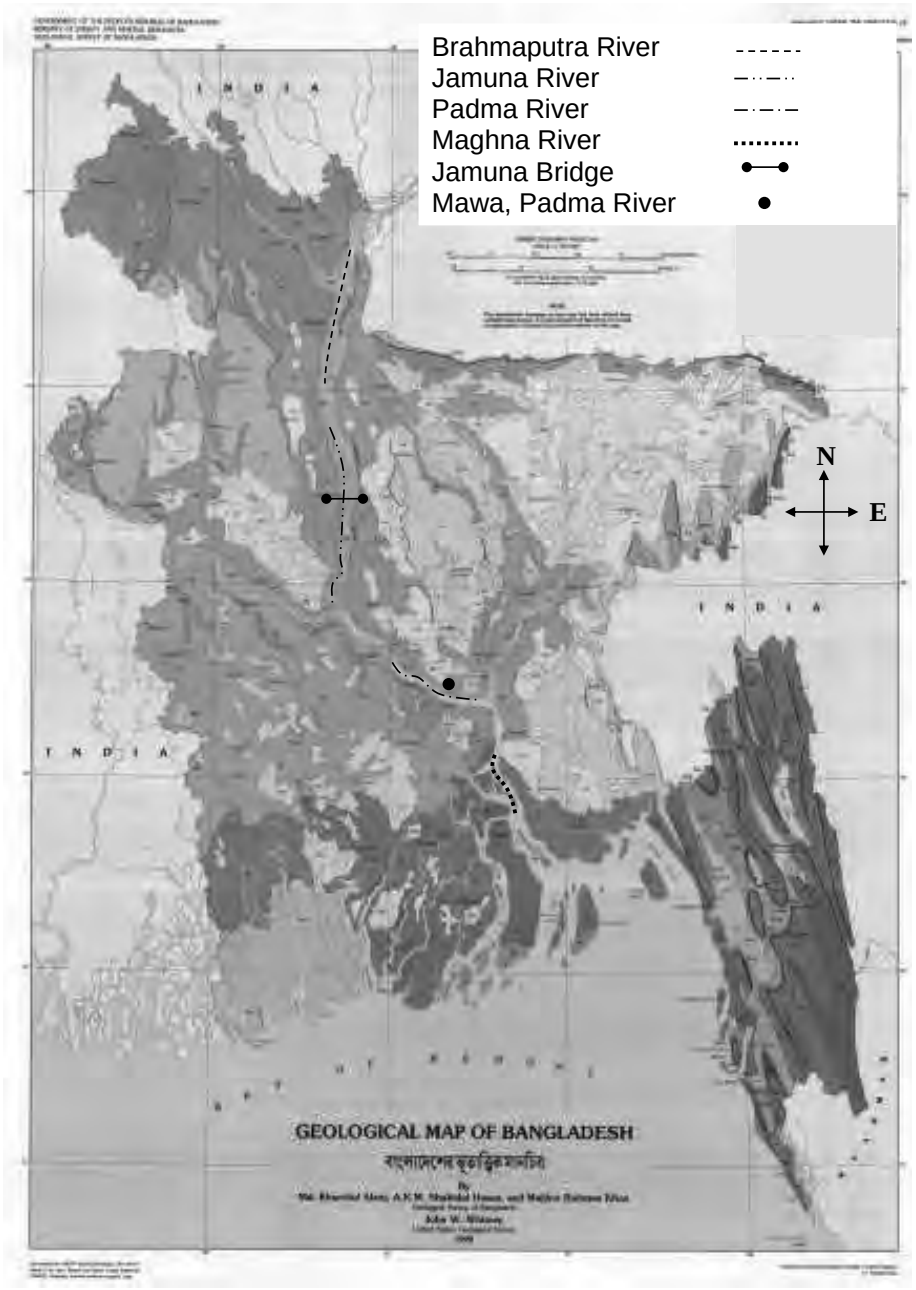

Figure 3-1. Geological map of Bangladesh [50].

(a)

(b)

Figure 3-2. Sample collection area (a) in dry season and (b) in rainy season.

(a)

(b)

Figure 3-3. Undisturbed sample (a) sand (b) silt.

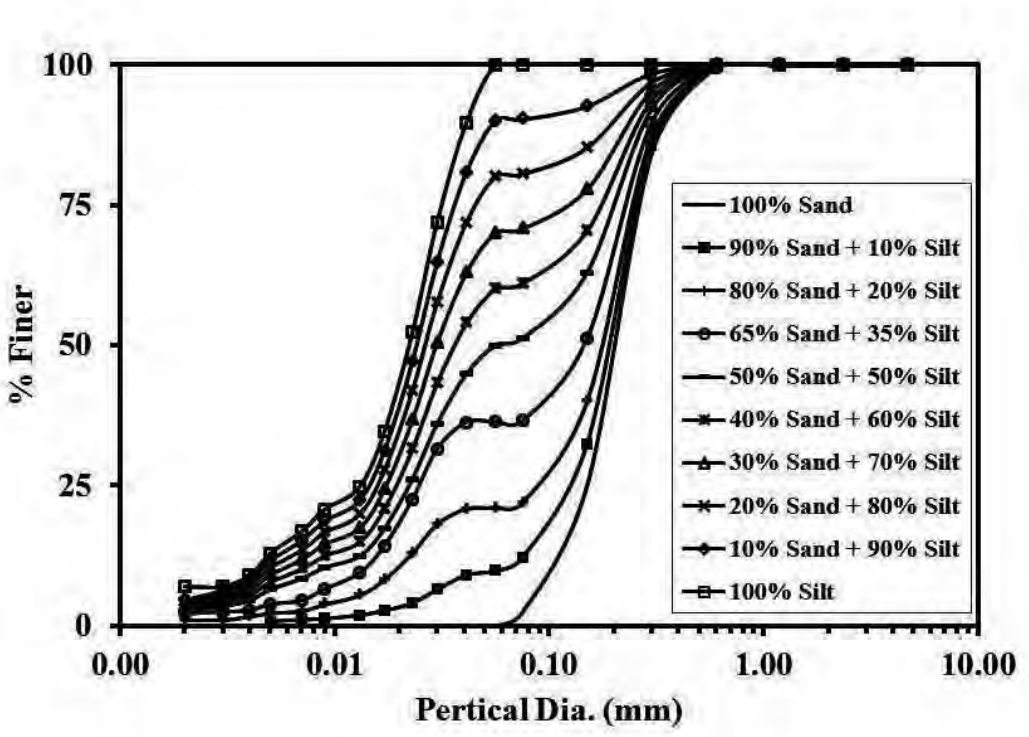

Figure 3-4. Particle size distribution curve.

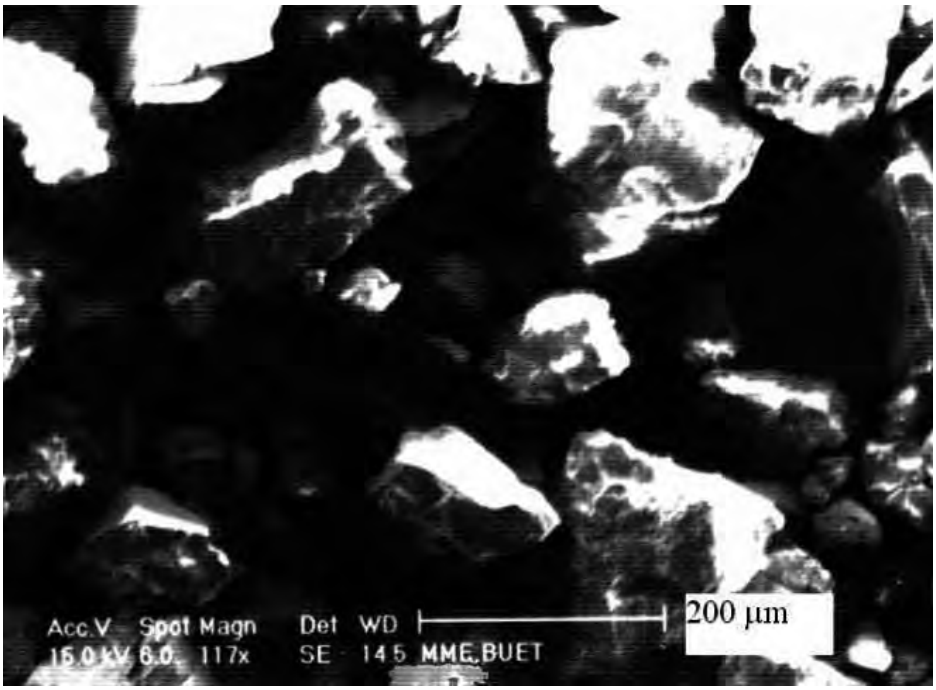

(a)

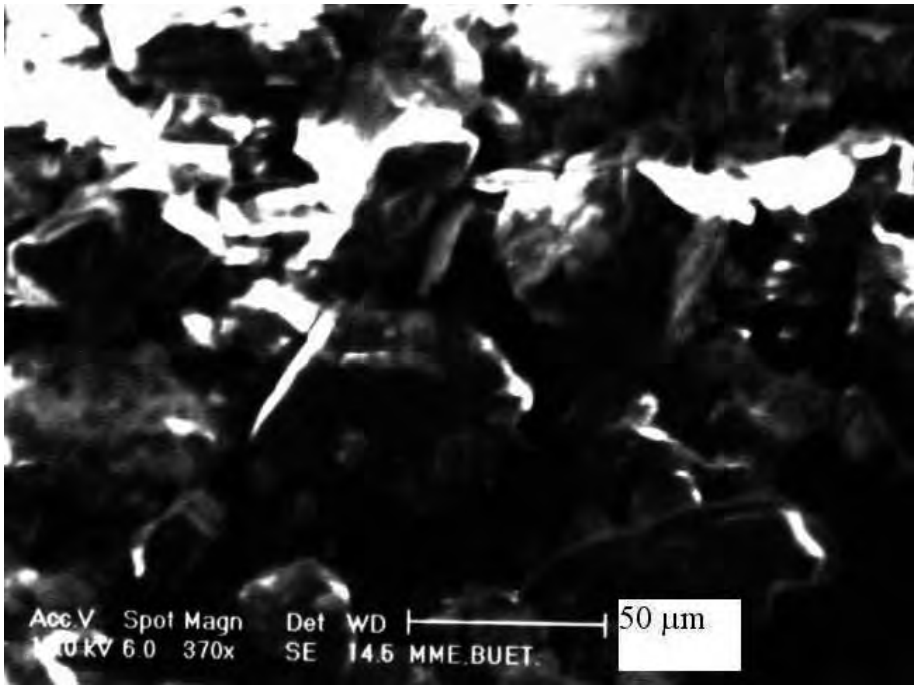

(b)

Figure 3-5. Electro microscopic view of (a) sand and (b) silt.

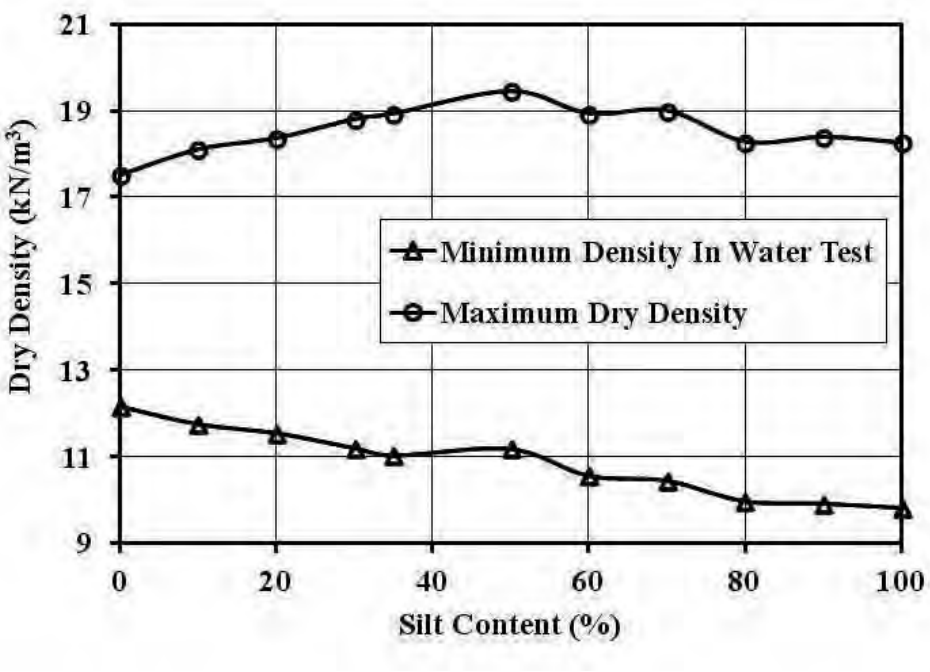

(a)

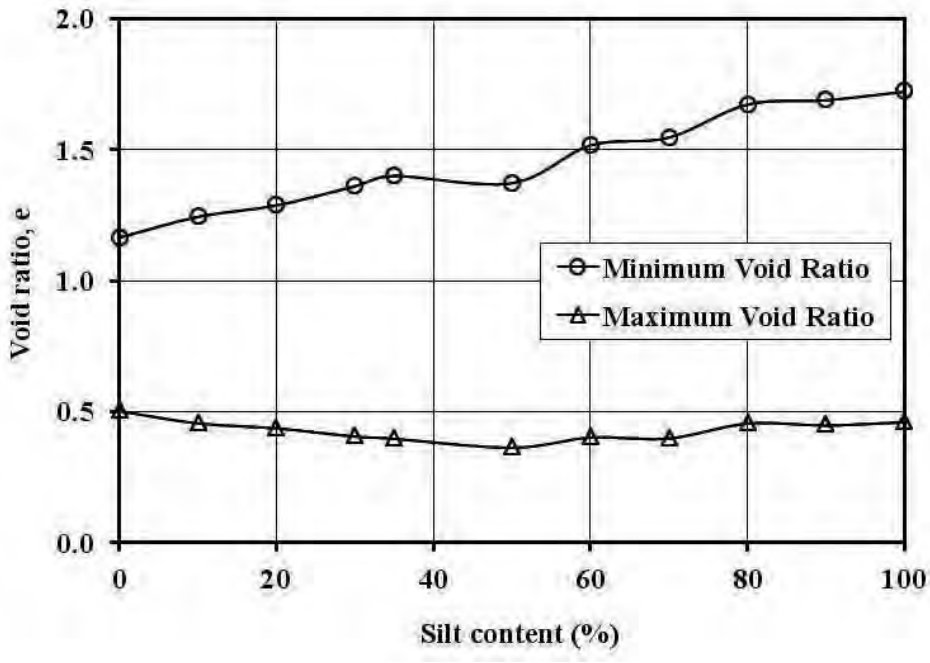

(b)

Figure 3-6. (a) Maximum and minimum density versus percent of silt content, (b) minimum and maximum void ratio versus percent of silt content.

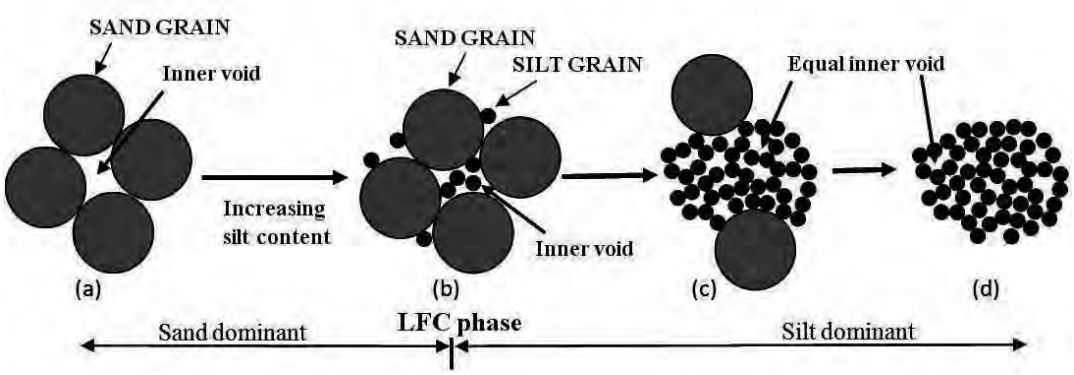

Figure 3-7. Schematic diagram demonstrating particle arrangement of sand-silt mixture with the variation of silt content.

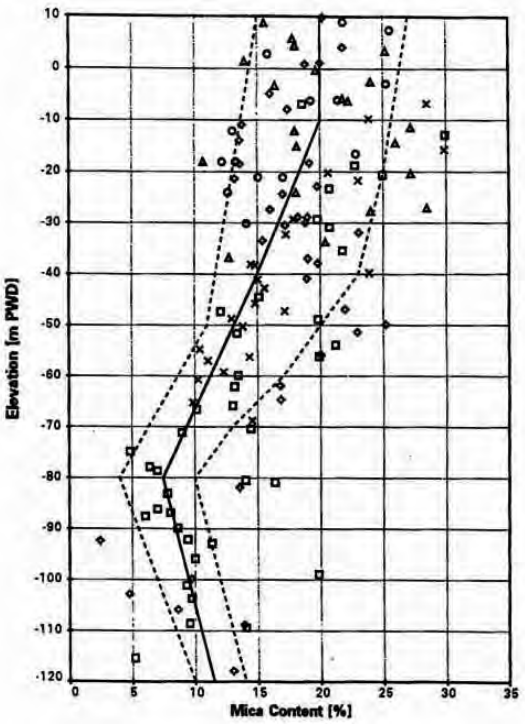

Figure 3-8. Distribution of mica content at sites of the Jamuna River [53].

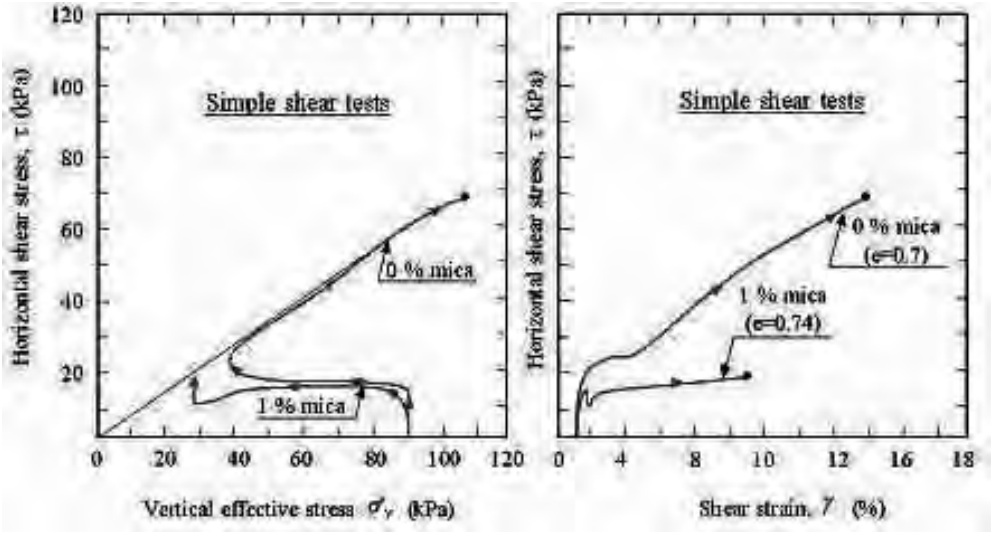

Figure 3-9. Effect of 1% mica on the undrained behaviour of sand in simple shear [53].

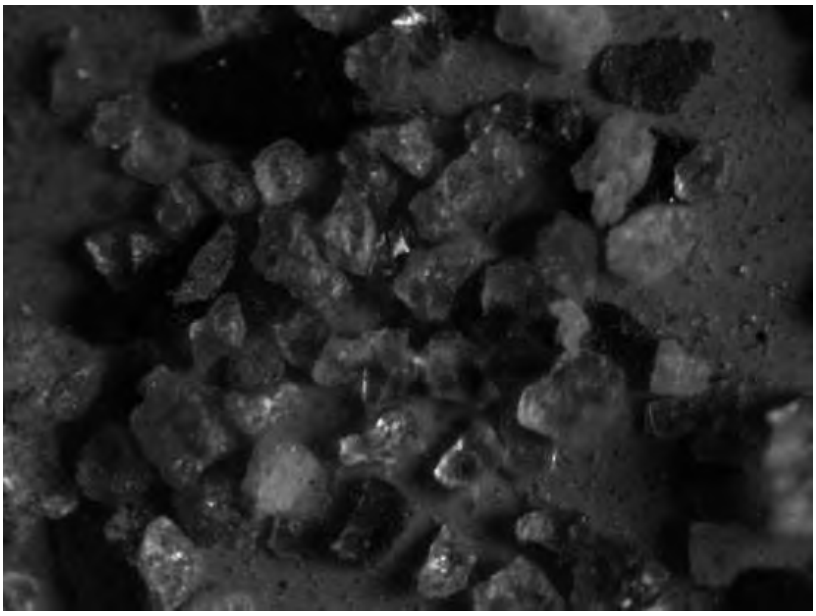

(a)

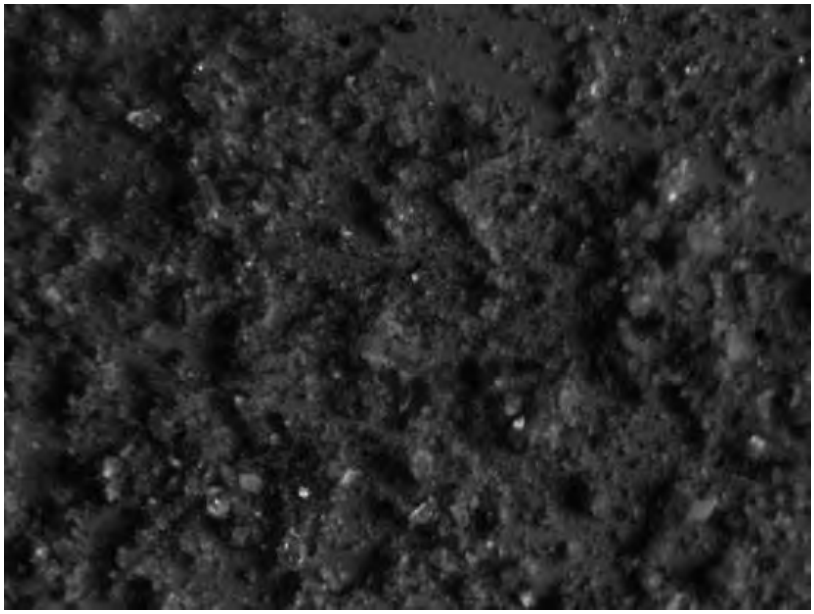

(b)

Figure 3-10. Stereo microscopic view of (a) sand and (b) silt at 40 times magnification.

(a)

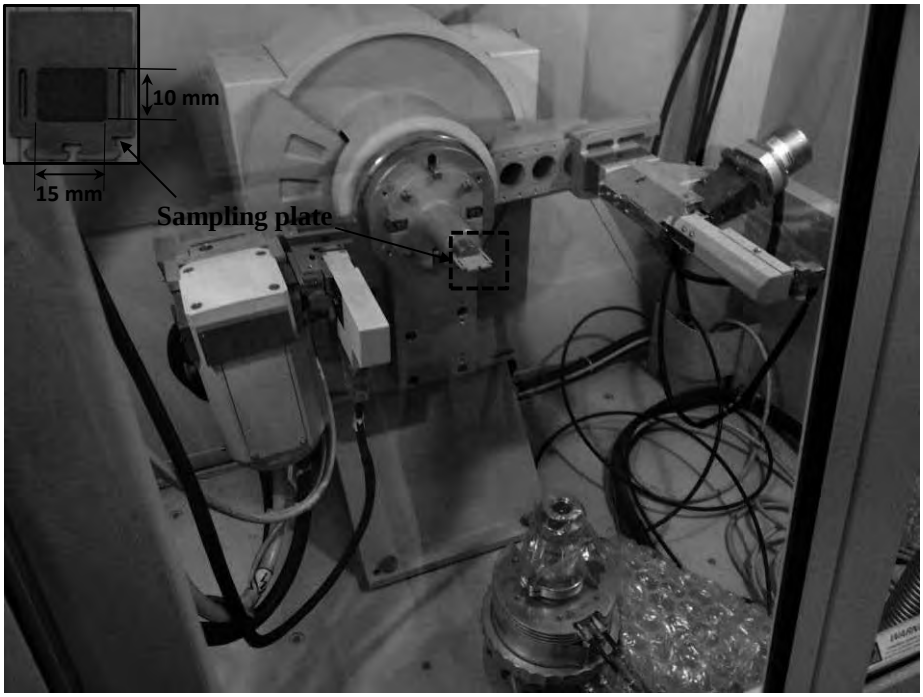

(b)

Figure 3-11. X-ray diffraction machine (a) full machine and (b) inside the machine, when the test was running.

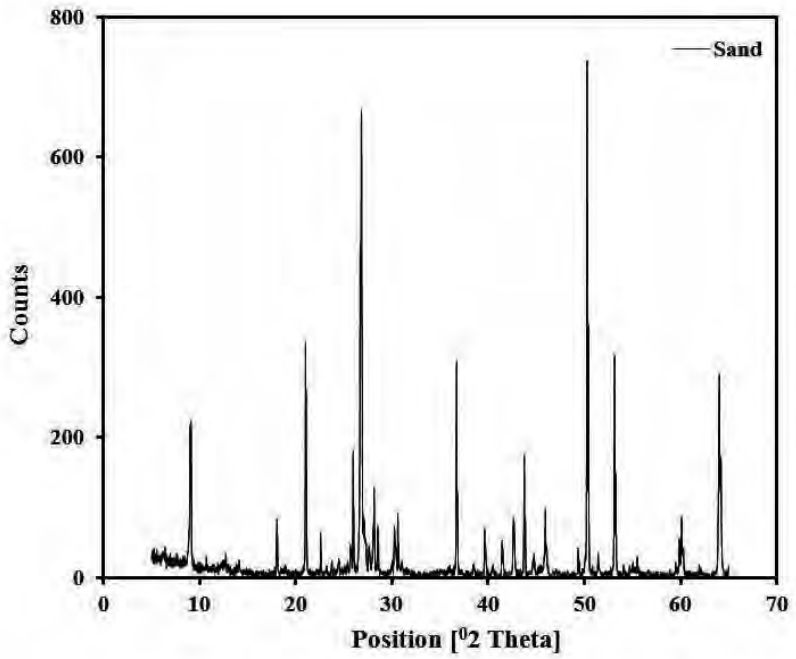

(a)

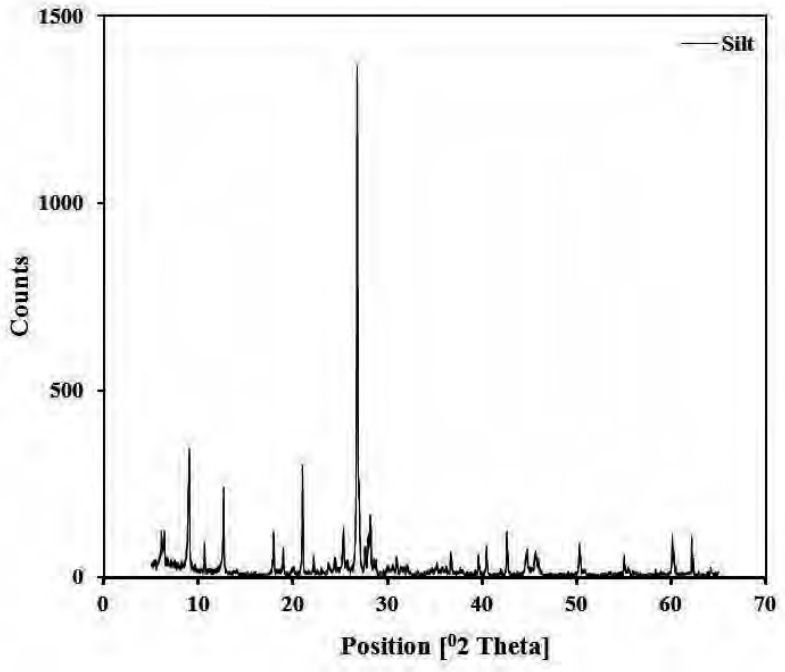

(b)

Figure 3-12. *X-RD* test result of (a) sand and (b) silt.

Figure 3-13. Sampling mold.

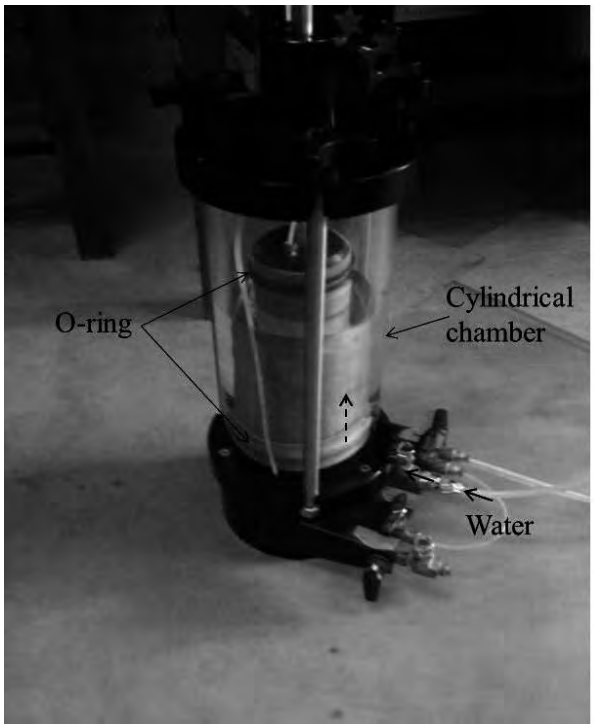

Figure 3-14. Plastic cylindrical chamber that was filling with water.

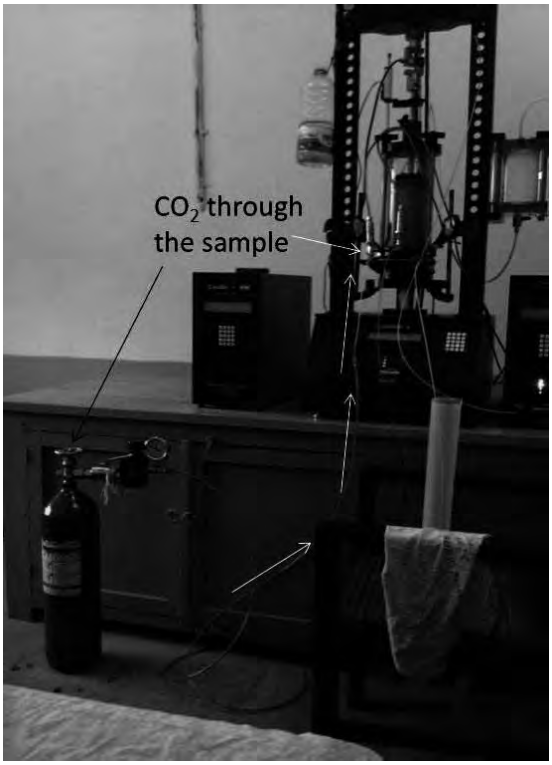

(a)

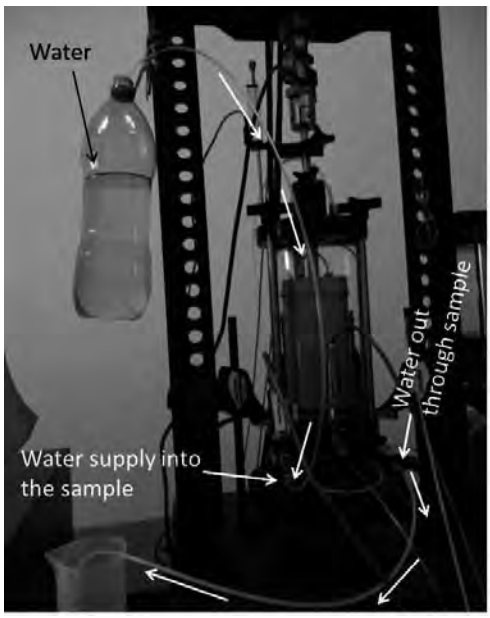

(b)

Figure 3-15. (a) Giving CO_2 on the specimen and (b) de-watering through specimen.

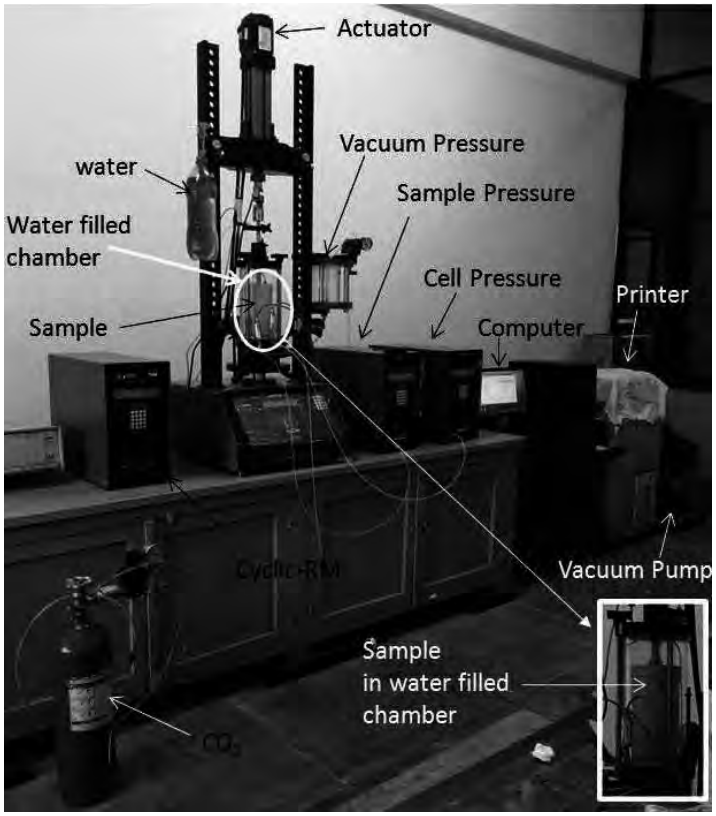

Figure 3-16. Triaxial system.

Figure 3-17. Air cushion before starting cyclic loading.

Figure 3-18. Permeability test by Falling Head method.

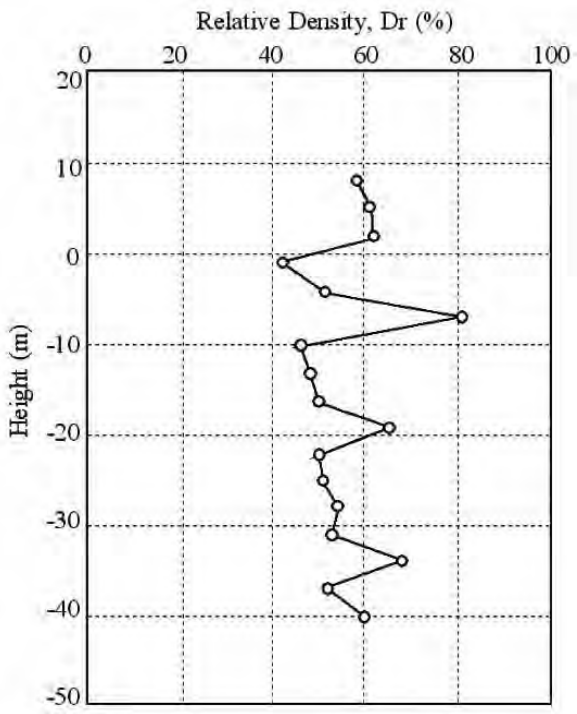

Figure 3-19. A typical profile of relative density at a site in Jamuna River [53].

Table 3-1. Quantitative *X-RD* test result.

	Compound name		**Percent (%) (By atomic weight)**	**Formula**
Sand	Quartz		81.10	SiO_2
	Albite		11.28	$Na(AlSi_3O_8)$
	Feldspar		7.62	$K_{0.5}Na_{0.5}AlSi_3O_8$
Silt	Quartz		66.62	SiO_2
	Chlorite		5.72	$(Mg, Al)_6(Si, Al)_4O_{10}(OH)_8$
	Albite		8.24	$Na(AlSi_3O_8)$
	Clay Mineral	Illite	8.11	$(K, H_3O)AlSiAlO_{10}(OH)_2$
	Mica	Muscovite	4.35	$KAl_2(AlSi_3O_{10})(OH)_2$
	Vermiculite		4.89	$Mg_{3.4}Si_{2.85}Al_{1.1}O_{10}(OH)_2(H_2O)_{3.7}$
	Magnesium iron silicate		2.07	$Mg_{0.8}Fe_{0.2}(SiF_6)(H_2O)_6$

Table 3-2. Index properties of component soils used in this study.

Soil type	**Sand**	**Silt**
USCS classification symbol	SP	ML
Mean grain size D_{50} (mm)	0.203	0.022
Uniformity coefficient (C_u)	2.25	5.82
Coefficient of gradation (C_z)	1.17	2.15
Specific gravity (G_s)	2.685	2.721
Minimum index density (kN/m^3)	9.814	12.167
Maximum index density (kN/m^3)	17.544	18.259
Minimum index void ratio (e_{min})	0.504	0.462
Maximum index void ratio (e_{max})	1.165	1.720
Liquid limit (%)	NP	38
Plastic limit (%)	ND	38
Plasticity index (%)	NP	NP

Table 3-3. Minimum and maximum density of various sand–silt mixtures used in this study.

Sample No.	**Soil Type**	**USCS classification Group Name**	**Minimum Density (kN/m^3)**	**Maximum Density (kN/m^3)**
1	Sand	SP	12.167	17.544
2	90% Sand + 10% Silt	SP	11.546	18.371
3	80% Sand + 20% Silt	SP	11.546	18.371
4	70% Sand + 30% Silt	SP	11.20	18.8
5	65% Sand + 35% Silt	SP	11.027	18.928
6	50% Sand + 50% Silt	SP	11.177	19.446
7	40% Sand + 60% Silt	ML	10.552	18.930
8	30% Sand + 70% Silt	ML	10.441	18.925
9	20% Sand + 80% Silt	Silt with sand	9.964	18.276
10	10% Sand + 90% Silt	Silt	9.913	18.259
11	Silt	Silt	9.814	18.259

Table 3-4. Programme of cyclic triaxial experiments.

Sample No.	**Soil Type**	***CSR***	σ_{3c} **(kPa)**	***Dr* (%)**	**Frequency *f* (Hz)**	**Total no. of expts**
1	Sand	0.20, 0.15, 0.12	100, 50	60, 30, 38	1	9
2	90% Sand + 10% Silt	0.10, 0.20	100	60	1	3
3	80% Sand + 20% Silt	0.15, 0.13, 0.10, 0.08	100	60	1	4
4	70% Sand + 30% Silt	0.12, 0.10, 0.08, 0.085	100	60, 30	1	5
5	65% Sand + 35% Silt	0.15, 0.10, 0.08, 0.05	100	60	1	6
6	50% Sand + 50% Silt	0.20, 0.10, 0.08	100	60	1	4
7	40% Sand + 60% Silt	0.13, 0.10, 0.08	100	60	1	3
8	30% Sand + 70% Silt	0.12, 0.10, 0.08, 0.085	100	60	1	4
9	20% Sand + 80% Silt	0.13, 0.01, 0.09, 0.08	100	60	1	4
10	10% Sand + 90% Silt	0.20, 0.10, 0.12, 0.09	100	60	1	4
11	Silt	0.20, 0.15, 0.12	100	60	1	7
Total test =						49

Table 3-5. Programme of monotonic triaxial experiments.

Sample No.	Soil Type	σ_{3c} (kPa)	D_r(%)	Total no. of experiments
1	Sand	100	60	1
2	10% Sand + 80% Silt	100	60	1
3	20% Sand + 80% Silt	100	60	1
4	30% Sand + 70% Silt	100	60	1
5	35% Sand + 65% Silt	100	60, 68	2
6	40% Sand + 60% Silt	100	60,68	2
7	10% Sand + 90% Silt	100	60,68,78	3
8	Silt	100	60, 83	2
Total test =				13

CHAPTER 4

CYCLIC TRIAXIAL TEST RESULT AND DISCUSSION

4.1 Introduction

To identify the effect of non-plastic silt on the cyclic behavior of sand-silt mixtures, total 49 stress-controlled cyclic triaxial stress-control tests have been done on sand-silt mixtures. These tests have been done on specimens of size 71 mm diameter and 142 mm height with frequency of 1 Hz. Specimens were prepared at a constant relative density and constant density approach. The effect of relative density, confining pressure as well as magnitude of cyclic loading was also studied. For a constant relative density (D_r = 60%) the effect of limiting silts content, pore pressure response and cyclic strength was observed. The rate of generation of excess pore water pressure with respect to cycles of loading was found to initially increase with increase in silt content till the limiting silts content and thereafter it reverses its trend when the specimens were tested at a constant relative density. The cyclic resistance behavior was observed to be just opposite to the pore pressure response. Permeability, *CRR* and Secant Shear Modulus decreased till Limiting Silts Content; after that they became constant with increasing silt content.

4.2 Test Result

The results of a typical cyclic triaxial test, performed on a specimen with 20% silt content prepared to a post consolidation relative density 60% and loaded at a cyclic stress ratio of 0.10, are presented in Figure 4-1. The constant load applied to the specimen till ±3% axial strain was developed as shown in Figure 4-1 (a). The employed actuator is a pneumatic device that is operated by air pressure. This is the reason why the cyclic load of 1 Hz frequency in Figure 4-1 could not achieve the prescribed amplitude when strain exceeded 3%. Use of lower frequency may solve the problem.

The corresponding axial strain induced on the specimen is presented in Figure 4-1 (b) against the cycles of loading. It is to be noted here that the specimen achieved the nearly 100% excess pore water pressure at the 9th cycle of uniform loading in the test for which the Figure 4-1 is presented. The pore water pressures generated in the

specimen as a result of the induced axial strains is presented in Figure 4-1 (c). It may be seen in these figures that the deviator stress remained unaltered till the end of the test. The axial strain development on the specimen remained very low at initial cycles of loading but it drastically increased towards the end. This drastic increase in axial strain started corresponding to around 80% excess pore water pressure generation. At this point stress state may touched the failure envelope. The effective stress path of the specimen is presented in Figure 4-1 (d) where the shear stress, $\tau = (\sigma_1' - \sigma_3')/2$ and normal stress, $\sigma' = (\sigma_1' + \sigma_3')/2$, where it can be seen that the specimen looses all its strength and stiffness corresponding to nearly 100% excess pore water pressure generation. Similar observation was made in all other tests. To identify the effective failure stress line, one strain controlled static triaxial test has been done at same relative density of 60% on specimen with 20% silt content. The angle of effective failure stress line is found to be 27^0, which is shown in Figure 4-1 (d). Again, a typical pore pressure response analysis is presented in Figure 4-1. The pore pressure response in specimens prepared to a constant post consolidation relative density 60% is presented in this Figure as per the method suggested by Lee and Albaisa, Dash and Sitharam [55, 47]. The peak excess pore water pressure ratio corresponding to various cycles of loading has been plotted in this Figure against the cycle ratio. Excess pore water ratio (R_u) is defined as the ratio of excess pore water pressure (u_{excess}) generated during a particular cycle of loading to the initial effective confining pressure (σ_{3c}). Similarly the peak pore pressure ratio is the maximum pore water pressure ratio at a particular cycle of loading. The cycle ratio (N/N_L) is defined as the ratio of cycle of loading (N) to the cycles of loading till 100% excess pore water pressure (i.e. the point of initial liquefaction) or ±3% axial strain is generated (N_L). It can be seen in Figure 4-2 that the peak pore pressures in sand-silt mixtures deviate the upper and lower bound values suggested by Lee and Albaisa [55] who performed stress controlled tests on Monterey sand specimens. However, peak pore pressures were consistent with lower and upper boundaries suggested by Dash and Sitharam [47] who performed stress controlled tests on Ahmedabad sand and Quarry dust as silt. This type of observation was observed for all the specimens with any silt content in this test program corresponding to any approach due to the presence of fines.

To determine the Cyclic Shear Strength or Cyclic Resistance Ratio (*CRR*) of a specimen of desired silt content and relative density corresponding to the concerned approach, a minimum of three cyclic tests were carried out at different Cyclic Stress Ratios (*CSR*) till the initial liquefaction (excess pore water pressure became equal to the initial consolidation stress, σ_{3c} or ±3% axial strain was reached as discussed earlier. Thereafter these cyclic stress ratios were plotted against the corresponding cycles to initial liquefaction (N_L) as shown in Figure 4-3 for a specimen with 80% silt content at post consolidation relative densities of 60%. *CRR* was determined as the *CSR* corresponding to liquefaction at 15 cycles.

4.3 Discussion

4.3.1 Constant dry density approach

Figure 4-4 illustrates the liquefaction susceptibility of sand-silt mixtures with varying percentage of non-plastic fines at a constant dry density of 13.6 kN/m^3 and *CSR*=0.10. As seen, the liquefaction potential is influenced by the non-plastic fines. This clearly indicates that the percentage of non-plastic fines in the sand samples has a significant effect on the liquefaction potential. It is seen that the liquefaction potential of the sand sample increases with increase of non-plastic fines up to 30% (till limiting silts content). However, with further increase in non-plastic fines (*FC*>30%) the liquefaction potential is found to be decreasing. This may be attributed due to the change in the sand matrix from sand controlled matrix to silt controlled matrix [56]. This result is in very good agreement with the experimental investigation of Dash and Sitharam, Sitharam et al. [47, 38]. The experimental results from the current study indicate that the threshold value (limiting value) of fine content is, approximately equal to 30% which is equal to the limiting fines content value calculated using Equation 3.1 [52].

4.3.2 Constant relative density approach

Initially the number of cycles required generating100% excess pore water pressure or ±3% axial strain in the specimens at a constant Cyclic Stress Ratio of 0.10 was studied and is presented in Figure 4-5. It is observed from this figure that the cycles of loading decreased till around the limiting silts content and beyond this point it remains more or less same with further increase in silt content till even pure silt [56]. This observation indicates that in constant relative density approach the cyclic

resistance decreases rapidly till around the limiting silts content and beyond limiting silts content it remains relatively same for all the silt contents till pure silt.

The peak pore pressure response as a function of cycles of loading is presented in Figure 4-6 where it was seen that the rate of generation of excess pore water pressure decreases rapidly till around the limiting silts content and finally it remains relatively same for all the silt contents till even pure silt thus justifying the cyclic resistance behaviour as described above. Figure 4-7 shows the variation of dry density of sand-silt mixture with silt content at constant relative density of 60%. After limiting silts content dry density decreases with increase of silt content. Therefore the variation of cyclic resistance with silt content cannot be attributed to dry density. The effect of fines in reducing the cyclic resistance despite an increase in dry density till the limiting silts content was found in line with Dash and Sitharam [47]. But it should be noted that Dash and Sitharam [47] have prepared the sample by the dry deposition method, where moist tamping method was used in this study. A comparison between materials used in this study and Dash and Sitharam [47] are given in Table 4.

Also the effect of fines can well be understood in keeping the cyclic resistance relatively same despite a decrease in dry density with increase in silt content beyond the limiting silts content because the presence of more fines in a specimen at a constant relative density resists the development of excess pore water pressure and this prevents the likely fall in cyclic resistance.

4.3.3 Effect of non-plastic silt on pore pressure generation

The data collected during the series of cyclic stress control triaxial tests to study the liquefaction potential of clean sand, silt and sand-silt mixtures with varying non-plastic silt content were used to understand in detail the development of excess pore water pressure in the sand samples. The effect of amplitude of cyclic shear strain, relative density, confining pressure, percentage of non-plastic fines and the number of loading cycles are presented here.

Figure 4-8 illustrate the relationship between the pore pressure ratio and number of loading cycles for 20% sand and 80% silt at different *CSR* values subjected to initial liquefaction. It is evident from Figure 4-8 that the development of pore pressure ratio

is a function of *CSR* and number of cycles. Pore pressure ratio increases with increase in *CSR*. For low amplitude of *CSR* (0.08), the pore pressure ratio develops gradually with number of cycles and for higher *CSR* (0.13) the pore pressure ratio develops suddenly within a few cycles.

Figure 4-9 illustrates the effect of relative density on pore pressure generation with number of loading cycles at *CSR* 0.10. It is clearly seen from this Figure that as the relative density increases there is decrease in the rate of build up of pore pressure, which signifies the influence of relative density on the generation of pore water pressure. Dash and Sitharam [47] also reported similar behaviour on Ahemedabad sand Quarry dust (silt) from stress controlled cyclic tests results.

Figure 4-10 shows the effect of non-plastic silt content on the pore pressure generation with number of loading cycles for a constant dry density of 13.6 kN/m^3 at 1Hz frequency under an effective confining pressure of 100kPa. It has been observed that pore pressure ratio increases with increase in percentage of non-plastic fines (*FC*<30%). With further increase in non-plastic fines (*FC*>30%) excess pore pressure ratio decreased. In addition, number of cycles for initial liquefaction decreases with increase in the percentage of non-plastic fines content (*FC*<30%). However, with further increase in the non-plastic fines (*FC*>30%) the number of cycles for initial liquefaction has been found to increase. This clearly indicates that for non-plastic fine content greater than 30%, there is a change in the matrix of the sand from sand controlled matrix to silt controlled matrix. As fine content dominates it prevents the building up of pore pressure thus in influences the potential for liquefaction.

4.3.4 Effect of non-plastic silt on permeability

According to the definition of limiting fines content after LFC the soil specimens behave as silt, for experimental evidence, permeability test by falling head method on sand-silt mixtures have been performed at a D_r=60%. Figure 4-11 shows the variation of permeability with silt content. For increasing silt content the permeability deceasing till *LFC*, after *LFC* the permeability become constant with silt content [56]. That means concept of limiting silts content worked well in permeability. This is the reason why liquefaction resistance decreases with the increase of silt content upto *LFC* and remain constant thereafter (as in Figure 4-5). After *LFC* permeability remain

constant at same relative density which proves that after *LFC* the inner void of fine particles remain almost same.

4.3.5 Effect of non-plastic silt on cyclic resistance ratio

Cyclic Resistance Ratio (*CRR*) of sand-silt mixture of desired silt content and relative density 60%, were determined as *CSR* at which liquefaction occurred for 15 cycles of loading. Figure 4-12 shows the variation of *CRR* with silt content. Up to *LFC, CRR* decreased, after that *CRR* remained constant. Concept of *LFC* worked for *CRR* well [56].

4.3.6 Effect of non-plastic silt on shear modulus

Secant shear modulus was determined at 2nd cycle. The target was to determine secant shear modulus at 2nd cycle for all specimens so that it can be compared. Figure 4-13 shows the secant shear modulus variation with silt content. It was observed that with increasing silt content the Secant Shear Modulus (G_{sec}) is decreasing till *LFC* = 30%, after *LFC* G_{sec} became constant [56]. Examining data it is found that shear strain ranges from 0.0009 to 0.0033 as shown in Figure 4-13. So, the change of secant shear modulus was due to strain level change.

4.4 Combined Pore Pressure Analysis

Lee and Albaisa [55] carried out around 22 numbers of cyclic triaxial tests with varying parameters on Monterey river sand to study the pore pressure response of sand. They varied the relative density from around 30% to 100%, confining pressure from 103 kPa to 1378 kPa and cyclic stress ratio from 0.24 to 0.38. They reported that all the curves generated by plotting the pore pressure response against the corresponding cycle ratio fall within a relatively narrow band. Results obtained from this investigation were utilized to study the limitations of this band when non-plastic fines are added to sand. For this purpose, peak pore pressures generated in sand-silt mixture specimens prepared at various relative densities corresponding to all the approaches over a wide range of parameters is presented as a function of cycle ratio (N/N_L) in Figure 4-14 to assess the upper and lower bound values as suggested by Lee and Albaisa [55]. Dash and Sitharam [47] carried out around 289 numbers of cyclic triaxial tests with varying parameters on Ahmedabad sand to study the pore pressure response of sand. They varied the relative density from around 14 to 91%, confining

pressure from 50kPa to 200 kPa and Cyclic Stress Ratio from 0.092 to 0.205 and proposed a new pore pressure band for sand–silt mixtures in line with Lee and Albaisa [55].

A check of pore pressure band for sand-silt mixtures have been presented in Figure 4-14. The peak pore pressures generated in sand-silt mixture specimens prepared at relative density 60% and confining pressure 100kPa and cyclic stress ratio from 0.08 to 0.20 are presented in the Figure 4-14. The pore pressure band proposed by Dash and Sitharam [47] was found to be valid for sand-silt mixtures used in this study.

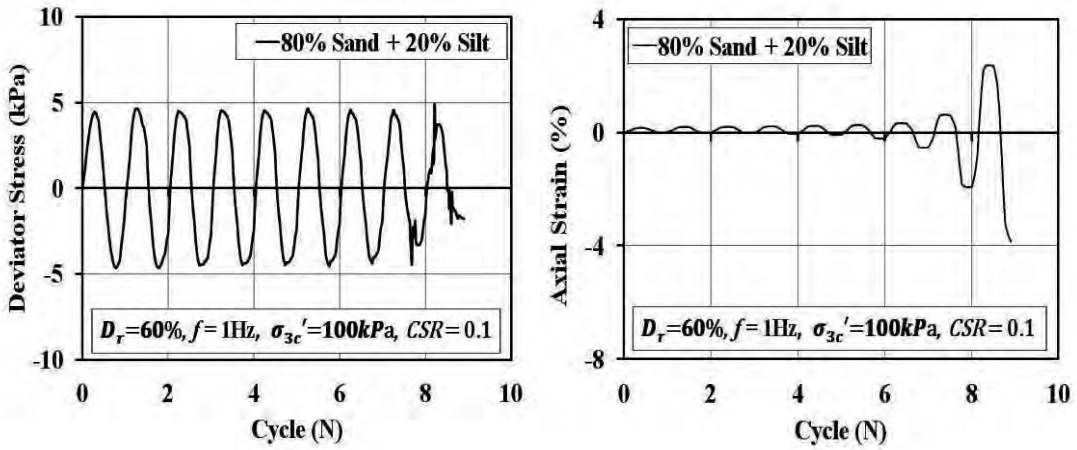

(a) (b)

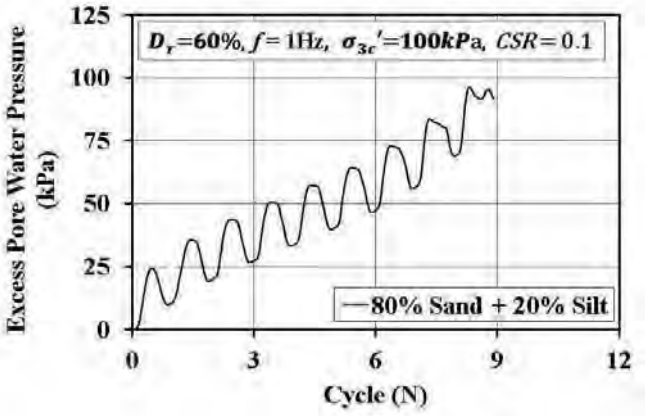

(c)

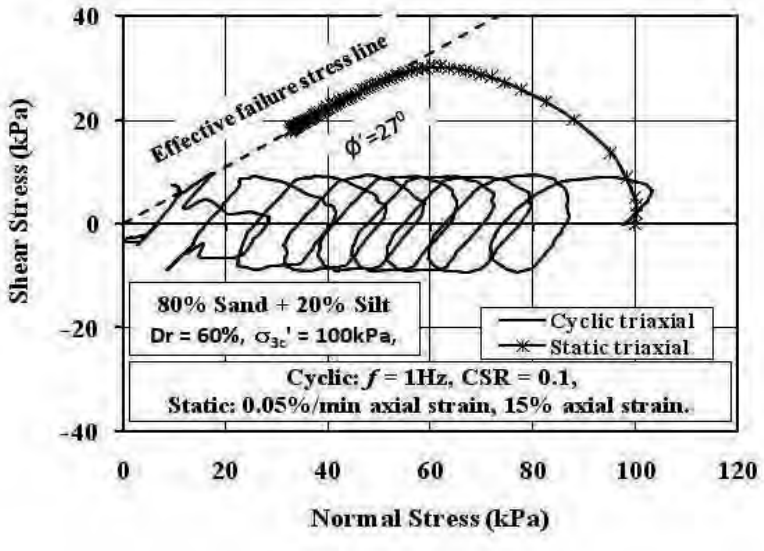

(d)

Figure 4-1. (a) Deviator stress versus cycles of loading till ±3% axial strain; (b) axial strain versus cycles of loading till ±3% axial strain; (c) pore water pressure response till ±3% axial strain; (d) effective stress path.

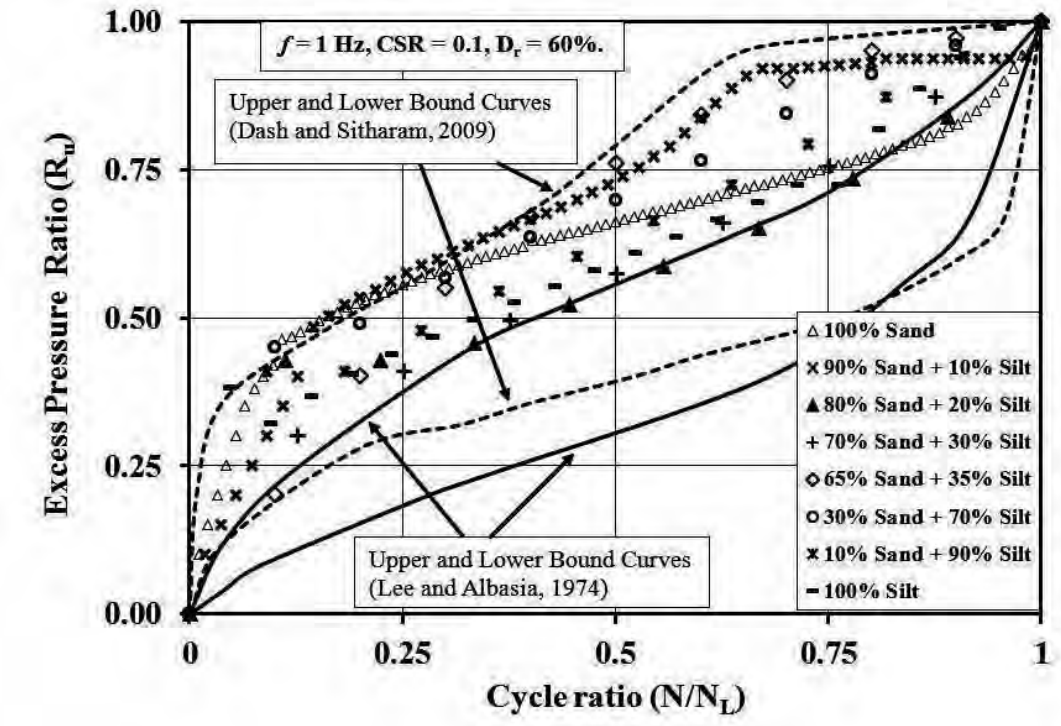

Figure 4-2. Typical pore pressure response against cycle ratio as per the method suggested by Lee and Albaisa; Dash and Sitharam [53, 47] [56].

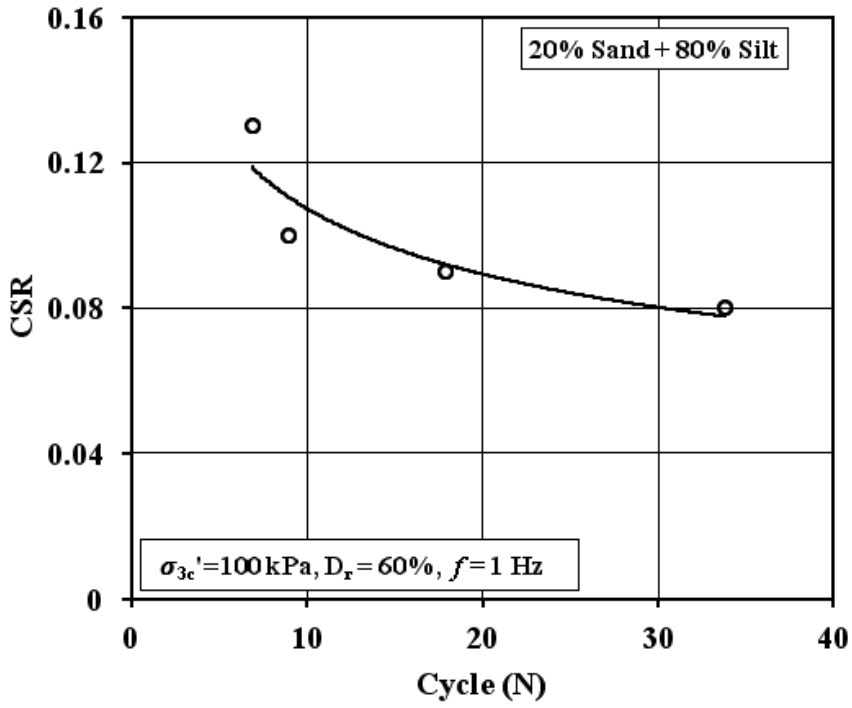

Figure 4-3. Typical Cyclic Stress Ratio curve.

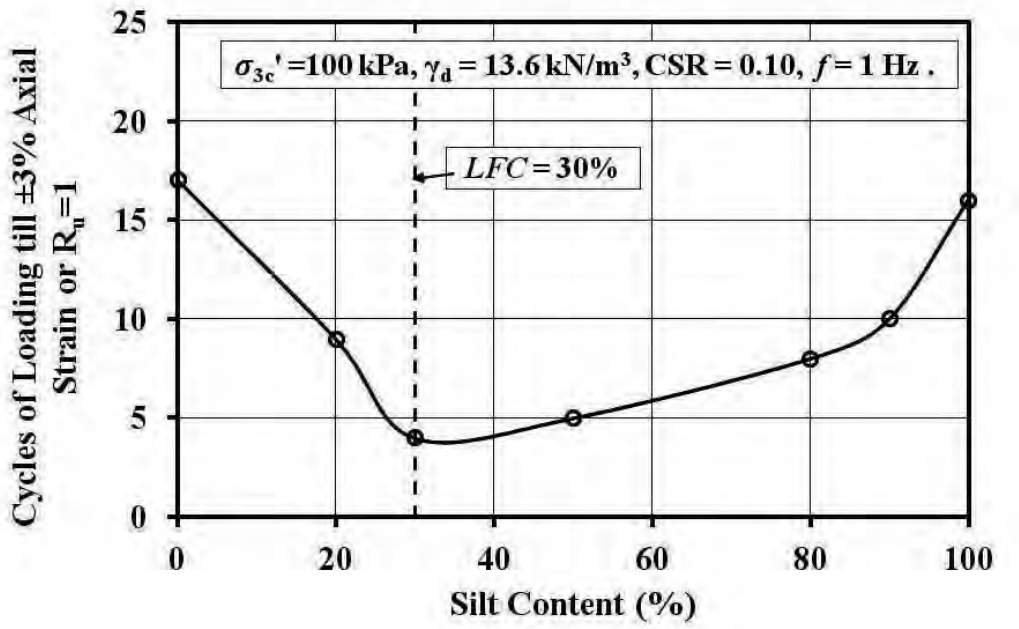

Figure 4-4. Cycles of loading till initial liquefaction with different percentage of non-plastic silt at *CSR* = 0.10 and constant dry density = 13.6 kN/m^3 [56].

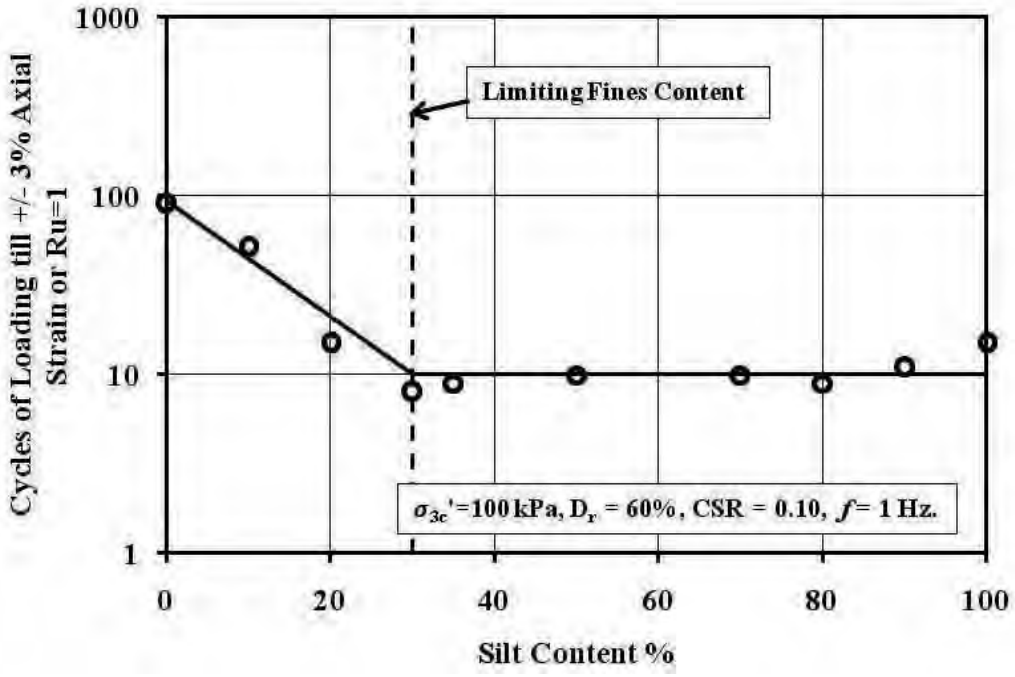

Figure 4-5. Cycles of loading till R_u = 1 or ±3% axial strain versus silt content at D_r = 60% and *CSR* = 0.10 [56].

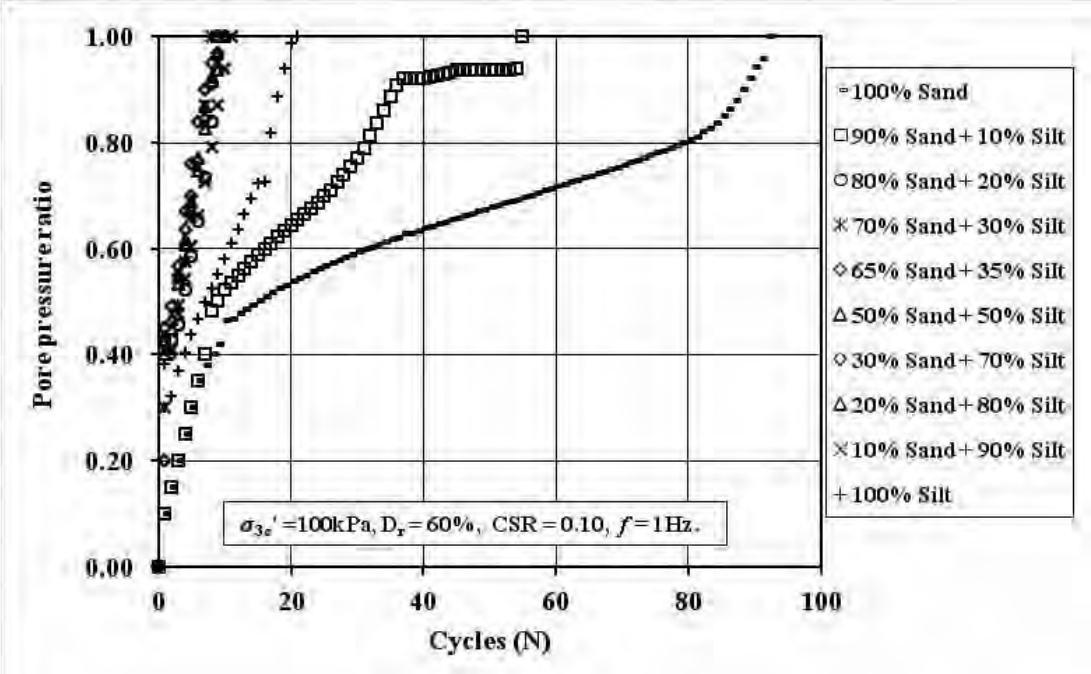

Figure 4-6. Pore pressure response as a function of cycles of loading at D_r = 60%.

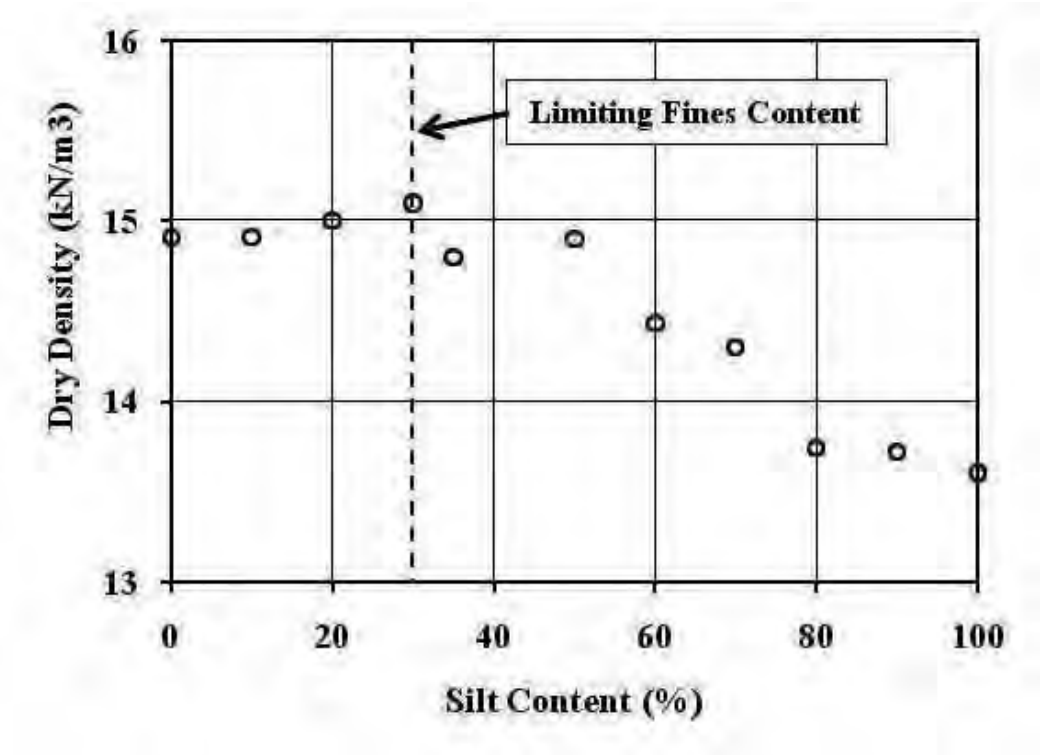

Figure 4-7. Variation of dry density with silt content at D_r=60%.

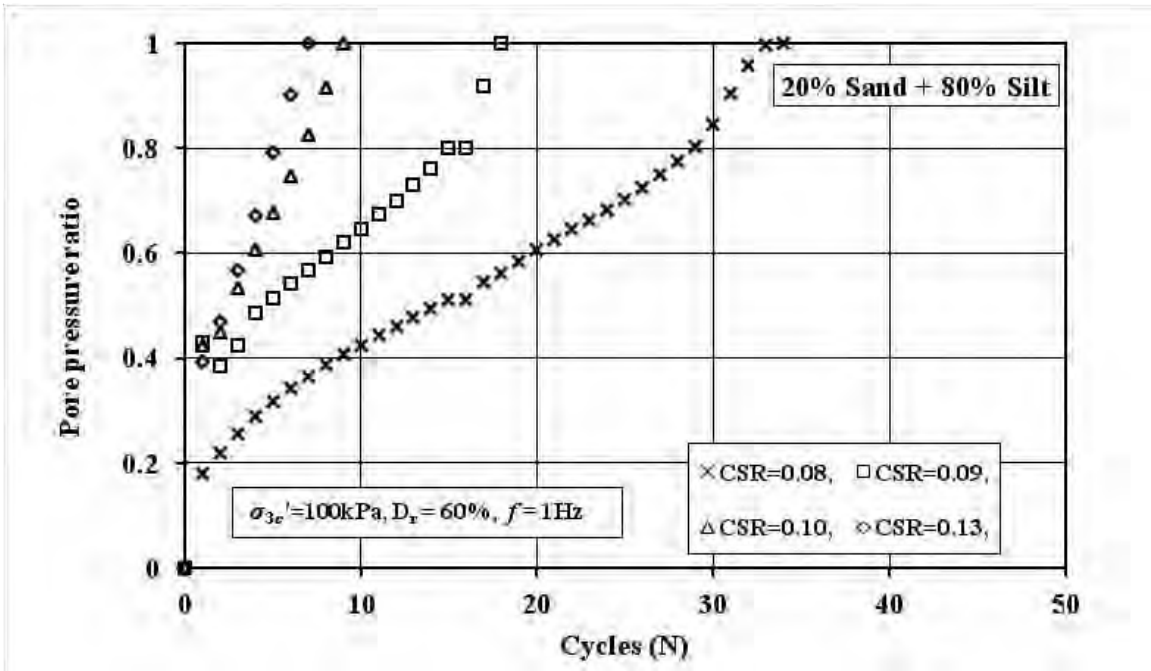

Figure 4-8. Relationship between pore water pressure ratio and number of cycle for 80% Silt, D_r=60% at various Cyclic Stress Ratio.

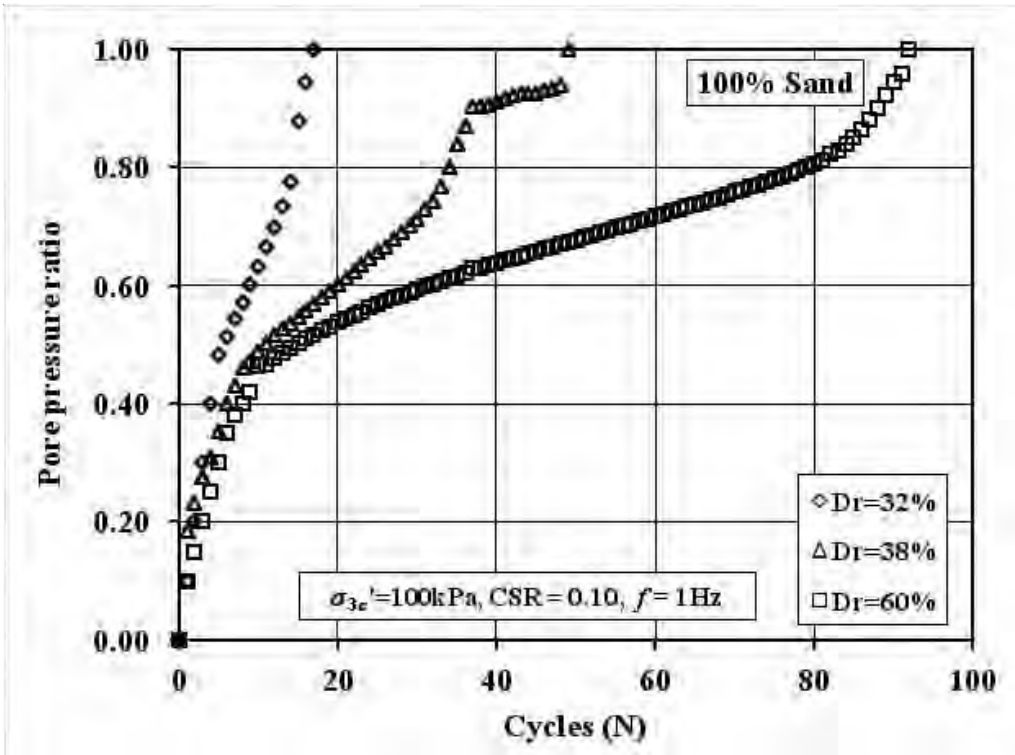

Figure 4-9. Effect of relative density on the pore pressure generation with number of loading cycles for clean sand at *CSR* = 0.10.

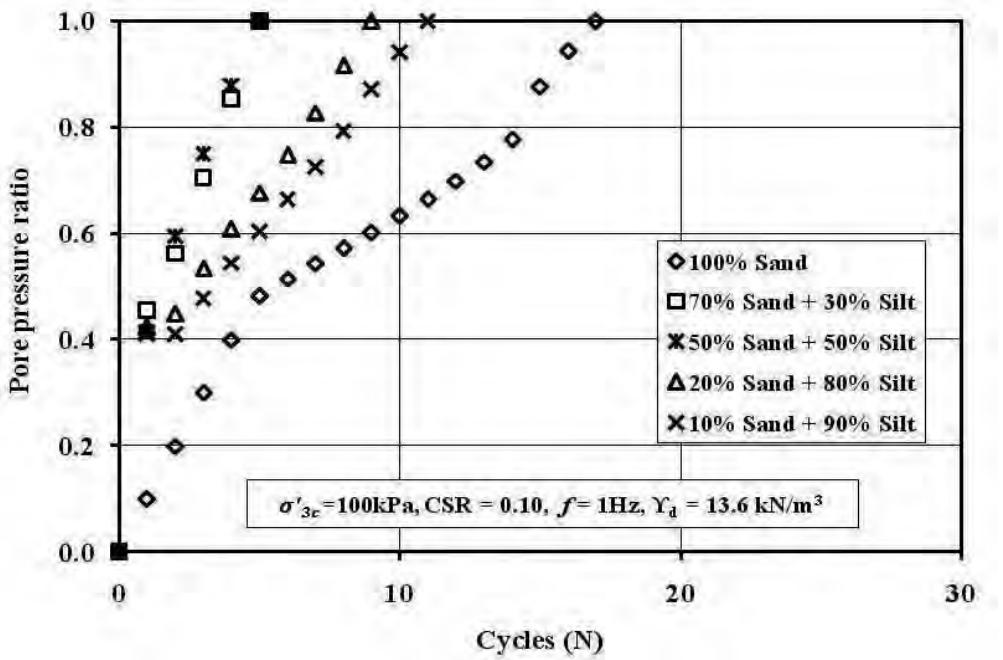

Figure 4-10. Variation of pore pressure ratio with numbers of cycles for different percentages of non-plastic fines.

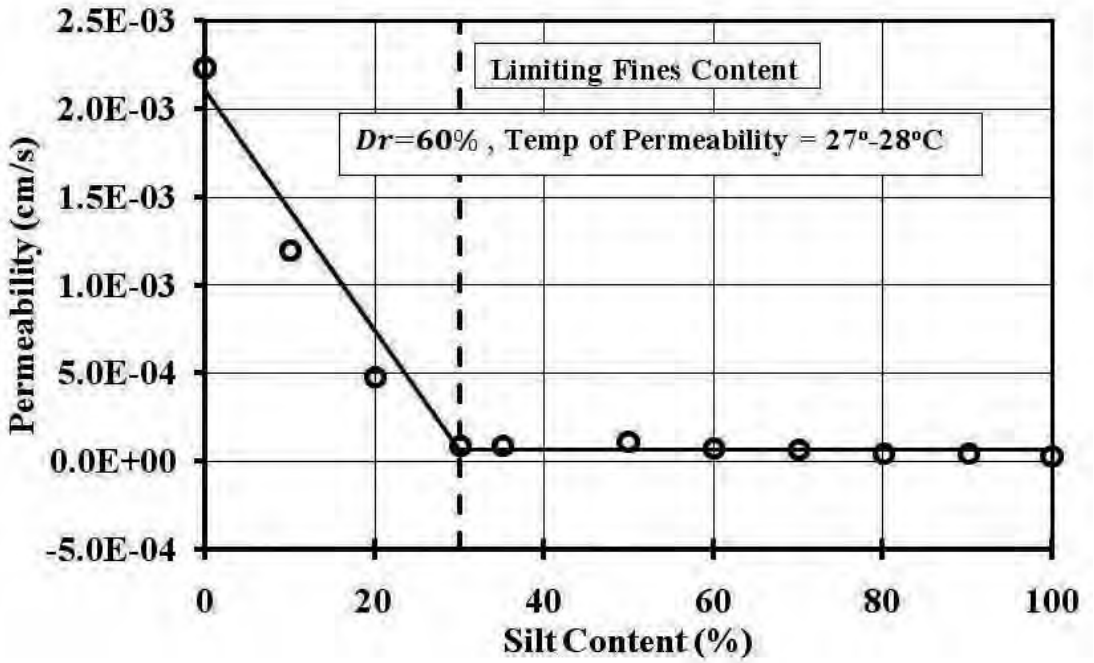

Figure 4-11. Variation of permeability with silt content [57].

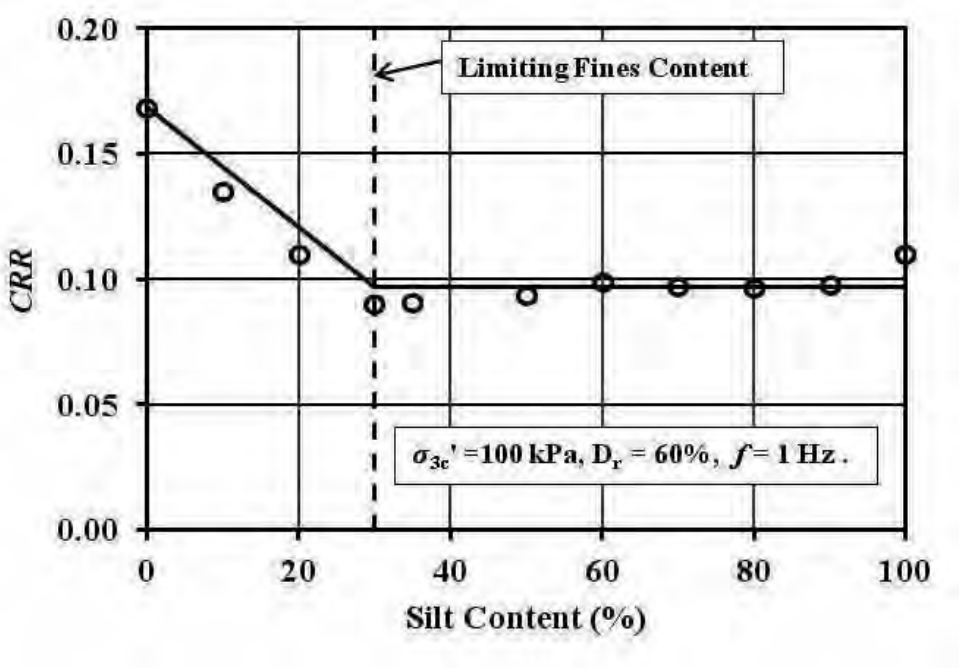

Figure 4-12. Variation of Cyclic Resistant Ratio (*CRR*) with silt content [56].

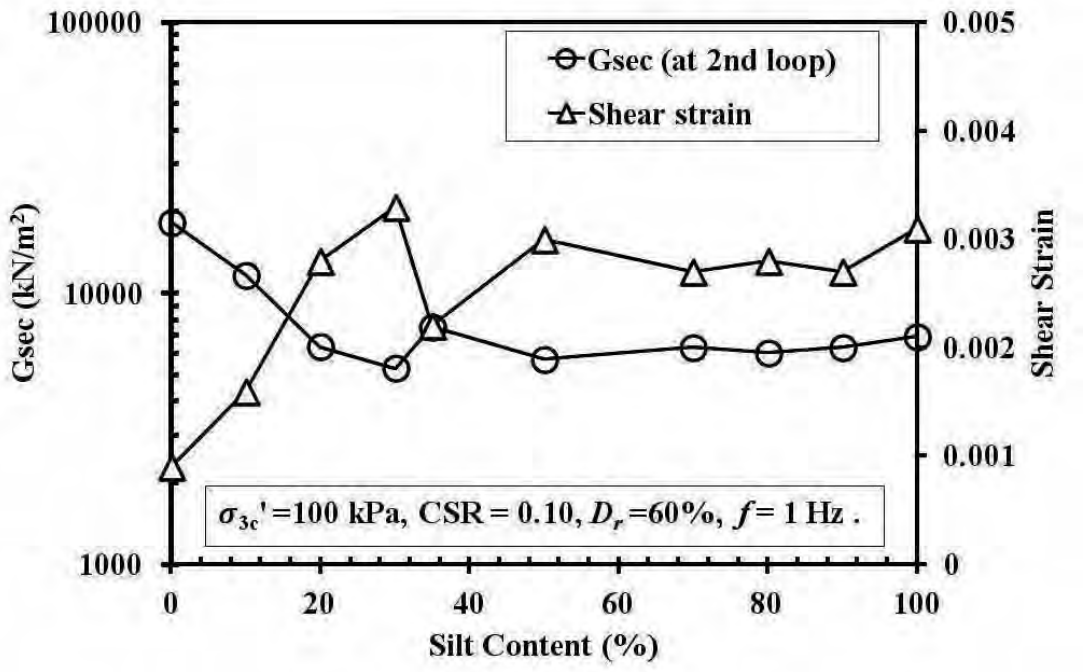

Figure 4-13. Variation of Secant Shear Modulus at 2nd cycle with silt content [56].

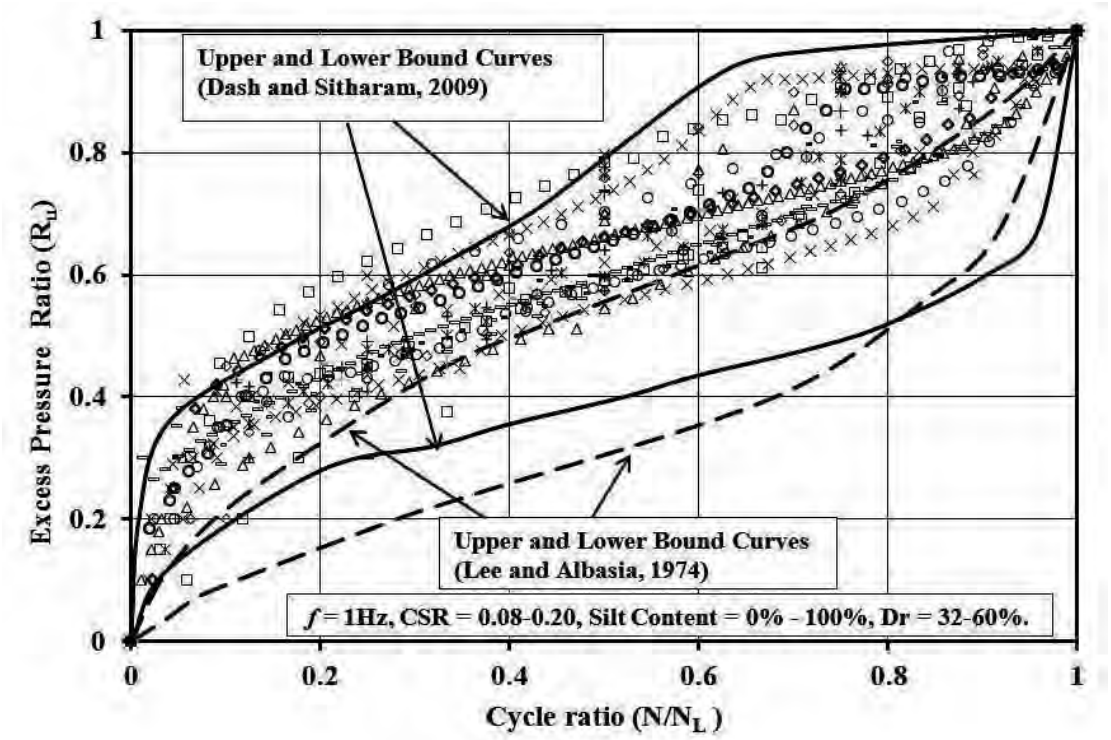

Figure 4-14. Maximum and minimum peak pore generation in sand and silt mixture specimens over a wide range of parameters and compared with Lee and Albasia; Dash and Sitharam [53, 47] [56].

CHAPTER 5

MONOTONIC TRIAXIAL TEST AND DISCUSSION

5.1 General

To assess the behavior of sand-silt mixture strain-controlled monotonic triaxial tests were carried out on sand-silt mixture of specimen size 71 mm diameter and 142 mm height with varying silt content at various relative densities at same isotropic effective confining pressure of 100 kPa. Concept of Limiting Fines Content (*LFC*) was verified by these undrained monotonic triaxial tests. Peak Shear strength of sand-silt mixture decreases with increase of silt content up to *LFC.* Peak Shear strength remains almost constant at silt content greater than *LFC*. At constant gross void ratio approach the undrained peak shear strength decreases with increase in silt content till *LFC* and for further increment of silt content the peak shear strength increases with increase in silt.

5.2 Monotonic Triaxial Test Result

To explain the behavior of non-plastic silt due to static undrained loading, Yamamuro and Lade [5] illustrarted five types of bahavior, namely, static liqufaction, temporary liquefaction, stable, temporary instability and instability as shown in Figure 5-1. On the other hand, Ishihara [57] illustrated five types of behavior, namely, 'Flow types or Contractive' and 'Non-flow type or Dilative' as shown in Figure 5-2.

The result of a series of undrained triaxial strain control compression tests on 90% silt with relative densities of 60, 68 and 78 percent are percent are presented in Figure 5-3 to Figure 5-5. Figure 5-3 shows the stress-strain response, where the deviator stress or stress different is assigned to the vertical axial ($\sigma_1 - \sigma_{3c}$) and axial strain is plotted on the horizontal axis. Again Figure 5-4 shows the excess pore pressure verses axial strain graph. It can be seen in this Figure 5-3 (a) that at relative density 60 percent the strain-softening behavior is exhibited in the sample with a drop in deviator stress (at 1.2% axial strain) accompanied by a 15 percent axial strain. In such a state is called "strain-softening" types and referred to as being "contractive or flow type" as in Figure 5-2.

On the other hand, when the density is large, as 68 and 78 percent relative density, the sample tends to exhibit strain-hardening behavior where the deviator stress always goes up with increasing shear strain. The dense samples in such a state is called "strain-hardening" type and referred to as begin "dilative or non-flow type". It is also observed from Figure 5-3 shows that, the rate of increasing deviator stress with respect to strain is higher for the dense specimen. The rate of increasing stress as well as the attainment of peak strength in all specimens is also can be verified from the development of excess positive (+u) or negative pore water pressure (-u) on the specimens as presented in Figure 5-4, using the equation $\sigma = \sigma'_{3c} + (\pm u)$. Where, σ'_{3c} is the effective confining pressure and σ is the normal stress. For expressing the soil behavior Rees [57], proposed increasing excess pore water pressure is contractive behavior and decreasing is dilative behavior (Figure 5-4). Figure 5-5 shows the undrained effective stress paths in which $p' = (\sigma'_1 + \sigma'_{3c})/2$ and $q = (\sigma'_1 - \sigma'_{3c})/2$. At 60 percent relative density q is decreasing with increasing p', after reaching a peak point (denoted as q_{max}) start decreasing. This type of behavior is entitled "static liquefaction" as in Figure 5-1. The static liquefaction is characterized by large pore pressure development that results in zero stress different at low axial strain [55]. In this regard near about 100 percent pore water pressure developed at 60 percent relative density (Figure 5-4). The result of 68 and 78 percent relative density are exhibiting the dilative behavior to Figure 5-2. These types of behavior are termed "stable" by Yamamuro and Lee [55]. In the Figure 5-4 at 68 and 78 percent relative density initially the pore water pressure reached at peak point at 2.6 and 0.7 percent axial strain respectively, later the excess pore water pressure decreased. This excess pore water pressure changing point is denoted as phase transformation point as in Figure 5-2, which can be clearly point out in Figure 5-5. 78 percent relative density got the phase transformation point rapidly, because of peak position excess pore water pressure at lower axial strain (0.7%).

The undrained monotonic compression test results were utilized for the purpose of determining the peak undrained shear strength of a specimen. The monotonic peak undrained shear strength of a specimen was determined from the plot of deviator stress verses the axial strain from a particular test which corresponds to the maximum deviator stress built up on a specimen within 15 percent axial strain.

5.3 Discussion

5.3.1 Constant relative density method

A total of 10 undrained monotonic triaxial tests were conducted on sand-silt mixture at a pre consolidation relative density of 60 percent. The stress-strain response of these specimens is presented in Figure 5-6. Figure 5-6 illustrates two types of stress-strain behavior obtained from undrained shear tests on saturated and consolidated samples of sand-silt mixture at 60% relative density. When it is clean sand, the sample tends to exhibit strain-hardening behavior where the shear stress always goes up with increasing shear strain. The clean sand in such a state is referred to as being dilative or non-flow type behavior [57]. The sand-silt mixture with 10 percent silt content also exhibited the similar type of behavior but showing less shear strength than that of clean sand. When the silt content with sand-silt mixture is equal or greater than 20 percent, the strain-softening behavior is exhibited by the sample with a drop in shear stress at very low strain of around less than 2 percent (Figure 5-6(b)). Figure 5-6(b) shows the stress-strain curves of specimens with silt content equal to or more than 20%. These specimens showed flow type behavior [57].

The excess pore pressure response of sand-silt mixture with 0 to 100 percent silt content is shown in Figure 5-7. For clean sand and 10 percent silt content, initially the excess pore water pressure increases at very low strain of around less than 2 percent axial strain and for further axial strain it decreases. The rate of decreasing is higher for clean sand than 10 percent silt content specimen. It means that increasing fines content decreases the rate of generation of negative excess pore water pressure. For sand-silt mixture with 20 to 100 percent silt content the excess pore pressure increases with increasing axial strain up to 5 to 10 percent axial strain, after that it becomes steady. Excess pore pressure generation was found to be maximum for sand-silt mixture with 35 percent silt content. Excess pore water pressure generation was less for other silt contents whether it is more than 35% or less than 35%. At 60 percent relative density all the specimen of sand-silt mixture except clean sand and 10% silt showed contractive behavior irrespective of silt content, since positive excess pore pressure generated for all specimens. Figure 5-7 (b) showed the excess pore pressure generation for specimens having silt content equal to or greater than 20 percent.

In Figure 5-8 the effective stress path of sand-silt mixture at 60 percent relative density is shown. The effective failure line and effective failure angle are also shown in this figure. The effective stress paths of clean sand and 10 percent silt content sample are seen to deviate upwards from phase transformation point increasing the strength which is termed as stable behavior [5]. For 20 percent silt content, the stress path neither decreased nor increased after touching the failure line. The samples having 20 to 100 percent silt content (see Figure 5-8 (b)), clearly showed the contractive behavior which is static liquefaction [5]. The average angle of effective failure line is calculated about 31 degrees.

The undrained monotonic peak shear strength verses percent of silt content is plotted in Figure 5-9. The shear strength is decreasing with increasing silt content till *LFC,* after *LFC* the strength becomes constant up to pure silt content [59]. After consolidation it was found that the relative density increased near about 1 percent for each of the specimens at 60 percent pre-consolidation relative density.

5.3.2 Constant gross void ratio method

The gross void ratio (e) of a soil specimen is the ratio of the volume of void (V_V) to the soil solids (V_S) in the specimen. It can be expressed as a function of dry density (γ_d) of the soil specimen and the specific gravity (G_S) of the soil solids.

$$\gamma_d = \frac{G_S \gamma_w}{1+e} \Rightarrow e = \frac{G_S \gamma_w}{\gamma_d} - 1 = \frac{G_S \gamma_w}{W_d/V} - 1 \ldots\ldots\ldots\ldots\ldots\ldots\ldots\ldots (5.1)$$

Specific gravity of sand and silt was 2.69 and 2.72 respectively. So the specific gravity of sand-silt mixture will vary from 2.69 to 2.72 depending on the silt content. As the unit weight of water (γ_w) is generally considered to be unique at normal temperature, the void ratio (e) solely depends on the dry weight (W_d) of the soil used and the volume (V) of the specimen, if the variation of specific gravity of sand-silt mixture is neglected.

In Figure 5-10 undrained monotonic peak shear strength verses silt content graph is shown. In this case total 7 undrained monotonic triaxial tests have been done at different percent of silt content at constant gross void ratio 0.76. It can be seen that the

undrained monotonic peak strength parameter initially decreases and reaches a minimum value at the *LFC* and thereafter the trend is reverse with further increase in silt content (Figure 5-10) [59].

5.3.3 Effect of dry density on relative density

The effect of relative density and fine content on undrained peak shear strength of sand-silt mixture is shown in Figure 5-9. Reduction of the monotonic peak shear strength with increasing silt content can be observed in this figure. Despite the fact that the dry density continue to increase a little bit with increase in silt content up to the point of *LFC* (Figure 5-11) for greater than 30 percent silt content dry density decreases with increase in silt content.

Before *LFC* the dry density is increasing with increase of silt content in a specimen, affects the peak shear strength (decreasing) as in Figure 5-9 and Figure 5-11. After the *LFC* dry density is decreasing with increase of silt content but the peak shear strength remains constant till pure silt. It is well understood that the peak shear strength is not depend on dry density for a constant relative density approach. Now what is the reason of this type of behavior is explained in the next section (see section 5.3.4).

5.3.4 Response at shear

In 60 percent relative density dilative and contractive both behavior is found for different percent of sand-silt mixture. So, a probable structure of sand-silt mixture at a constant relative density (60 percent) is presented in Figure 5-12. When clean sand is mixed with increasing amount of nonplastic silts, the minimum and maximum void ratios as well as the range of void ratios change. This particle structure is shown in the schematic drawings in Figure 5-12.

Figure 5-12 (i) shows a soil structure before shearing. The void spaces between the large grains are relatively unoccupied in Figure 5-12 (i) (a). In Figure 5-12 (i) (a) the large sand grains, which will make up the load bearing skeleton, are held slightly apart by smaller silt particle near the contact points in Figure 5-12 (i) (b). In Figure 5-12 (i) (c) the large grain particles become significantly displaced from each other by the large quantity of smaller particles until only small particles are present at Figure 5-12 (i) (d). Figure 5-12 (ii) shows the applied shear and normal effective stress in this

stable particle structure. In the shearing phase inner slip occur among the sand particles (Figure 5-12 (ii) (a)) which procreate inner voids. As it is undrained triaxial test whereupon a large amount of suction pressure (excess negative pore water pressure) develop in the voids which increases effective mean pressure. Consequently the peak shear stress is higher ($\sigma = \sigma'_{3c} + (\pm u)$) for clean sand. Due to the presence of more silt (increment of silt) in sand specimen the sand particles are separated by the smaller silt particles as in Figure 5-12 (i) (b). At the shearing phase the silt particles are forced into the void spaces by the sand particles as in Figure 5-12 (ii) (b). At that the inner voids (as in clean sand, explained above) are filled with fine silt particles which reduce the suction pressure (excess negative pore water pressure). So, the excess negative pore of 10 percent silt content specimen is less than that of the clean sand as in Figure 5-7 (a). Negative excess pore pressure decrease with increase in silt content and reach to positive excess pore pressure (after *LFC*) at 60 percent relative density (see Figure 5-7 (a)).In silt dominant part (silt content greater than 30 percent) the dry density decreases with increase in silt content (Figure 5-11), but the inner voids (void among silt particles only) are equal as in Figure 5-12 (i) (c) and (d).The reason of these same responses in Figure 5-9 is the equal inner void after *LFC*.

After 30 percent silt content (*LFC*) the sand particles become completely separated by fine silt particles, so these sand-silt mixtures exhibits silt dominant behavior. The silt particles make their own packing where some voids develop (inner void). Those inner voids are equal for all percent of silt content greater than 30. This is the reason why beyond *LFC* sand-silt mixture shows constant peak shear strength.

Permeability test by falling head method has been done to verify the equal inner void after *LFC*. In Figure 5-13 permeability test result of sand-silt mixtures is shown. Increasing silt content decreases the permeability till *LFC*, for further increment of silt content, permeability remains constant till pure silt. Consequently it is apparent that after *LFC* the inner voids are equal for all specimens.

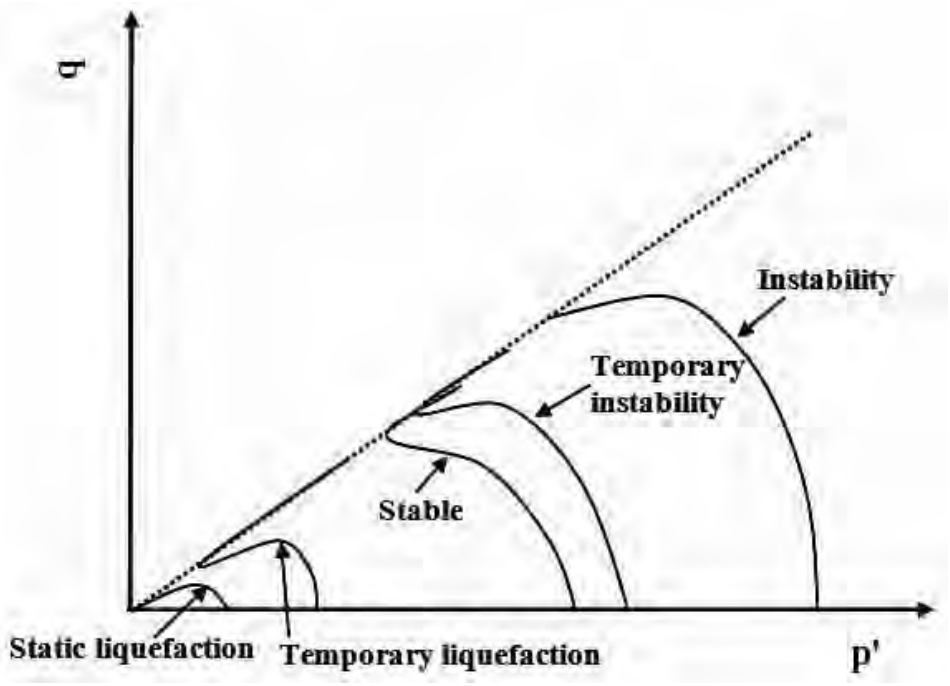

Figure 5-1. Static liquefaction, temporary liquefaction, temporary in stability and in stability behavior [5].

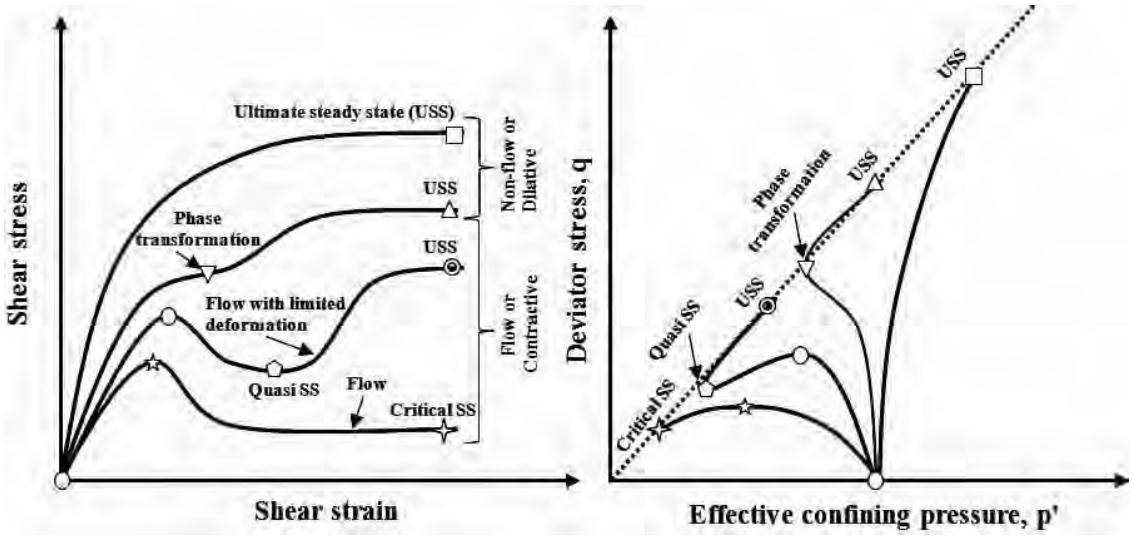

Figure 5-2. Classification of undrained behavior of sandy soils based on contractiveness and diativeness [57].

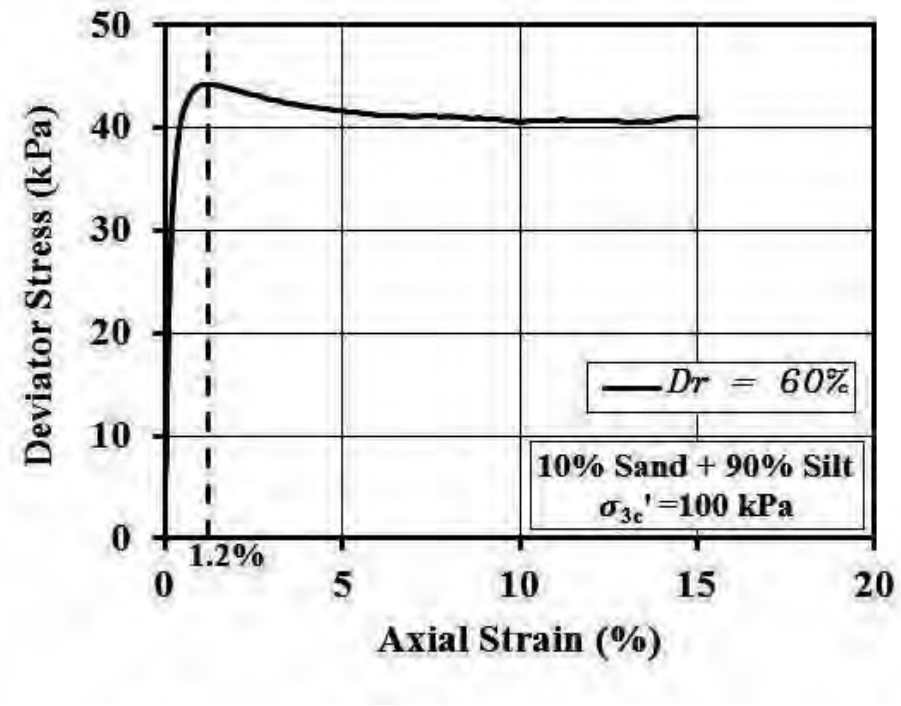

(a)

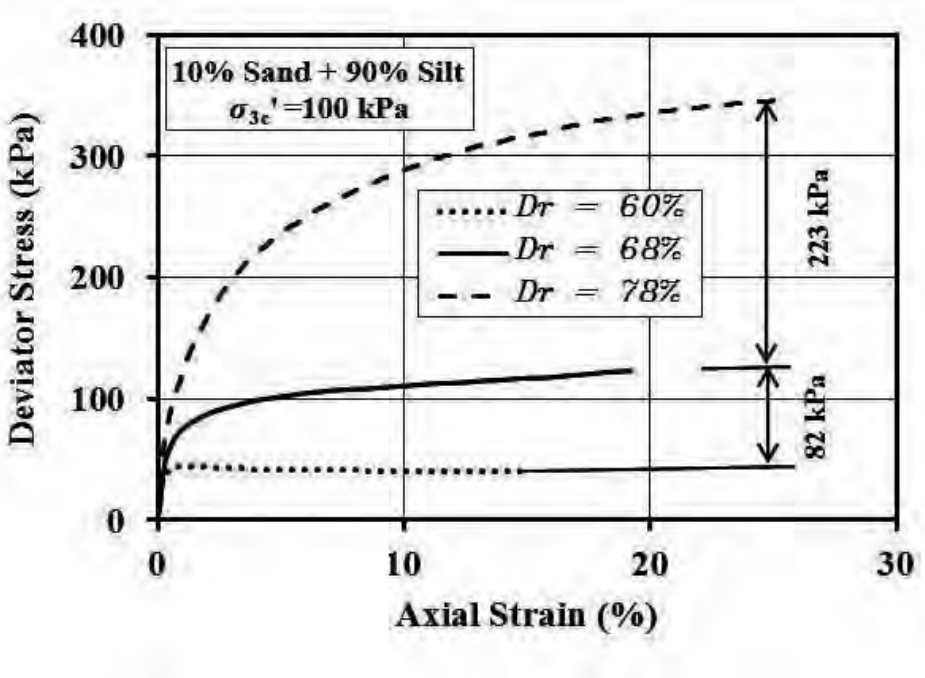

(b)

Figure 5-3. Stress-strain relationship, (a) at 60 percent relative density and (b) at different relative density.

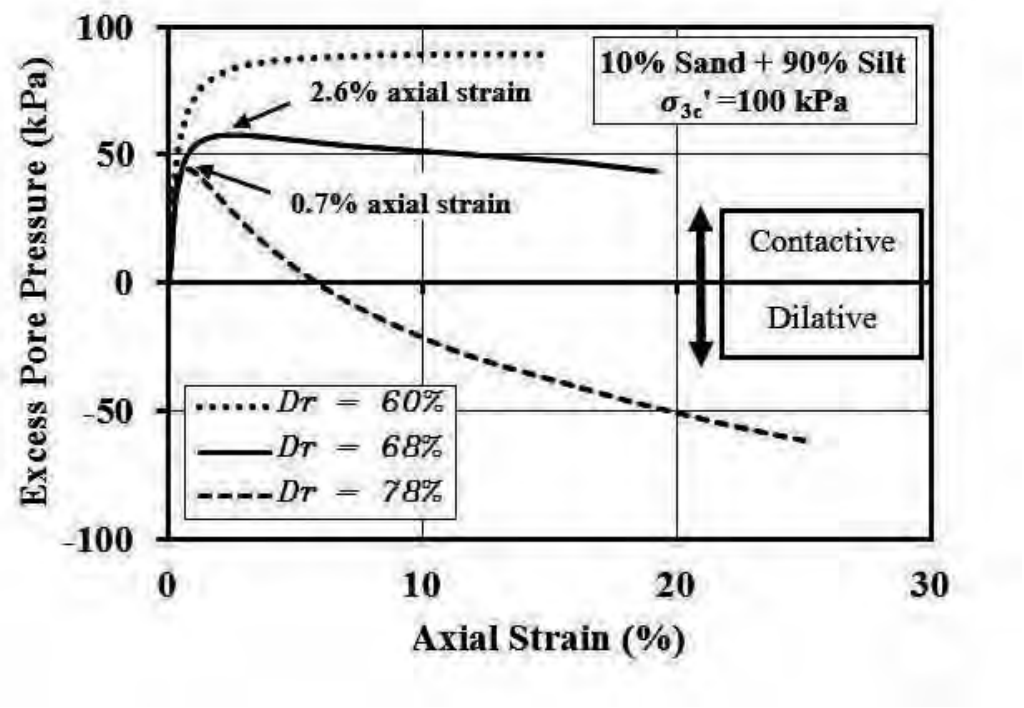

Figure 5-4. Excess pore water pressure versus axial strain curve.

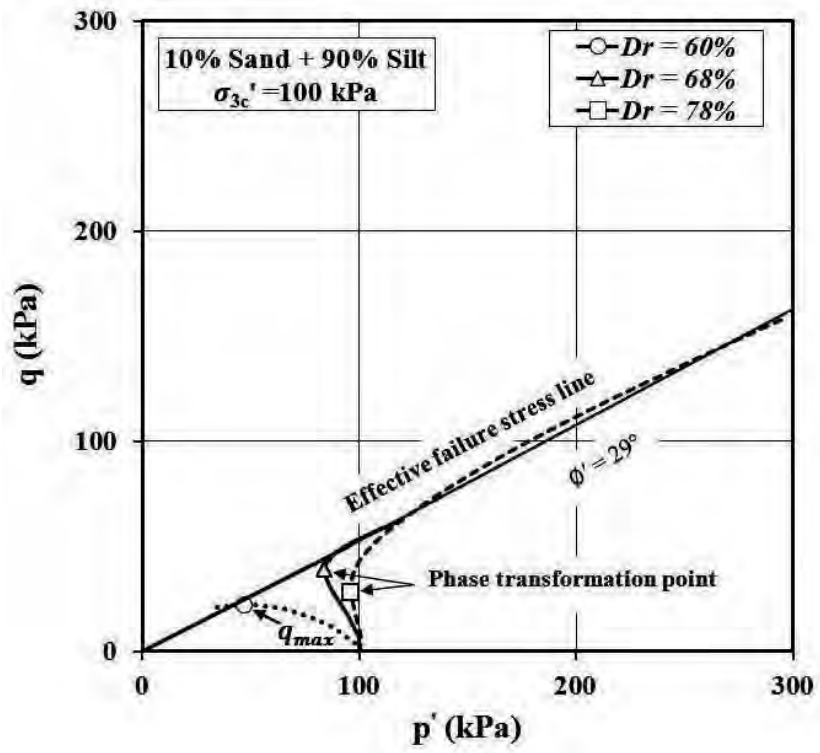

Figure 5-5. Effective stress path of three specimens with different relative density.

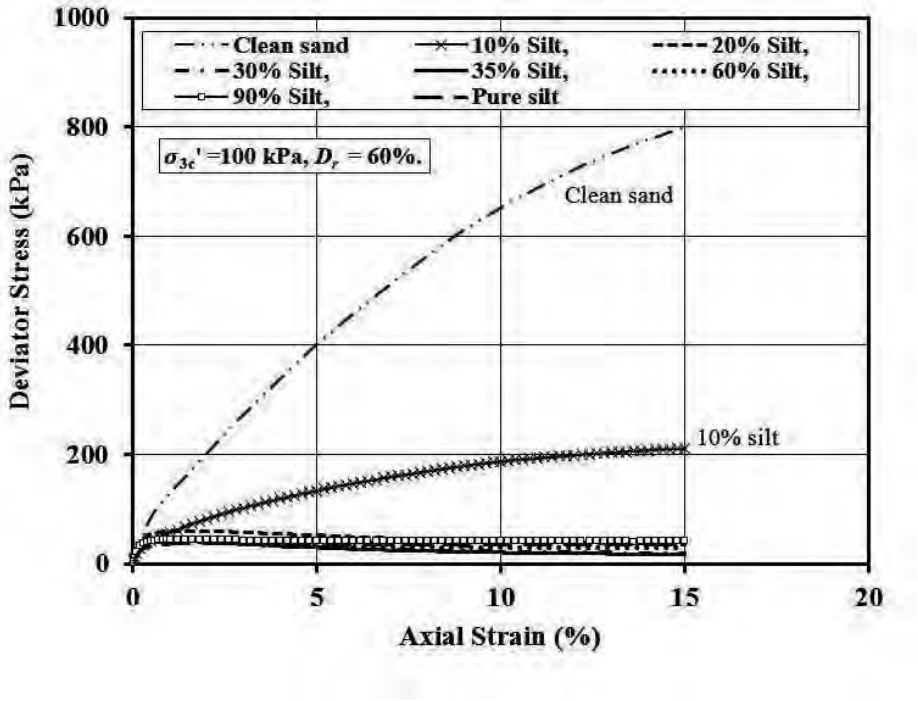

(a)

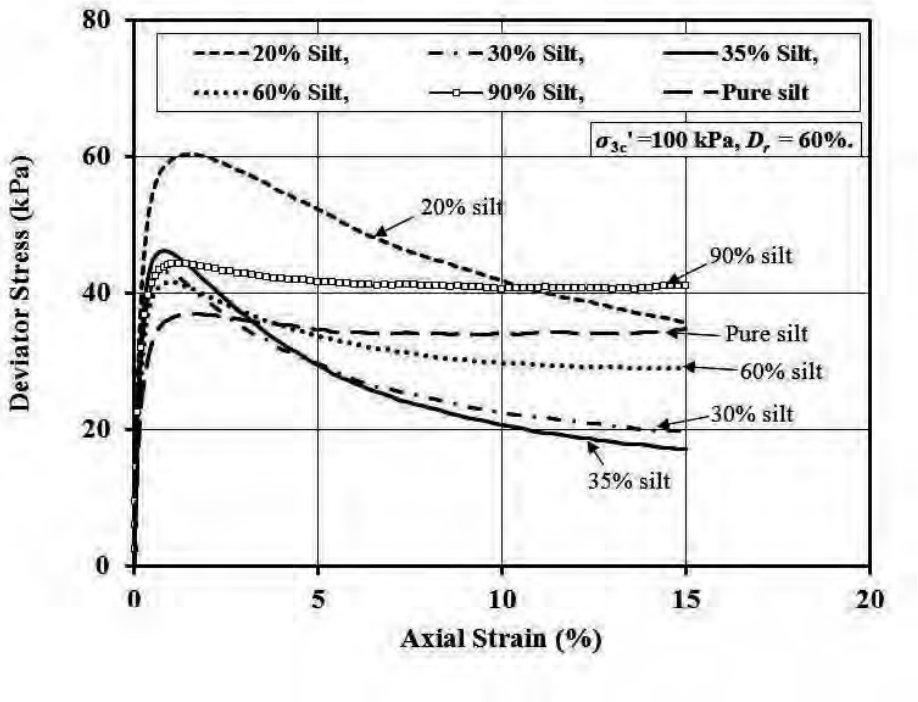

(b)

Figure 5-6. Stress-strain relationship at 60 percent relative density. (a) silt content 0 to 100 percent and (b) silt content 20 to 100 percent silt.

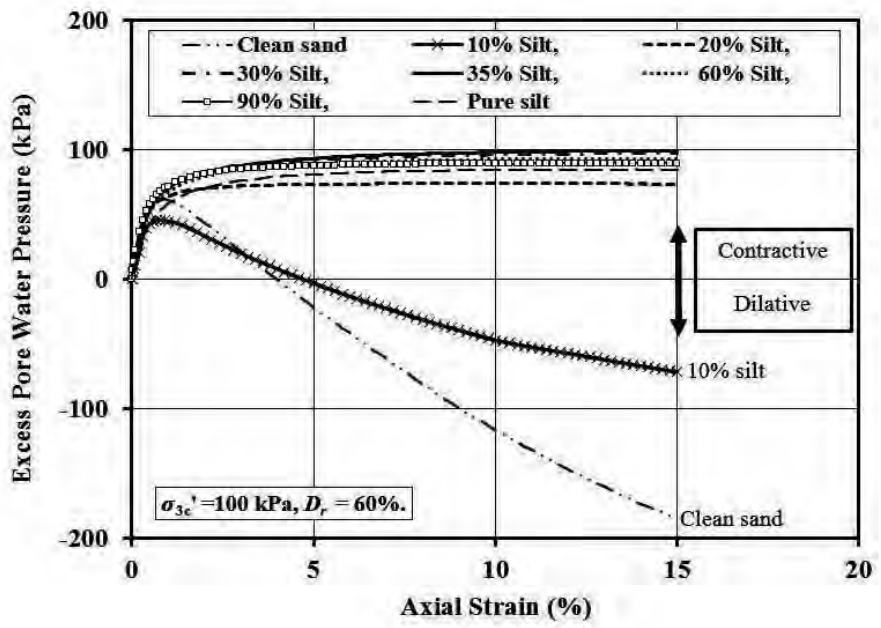

(a)

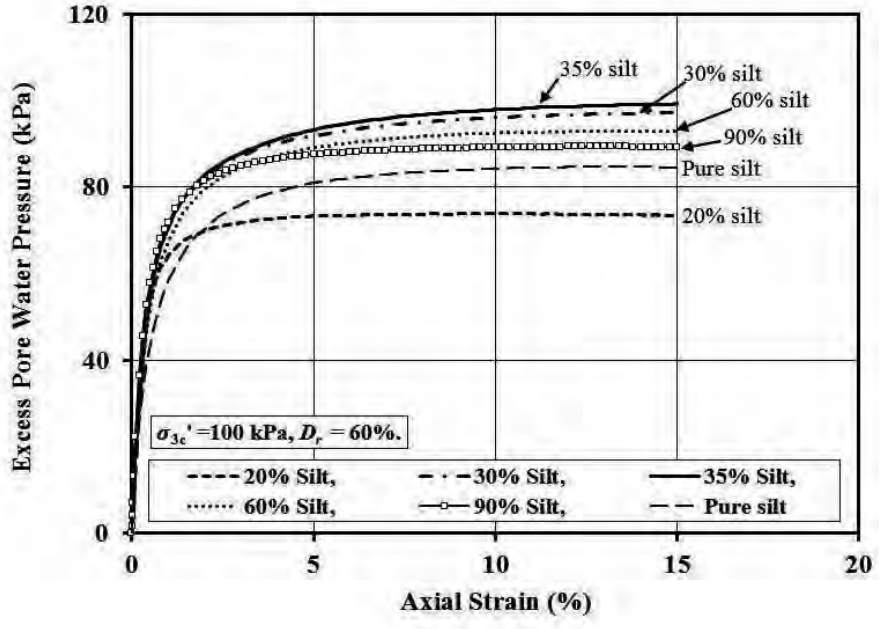

(b)

Figure 5-7. Excess pore pressure verses strain curve at 60 percent relative density. (a) silt content 0 to 100 percent and (b) silt content 20 to 100 percent silt.

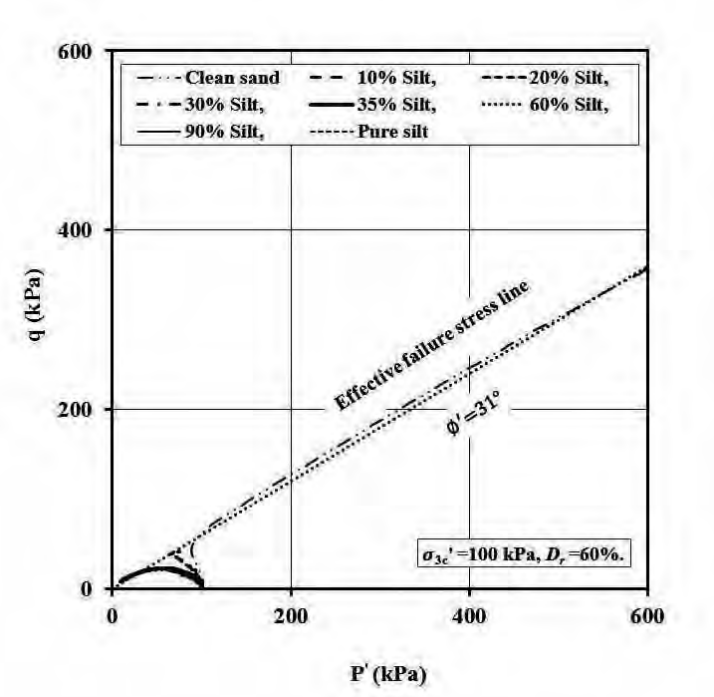

(a)

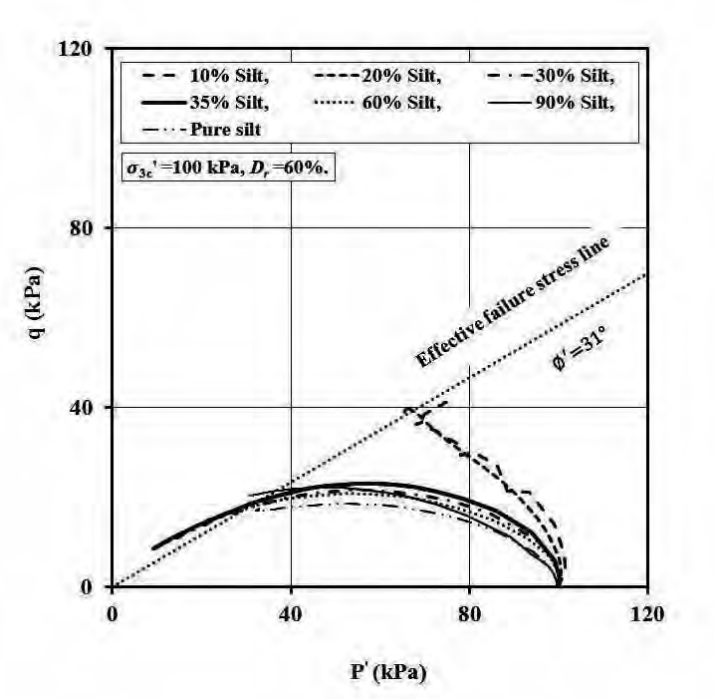

(b)

Figure 5-8. Effective stress path of tested specimens at 60 percent relative density. (a) silt content 0 to 100 percent and (b) silt content 20 to 100 percent silt.

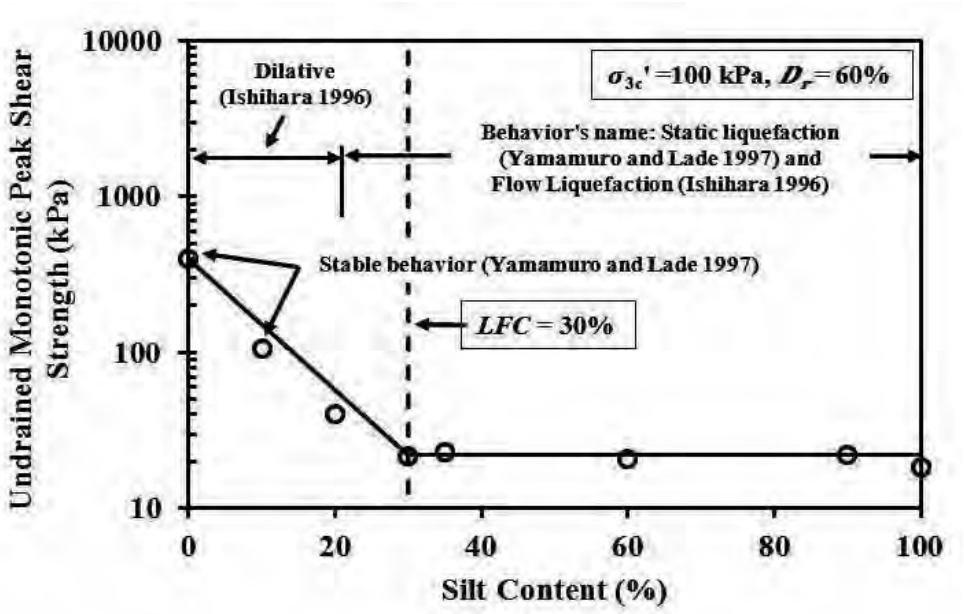

Figure 5-9. Effect of silt content on undrained monotonic peak shear strenght of sand-silt mixture at canstant relative density of 60 percent [59].

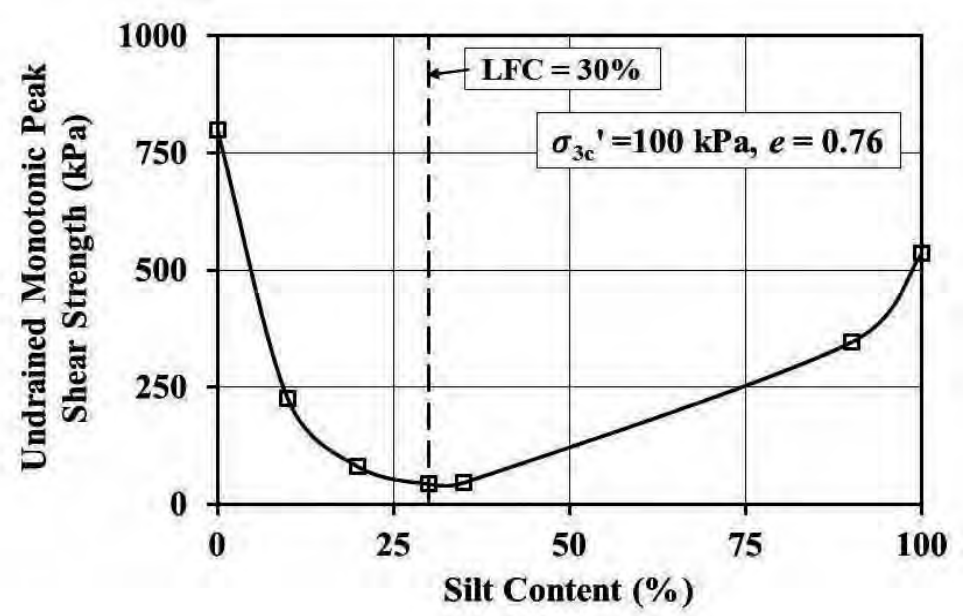

Figure 5-10. Effect of silt content on undrained monotonic peak shear strenght of sand-silt mixture at canstant gross void ratio 0.76 [59].

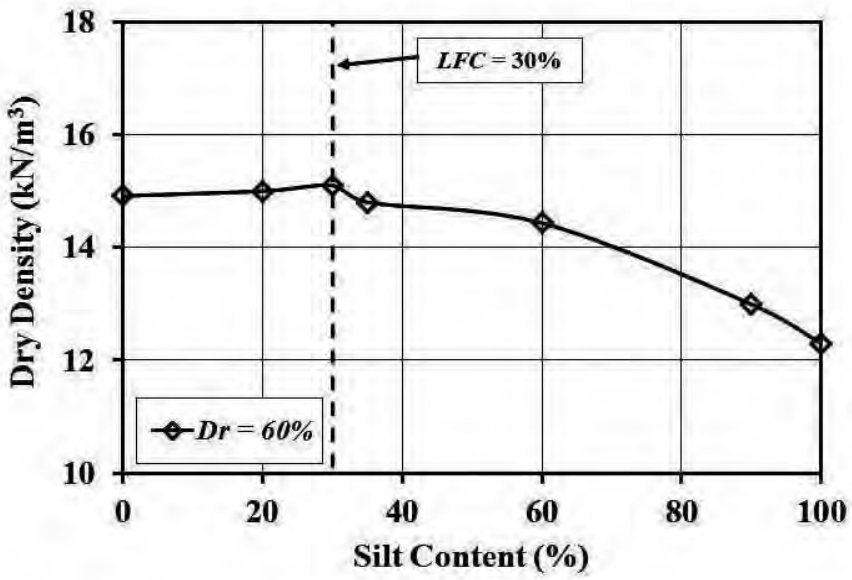

Figure 5-11. Variation of dry density with silt content at constant relative density.

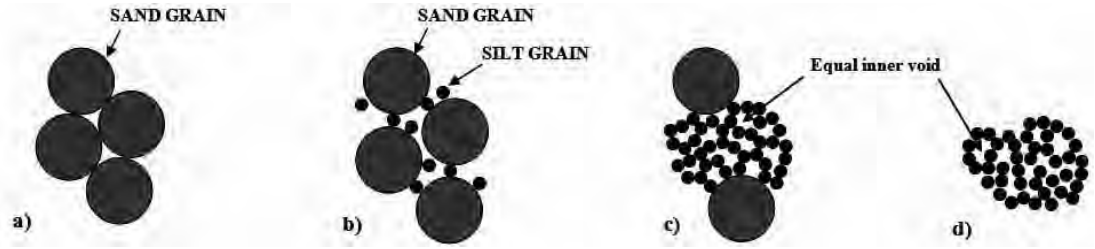

i) Before Shearing

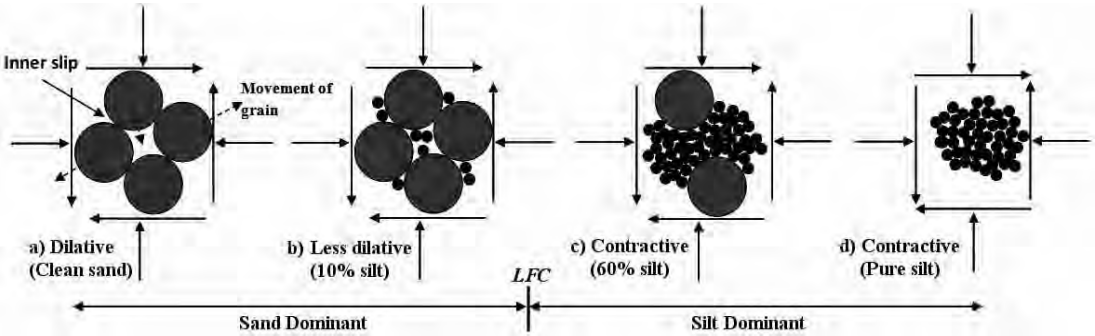

(ii) At Shearing

Figure 5-12. Probable structure of sand-silt mixture at different percent of silt at 60 percent silt content. (i) before shearing and (ii) at shearing.

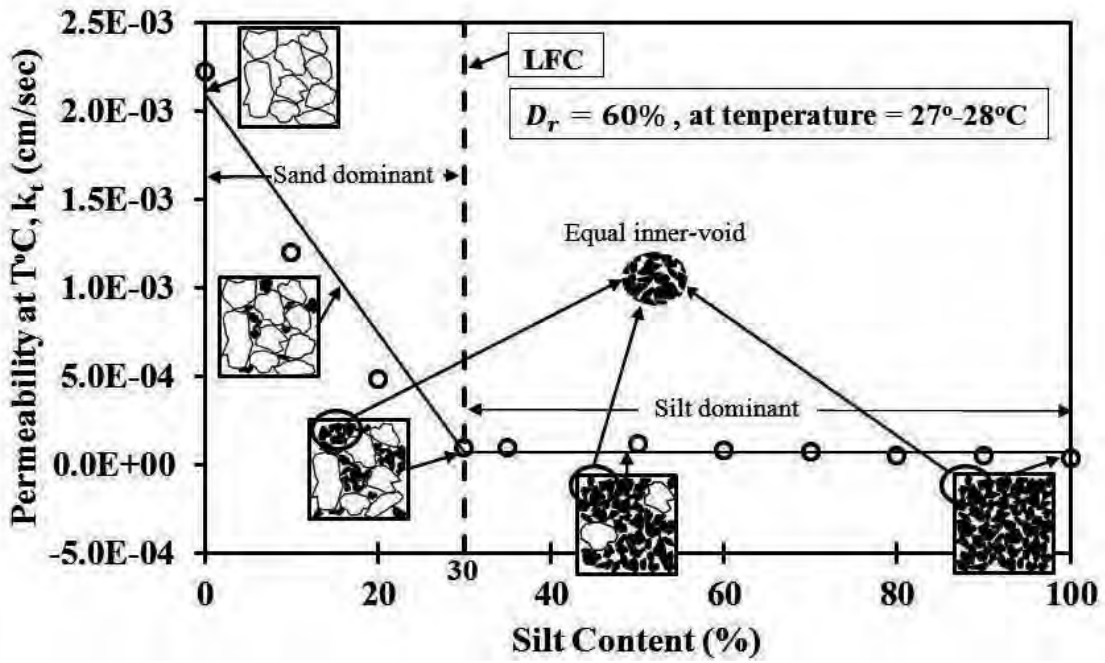

Figure 5-13. Effect of silt content on coefficient of permeability of sand-silt mixture at canstant relative density of 60 percent.

CHAPTER 6

CONCLUSION AND RECOMMENDATION

6.1 Introduction

A series of cyclic and monotonic triaxial tests has been done on different percents of silt (0 to 100) content in sand specimens, with constant relative density and void ratio approach, effective confining pressure 100 kPa. The diameter and height of the specimen was 71 mm and 142 mm respectively. The specimens were prepared by moist tamping method.

Investigating the cyclic and monotonic triaxial test results (specimens prepared by moist tamping method) the essence comes out that in both cyclic and monotonic triaxial test the shear strength decreases with increase in silt content till *LFC*, later the shear strength becomes study with increase in silt content till pure silt. After justifying all the literature and test results, concur with the conclusion of Dash and Sitharam [47].

6.2 Conclusion

The cyclic, monotonic triaxial tests at 100 kPa confining pressure and permeability tests were conducted on sand-silt mixtures, the acquirement are given bellow respectively.

6.2.1 Cyclic loading

In this research work cyclic loading conducted with 1 Hz frequency for all sand-silt mixtures. From the experimental result the following conclusions can be drawn:

1) The rate of generation of excess pore water pressure with respect to cycles of loading was found to initially increase with increase in silt content till the limiting silts content (*LFC*) is reached and thereafter it reverses till pure sit its trend when the specimens were tested at a constant dry density.

2) The cyclic resistance behaviour was observed to be just opposite to the pore pressure response.

3) In constant relative density approach, the excess pore pressure generation rate with respect to cycles of loading was found to initially decrease till limiting fines content and thereafter a more or less same. This pore pressure response implies that the cyclic resistance decreases till the limiting fines content and thereafter remains relatively constant.

4) *CRR* and Secant Shear Modulus decreased till Limiting Silts Content; after that they became constant with increasing silt content.

6.2.2 Monotonic loading

An experimental study on sand with different percent of silt content at constant relative density and void ratio were conducted. Undrained monotonic strain control triaxial tests were performed on sand-silt mixtures. In the light of the experimental evidences, the following conclusions can be drawn:

1) Limiting Fines Content (*LFC*) defined by Polito & Martin II [37] was found valid in this study.

2) In the shearing phase inner slip occur among the sand particles which procreate inner voids. As it is undrained triaxial test whereupon a large amount of suction pressure (excess negative pore water pressure) develop in the voids which increases effective mean pressure. For increasing silt, inner voids were occurred by inner slip of the particles filled with fine silt particles which reduce the suction pressure. For further increment of silt the excess negative pore pressure change to excess positive pore pressure at *LFC* (30 percent silt content), later it remains constant till pure silt content.

3) At constant relative density, increase in silt content decrease the undrained peak shear strength till *LFC* after *LFC* the strength become near about same till pure silt sample. This behavior is due to the equal inner void in the fine silt particles after *LFC* at constant relative density.

4) At constant gross void ratio, the peak shear strength decreases with increase in silt content till *LFC* and for further increment of silt content the peak shear strength increases.

6.2.3 Permeability test

Increasing silt content decreases the permeability till *LFC*, for further increment of silt content, permeability remains constant till pure silt. Consequently it is apparent that after *LFC* the inner voids are equal for all specimens. So, after *LFC* the *CRR,* Secant Shear Modulus and undrained peak shear strength of increasing silt content till pure silt is near about constant.

6.3 Recommendation for Further Study

On completion of these experimental studies of both cyclic and monotonic triaxial tests on sand silt mixtures, it is felt necessary that further investigation needed especially with particles size (sand and silt). Following studies could be done in the context of this study.

(i) Different sample preparation methods could be used to understand the effect of sample preparation method of sand-silt mixtures. Such as air pluviation method, water pluviation method, rodding dry soil, several vibration techniques.

(ii) This study only considered the constant relative density and constant dry density or void ratio approach. Other approach could be used to check the behavior of sand-silt mixture. Namely, sand skeleton void ratio approach, interfine void ratio approach.

(iii) Effect of different confining pressures on sand-silt mixture at different approach and different approach's different values may also be investigated.

(iv) Changing the loading frequency (cyclic test) and axial strain rate (monotonic test) the effect can be justify.

(v) Effect of sand and elastic silt (plastic silt) mixtures, effect of sand-clay mixtures can be investigated.

(vi) The effect of mica content on sand-silt mixture may be investigated.

References

[1] Zlatovic, S., and Ishihara, K., "On the Influence of Non-Plastic Fines on Residual Strength," *Proceedings of the first International Conference on Earthquake Geotechnical Engineering*, Tokyo, pp. 14-16, 1995.

[2] Lade, P. V., and Yamamuro, J. A., "Effects of Non-Plastic Fines on Static Liquefaction of Sands," *Canadian Geotechnical Journal*, Vol. 34, pp. 918-928, 1997.

[3] Thevanayagam, S., and Ravishankar, K., and Mohan, S., "Effects of Fines on Monotonic Undrained Shear Strength of Sandy Soils," *ASTM Geotechnical Testing Journal*, Vol. 20, No. 1, pp. 394-406, 1997.

[4] Thevanayagam, S., "Effect of Fines and Confining Stress on Undrained Shear Strength of Silty Sands", *J. Geotech. Geoenviron. Eng. Div.*, ASCE, 124, No. 6, pp. 479-491, 1998.

[5] Yamamuro, J. A., Lade, P. V., "Steady-state Concepts and Static Liquefaction of Silty Sands", *Journal of Geotechnical and Geoenvironmental Engineering*, ASCE, Vol. 124, No. 9, pp. 868-877, 1998.

[6] Amini, F., and Qi, G. Z., "Liquefaction Testing of Stratified Silty Sands", *Journal of Geotechnical Geoenvironmental Engineering*, Proc. ASCE, 2000, Vol. 126, No. 3, pp. 208-217, 2000.

[7] Naeini, S. A., "The Influence of Silt Presence and Sample Preparation on Liquefaction Potential of Silty Sands", PhD Dissertation, Tehran, Iran: Iran University of Science and Technology, 2001.

[8] Naeini, S. A., and Baziar, M. H., "Effect of Fines Content on Steady-State Strength of Mixed and Layered Samples of a sand", *Soil Dynamics and Earthquake Engineering*, Elsevier, Vol. 24, pp. 181-187, 2004.

[9] Belkhatir, M., Arab, A., Della, N, Missoum, H., and Tom Schanz, T., "Liquefaction Resistance of Chlef River Silty Sand: Effect of Low Plastic Fines and other Parameters." *Acta Polytechnica Hungarica*, Vol. 7, No. 2, 2010.

[10] Finn, W. D. L., "State-of-the-art of Geotechnical Earthquake Engineering Practice", *Soil Dynamic and Earthquake Engineering*, Elsevier, Vol. 20, pp.1-15., 2002.

[11] Singh, S., "Liquefaction Characteristics of Silt", *Ground Failures under Seismic Condition Geotechnical Special Publication*, No. 44, ASCE, pp. 105-116, 1994.

[12] Shen, C. K., Vrymoed, J. L., and Uyeno, C. K., "The Effects of Fines on Liquefaction of Sands", *Proc. 9th Int. Conf. Soil Mech. and Found. Eng*, Tokyo, Vol. 2, pp. 381-385, 1977.

[13] Troncoso, J. H., Verdugo, R., "Silt Content and Dynamic Behaviour of Tailing Sands" *Proc. 12th Int. Conf. on Soil Mech. and Found. Eng.*, San Francisco, pp. 1311-1314, 1985.

[14] Georginnou, V. N., Burland, J. B., and Hight, D. W., "The Undrained Behaviour of Clayey Sands in Triaxial Compression and Extension", *Geotechnique 40*, No. 3, pp. 431-449, 1990.

[15] Finn, W. L., Ledbetter, R. H., Wu, G., "Liquefaction on Silty Soils: Design and Analysis", *Ground Failures under Seismic Condition Geotechnical Special Publication*, No. 44, ASCE, pp. 51-76, 1994.

[16] Vaid, V. P., "Liquefaction of Silty Soils", *Ground Failures under Seismic Condition Geotechnical Special Publication*, No. 44, ASCE, pp. 1-16, 1994.

[17] Erten, D., Maher, M. H., "Cyclic Undrained Behaviour of Silty Sand", *Soil Dynamics and Earthquake Engineering*, Elsevier, Vol. 14, pp. 115-123, 1995.

[18] Zlatovic, S., and Ishihara, K., "Normalised Behaviour of Very Loose Non-Plastic Soils: Effects of Fabric", *Soils and Foundations*, Vol. 37, No. 4, pp. 47-56, 1997.

[19] Law, K. T., and Ling, Y. H., "Liquefaction of Granular Soils with Non-Cohesive and Cohesive Fines", *Proc. of the 10th World Conference on Earthquake Engineering, Rotterdam*, pp. 1491-1496, 1992.

[20] Koester, J. P., "The Influence of Fine Type and Content on Cyclic Strength", *Ground Failures under Seismic Condition*, Geotechnical Special Publication, No. 44, ASCE, pp. 17-33, 1994.

[21] Das, B. M., and Ramana, G. V., "Principal of Soil Dynamics", Second Edition, *Printed in the United States of America*, chap. 10, pp. 398-399, USA, 2011.

[22] Baziar, M. H., Shahnazari, H., and Sharafi, H., "A Laboratory Study on The Pore Pressure Generation Model for Firouzkooh Silty Sands Using Hollow Torsional Test." *International Journal of Civil Engineering*, Vol. 9, No. 2, 2011.

[23] Lee, K. L. and Seed, H. B., "Cyclic Stress Conditions Causing Liquefaction of Sand," *Journal of the Soil Mechanics and Foundations Division*, ASCE, 93(1), 47–70, 1967.

[24] Seed, H. B., "Landslides During Earthquakes Due to Liquefaction," *Journal of the Soil Mechanics and Foundations Division*, ASCE, 94(5), 1053–1122, 1968.

[25] Seed, H. B. and Idriss, I. M., "Simplified Procedure for Evaluating Soil Liquefaction Potential," *Journal of the Soil Mechanics and Foundations Division,* ASCE, 97(9),1249–1273, 1971.

[26] Finn, W. D. L., Pickering, D. J. and Bransby, P. L., "Sand Liquefaction in Triaxial Test Simple Shear Tests," *Journal of the Soil Mechanics and Foundations Division*, ASCE, 97(4), 639–659, 1971.

[27] Castro, G., "Liquefaction and Cyclic Mobility Of Saturated Sands," *Journal of the Geotechnical Engineering Division*, ASCE, 101(6), 551–569, 1975.

[28] Youd, T. L., "Liquefaction, Flow and Associated Ground Failure," *Proceedings of the US National Conference*, Ann Arbor, MI, USA, June, 146–155, 1975.

[29] Kishida, H., "Characteristics of Liquefied Sands During Mino-Owari, Tohnankai, and Fukui Earthquakes". *Soils and Foundations*, 9(1): 75-92, 1969.

[30] Tohno, I. and Yasuda, S., "Liquefaction of the Ground During the 1978 Miyagiken-Oki earthquake" *Soils and Foundations*, 21(3), 18-34, 1981.

[31] Ishihara, K., "Post-Earthquake Failure of a Tailings Dam Due to Liquefaction of the Pond Deposit". *Proc. Int. Conf. on Case Histories in Geotechnical Engrg. St. Louis*, Missouri, Vol. 3, 1129-1143, 1984.

[32] Hazirbaba, K., and Rathje, E., M., "Pore Pressure Generation of Silty Sands Due to Induced Cyclic Shear Strains." *J. Geotech. Geoenviron. Eng.* 2009.135:1892-1905. ASCE, 2009.

[33] Seed, H. B. and Lee, K. L., "Liquefaction of Saturated Sands During Cyclic Loading," *Journal, Soil Mechanics and Foundations Division*, ASCE, Vol. 92, No. SM6, pp. 105-134, 1966.

[34] Shamsher, P. and Vijay, K. P., "Past and Future of Liquefaction," *Indian Geotechnical Conference-2010*. GEO trendz, 2010, IGS Munbai Chapter and IIT Bombay.

[35] http://www.gns.cri.nz/Home/Our-Science/Natural-Hazards/Recent-Events/Canterbury-quake/Darfield-Earthquake.

[36] Amini, F., and Qi, G. Z., "Liquefaction Testing of Stratified Silty Sands." *J. Geotech. Geoenviron. Eng.*, 126(3), 208–217, 2000.

[37] Polito, C. P., and Martin, J. R., "Effects of Non-Plastic Fines on the Liquefaction Resistance of Sands." *J. Geotech. Geoenviron. Eng.*, 127(5), 408–415, 2001.

[38] Sitharam, T. G., Ravishankar, B. V., and Vinod. J. S., "Liquefcation and Pore Water Pressure Generation in Sand - a Cyclic Strain Approach." *Journal of Earthquake and Tsunami*, Vol. 2, No. 3, pp. 227–240, 2008.

[39] Dash, H. K., and Sitharam, T. G., "Undrained Cyclic and Monotonic Strength of Sand-Silt Mixtures." *Geotech Geol Eng*, 29:555–570, 2011.

[40] Baziar, M. H., Shahnazari, H., and Sharafi, H., "A Laboratory Study on the Pore Pressure Generation Model for Firouzkooh Silty Sands Using Hollow Torsional Test." *International Journal of Civil Engineering*, Vol. 9, No. 2, June 2011.

[41] Tsuchida, H., "Prediction and counter measure against the liquefaction in sand deposits," Abstract of the seminar in the Port and Harbor Research Institute, 3.1–3.33, 1970.

[42] Xenaki, V. C., and Anthanasopoulos, G. A., "Liquefaction Resistance of Sand-Mixtures: an Experimental Investigation of the Effect of Fines," *Soil Dynamics and Earthquake Engineering*, Elsevier, 183–194, 2003.

[43] Ishihara. K., "Liquefaction and Flow Failure During Earthquakes", *Geotechnique*, Vol. 43, No. 3, pp. 351-415, 1993.

[44] IS: 1498–1970: ''Classification and identification of soils'' (1992). IS: 2720: (Part 1)–1983. ''Preparation of dry soil samples.'' (Part 3) Section 1: 1980. ''Specific gravity-fine grained soils.'' (1992), Section 2: 1980. ''Specific gravity– fine, medium and coarse grained soils.'' (1992). (Part 4)–1985. ''Grain size analysis.''(1995). (Part 5)–1985. ''Determination of liquid and plastic limit.''(1995). (Part 14)–1983. ''Determination of density index (relative density) of cohesionless soils.''

[45] Seed, H. B., Tokimatsu, K., Harder, L. F., Chung, R., "Influence of SPT Procedures in Soil Liquefaction Resistance Evaluations." *J Geotech Eng*, ASCE 111(12):861–878, 1985.

[46] Ladd, R. S., ''Preparing Test Specimens Using Under Compaction.'' *Geotech. Testing J.*, 1(1), 16–23, 1978.

[47] Dash, H. K., and Sitharam, T. G., “Undrain Cyclic Pore Pressure Response of Sand-Silt Mixtures: Effect of Nonplastic Fines and Other Parameters.” *Geotech Geol Eng*, 27:500-517, 2009.

[48] Bray, J. D., Sancio, R. B., Reimer, M. F., and Durgunoglu, H. T., “Liquefaction Susceptibility of Fine-grained Soils.” *proc., 11th Int. Conf. On Soil Dynamics and Earthquake Engineering and 3rd Int. Conf. On Earthquake Geotechnical Engineering. 1*, pp. 655-662. Berkeley, California: Stallion Press, 2004.

[49] Ishihara, K., "Stability of Natural Deposits During Earthquakes," *Proc. 11th Int. Conf. Soil Mech. and Found. Eng*., 1, pp. 321-376, 1985.

[50] Alam, M. K., Hasan, A. S., Khan, M. R., and Whitney, J. W., "Geological Map of Bangladesh." *Government of the peoples republic of bangladesh ministry of energ and resources geological survey of bangladesh*. Bangladesh, 1990.

[51] Head, K. H., “Manual of Soil Laboratory Testing.”Vol. 1, chap. 3, pp. 139-140, *ELE International Ltd*, London, 1984.

[52] Hazirbaba, K. “Pore Pressure Generation Characteristics of Sands and Silty Sands: a Strain Approach.” Dissertation presented for PhD program to the faculty of Graduate School at the University of Texas at Austin, 2005.

[53] Hight, D. W., Georgiannou, V. N., Matin, P. L. and Mundegar, A. K., “Flow Slides in Micaceous Sands”, *Proc. International Symposium on Problematic Soils. Sendai*, Japan, Vol. 2, 945-958, 1999.

[54] ASTM 4258-09, Standard Test Method for Consolidated Undrained Triaxial Compression Test for Cohesive Soils.

[55] Lee, K. L., and Albaisa, A., “Earthquake Induced Settlements in Saturated Sands.” *J Geotech Eng Div* 100(GT4):387–406, 1974.

[56] Karim, M. E. and Alam, M. J., " Effect of Non-Plastic Silt Content on Liquefaction Behavior of Sand-Silt Mixture." (revised manuscript is submitted as per comments' of reviewers), *Soil Dynamic and Earthquake Engineering*, Elsevier, 2014.

[57] Ishihara, K., "Soil Behaviour in Earthquake Geotechnics." *Oxford science publications*, chap. 11, pp. 248, New York, 1995.

[58] Rees, S. D., "Effect of Fines on the Undrained Behavior of Christchurch Sandy Soils." Ph.D. thesis submission to University of Canterbury Christchurch, New Zealand, 2010.

[59] Karim, M. E. and Alam, M. J., "Effect of Nonplastic Silt Content on Un-drained Shear Strength of Sand-Silt Mixture." (submitted), *KSCE Journal of Civil Engineering*, Springer, 2013.

APPENDIX A

MONOTONIC TRIAXIAL TESTS RESULT

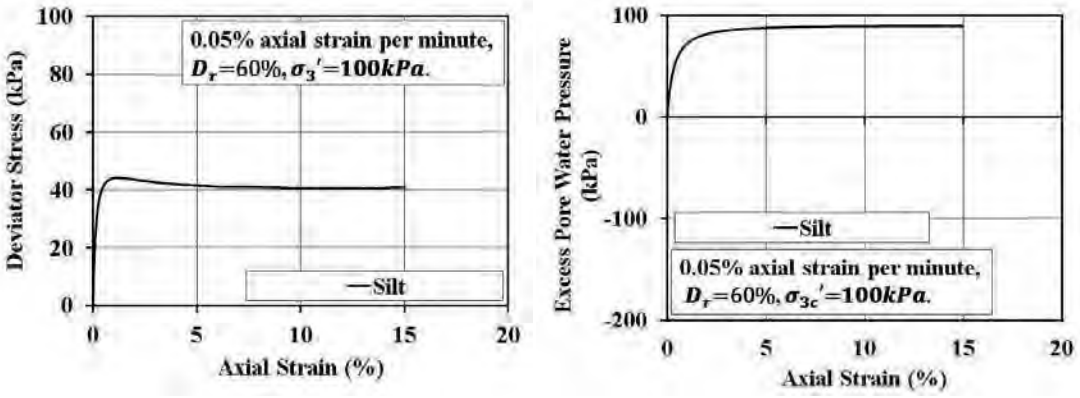

(a) (b)

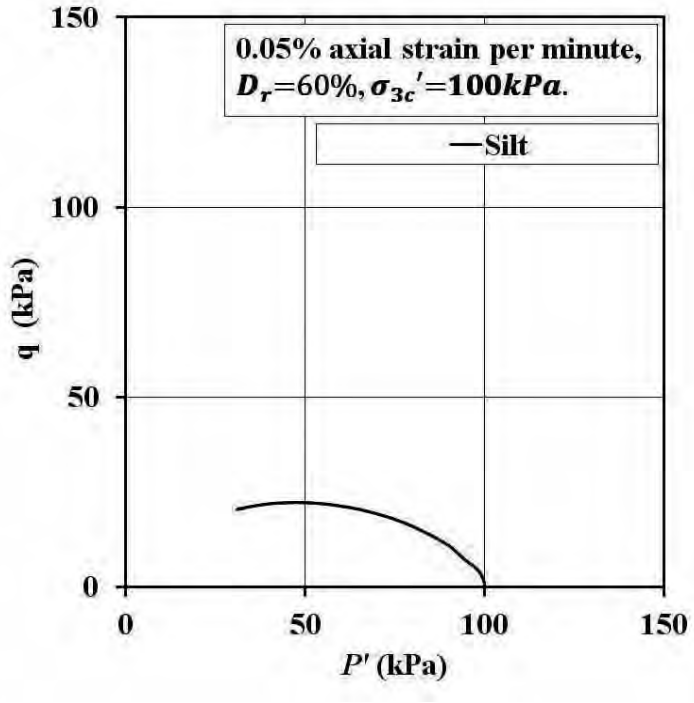

(c)

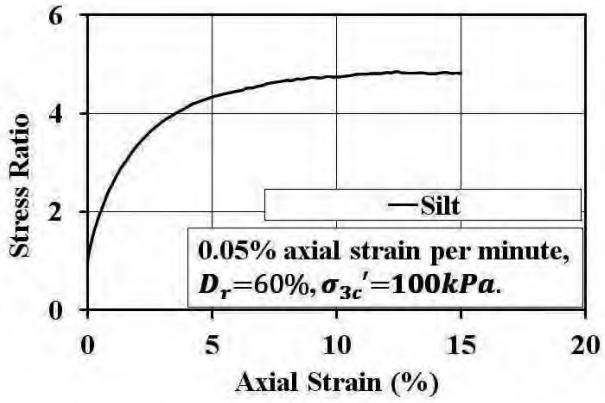

(d)

Figure A. 1. (a) Stress-strain response, (b) excess pore pressure response, (c) effective stress path and (d) stress ratio verses axial strain graph of silt specimen at D_r=60%.

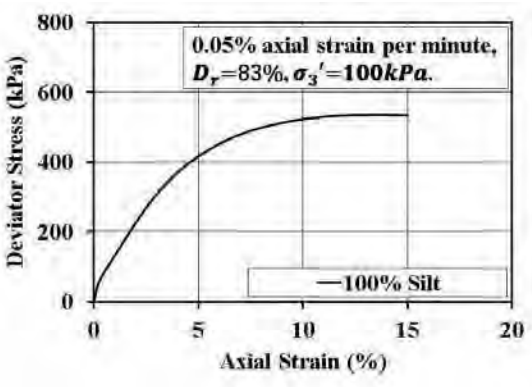

(a)

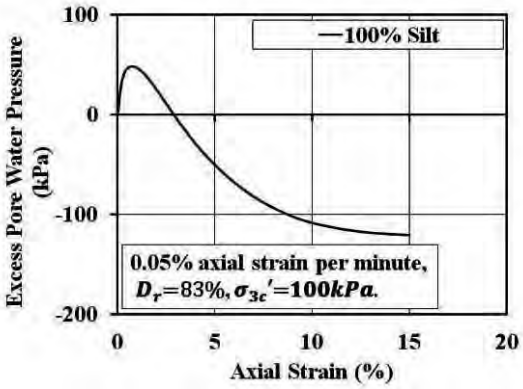

(b)

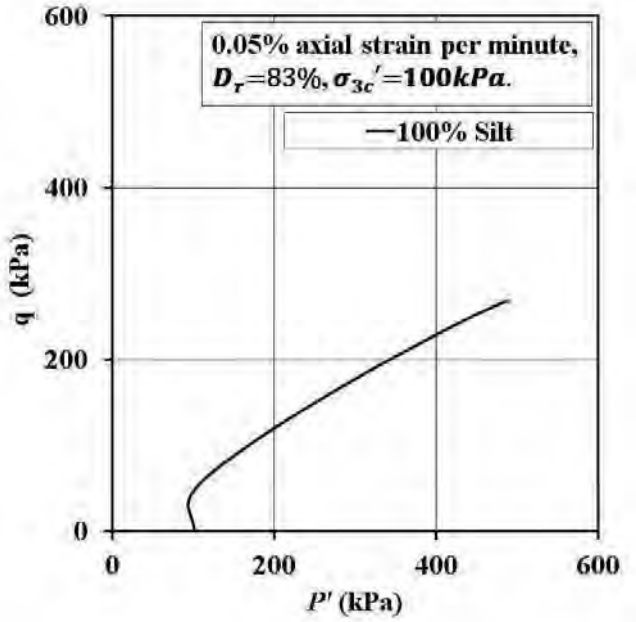

(c)

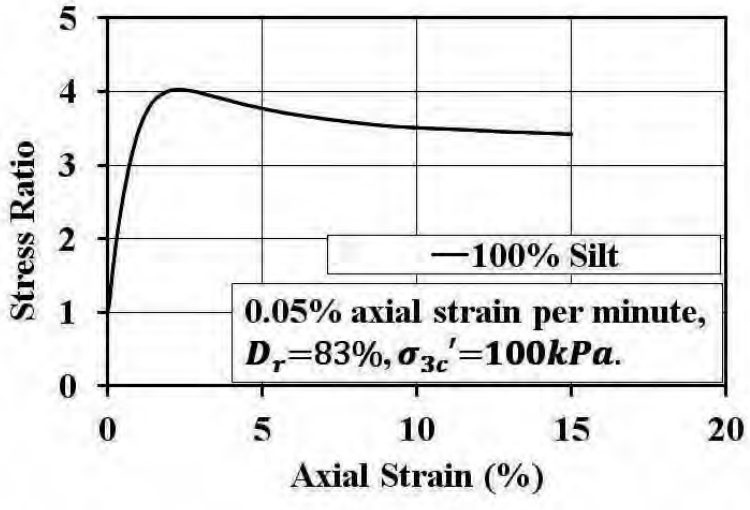

(d)

Figure A. 2. (a) Stress-strain response, (b) excess pore pressure response, (c) effective stress path and (d) stress ratio verses axial strain graph of silt specimen at D_r=83%.

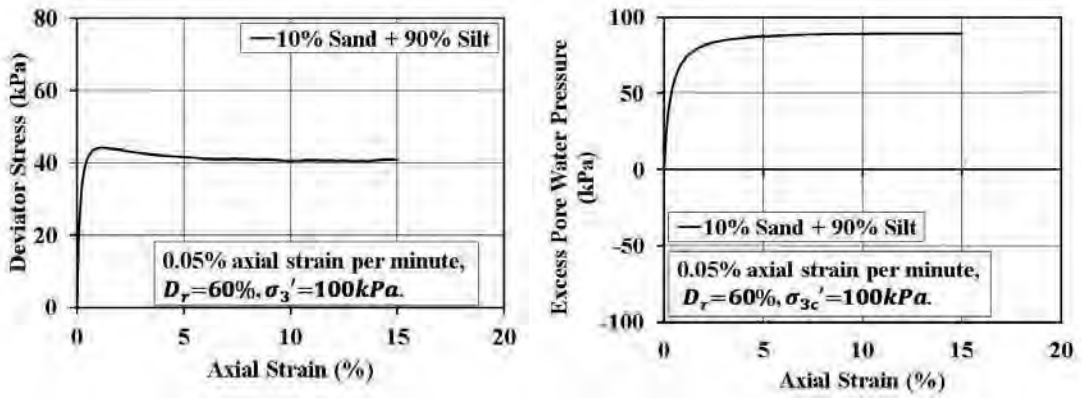

(a) (b)

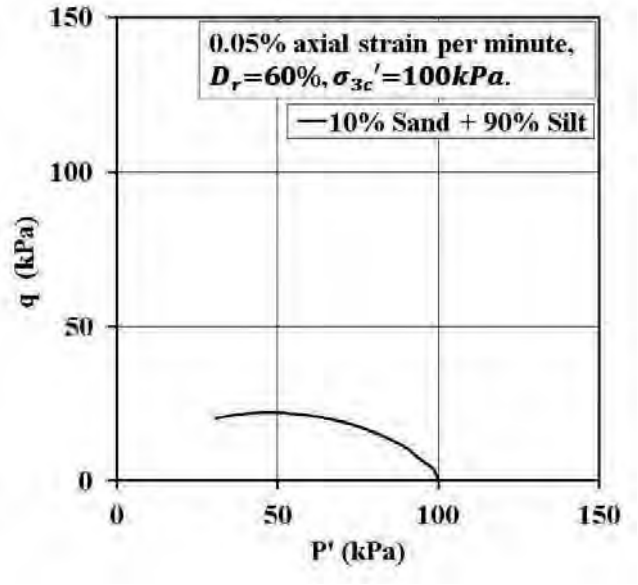

(c)

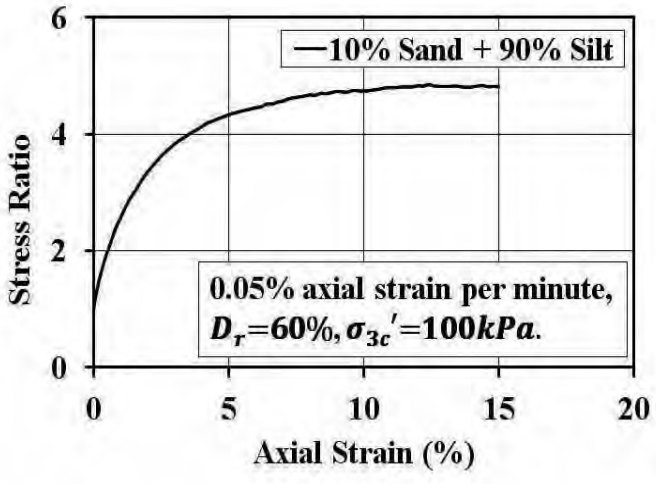

(d)

Figure A. 3. (a) Stress-strain response, (b) excess pore pressure response, (c) effective stress path and (d) stress ratio verses axial strain graph of 10% sand + 90% silt specimen at D_r=60%.

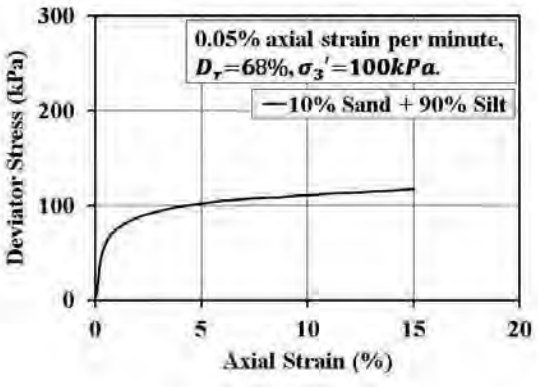

(a)

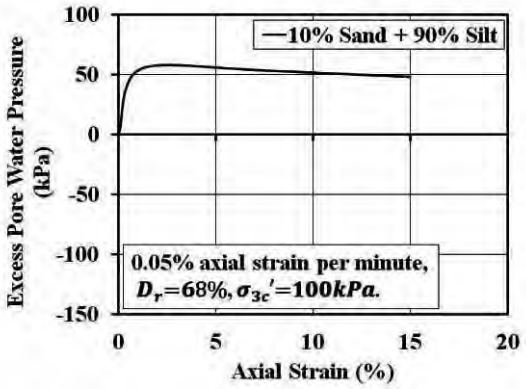

(b)

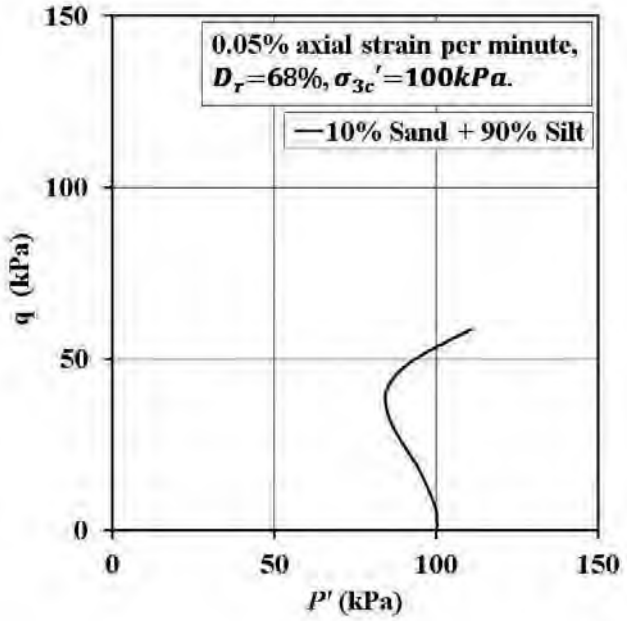

(c)

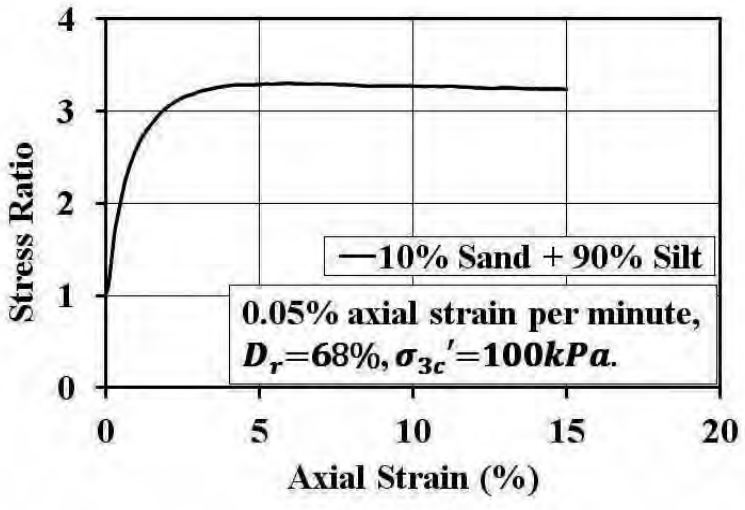

(d)

Figure A. 4. (a) Stress-strain response, (b) excess pore pressure response, (c) effective stress path and (d) stress ratio verses axial strain graph of 10% sand + 90% silt specimen at D_r=68%.

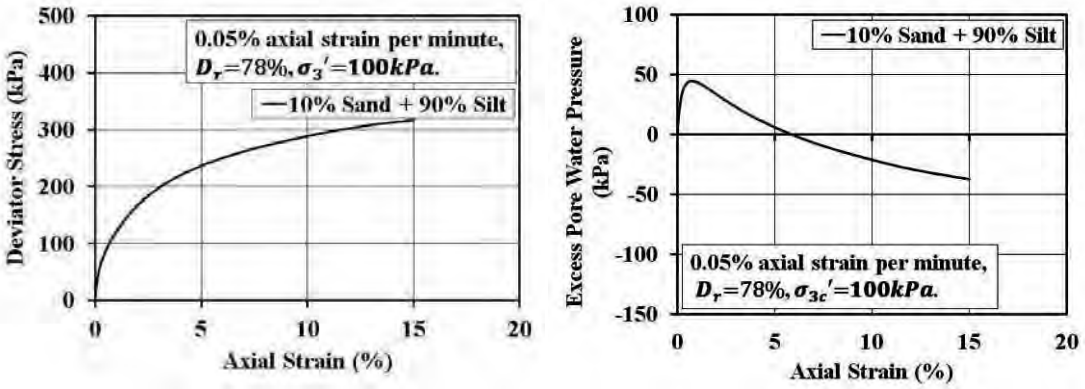

(a)

(b)

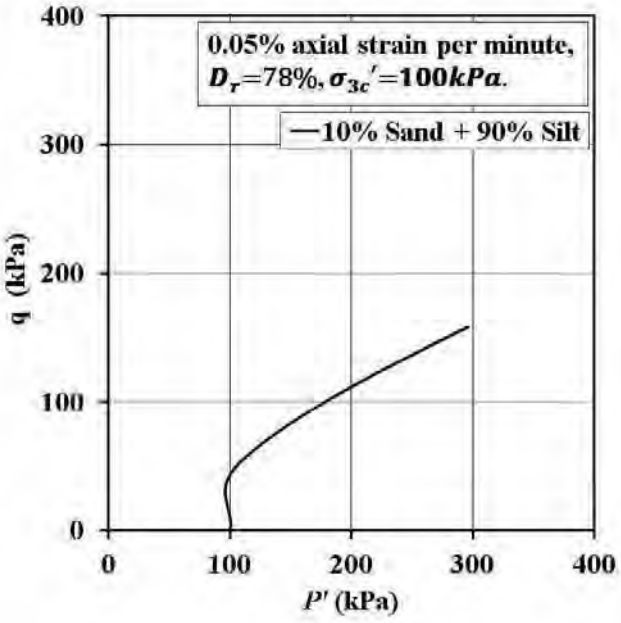

(c)

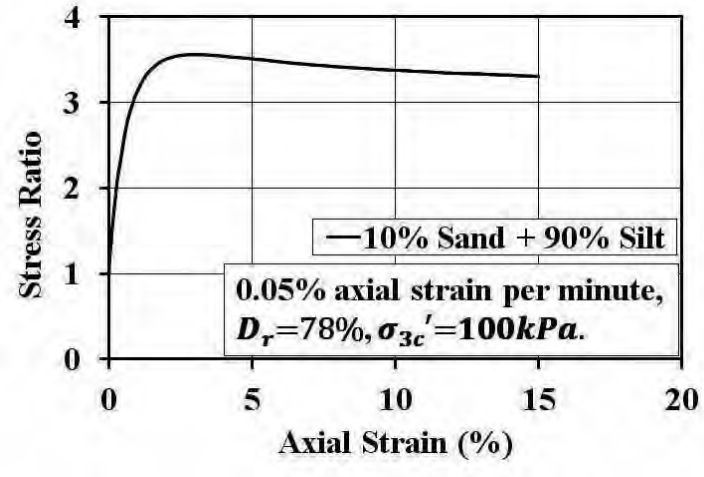

(d)

Figure A. 5. (a) Stress-strain response, (b) excess pore pressure response, (c) effective stress path and (d) stress ratio verses axial strain graph of 10% sand + 90% silt specimen at D_r=78%.

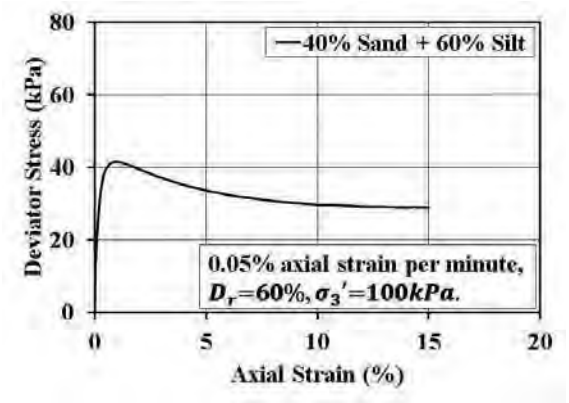

(a)

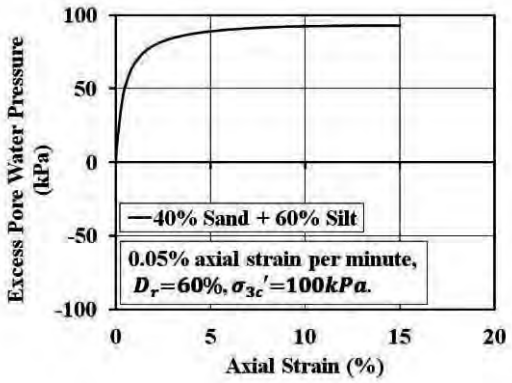

(b)

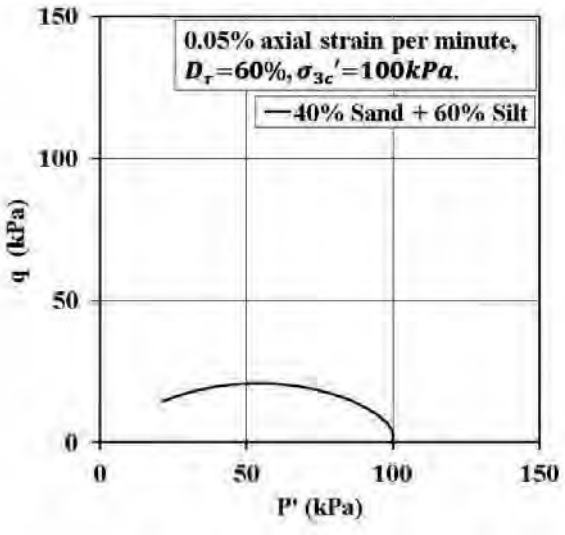

(c)

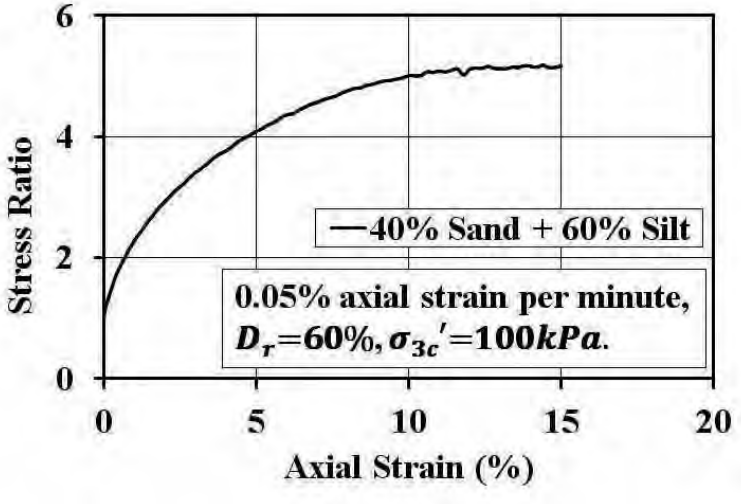

(d)

Figure A. 6. (a) Stress-strain response, (b) excess pore pressure response, (c) effective stress path and (d) stress ratio verses axial strain graph of 40% sand +60% silt specimen at D_r=60%.

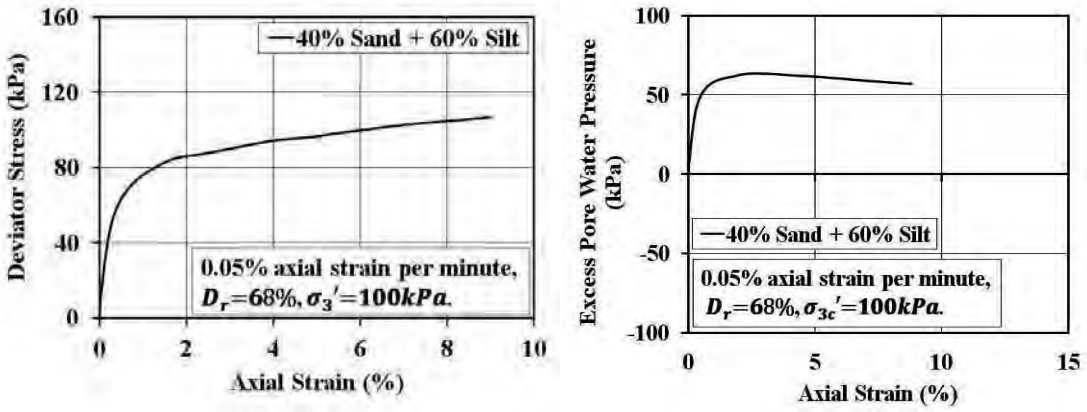

(a)

(b)

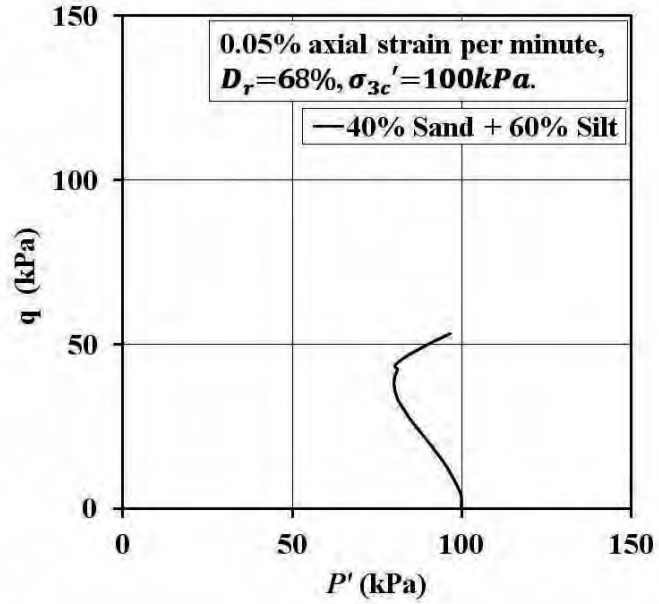

(c)

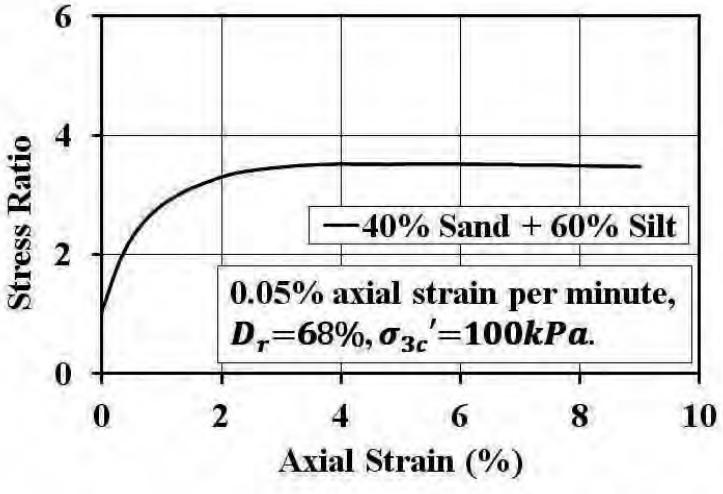

(d)

Figure A. 7. (a) Stress-strain response, (b) excess pore pressure response, (c) effective stress path and (d) stress ratio verses axial strain graph of 40% sand +60% silt specimen at D_r=68%.

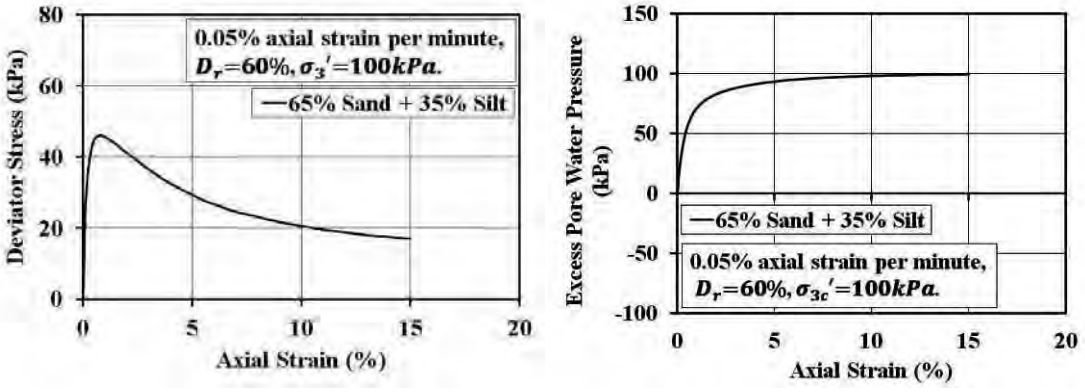

(a) (b)

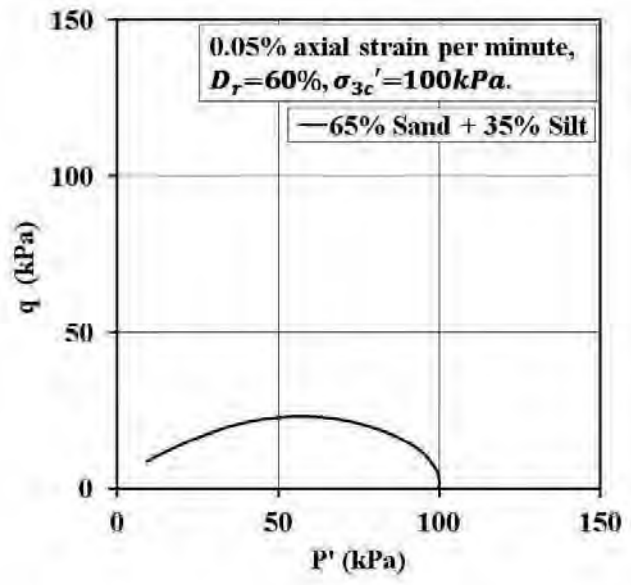

(c)

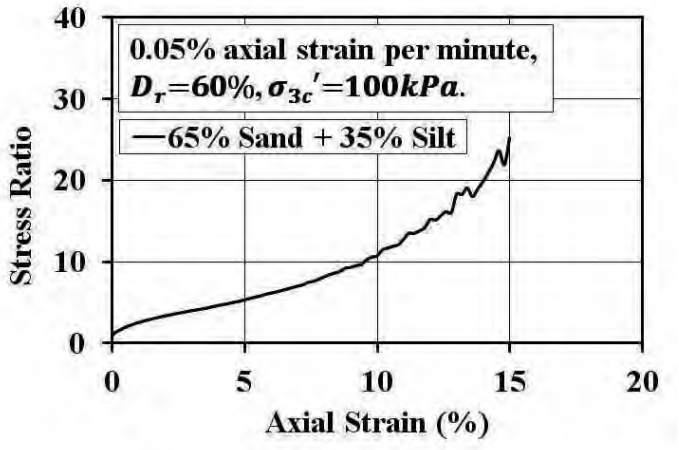

(d)

Figure A. 8. (a) Stress-strain response, (b) excess pore pressure response, (c) effective stress path and (d) stress ratio verses axial strain graph of 65% sand + 35% silt specimen at D_r=60%.

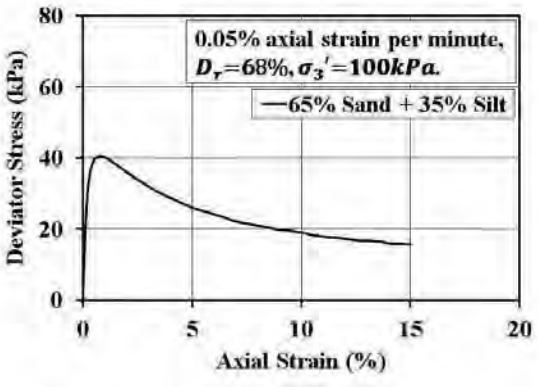

(a)

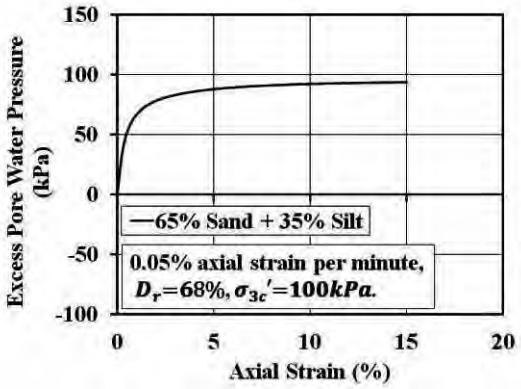

(b)

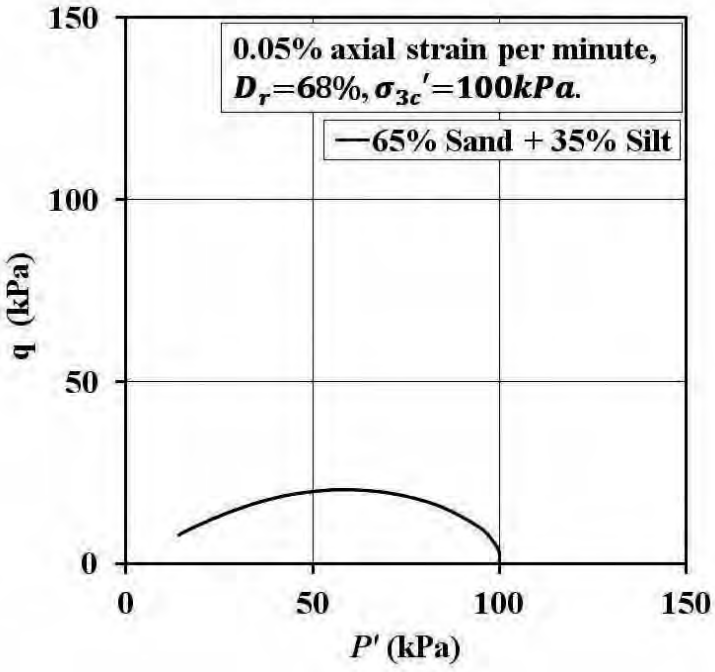

(b)

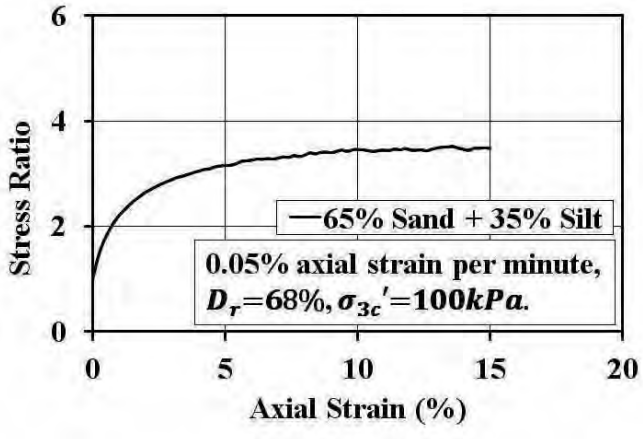

(d)

Figure A. 9. (a) Stress-strain response, (b) excess pore pressure response, (c) effective stress path and (d) stress ratio verses axial strain graph of 65% sand + 35% silt specimen at D_r=68%.

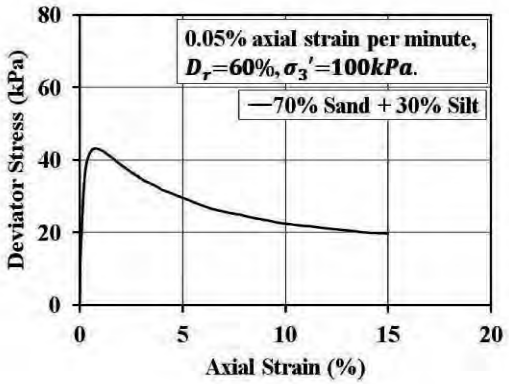

(a)

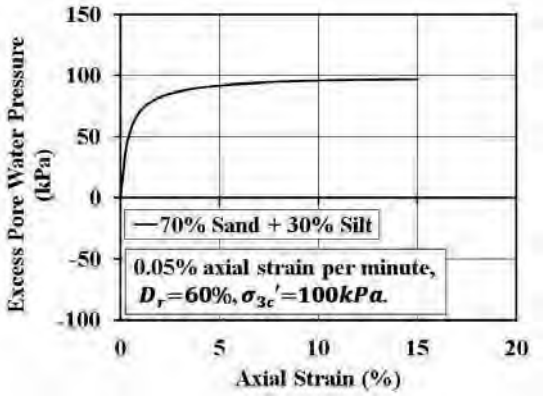

(b)

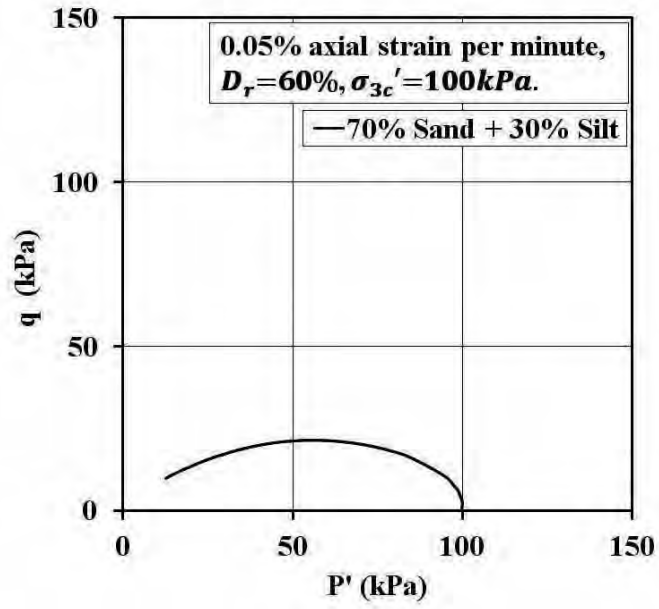

(c)

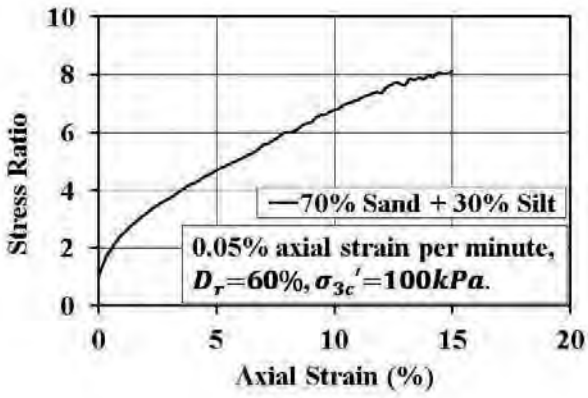

(d)

Figure A. 10. (a) Stress-strain response, (b) excess pore pressure response, (c) effective stress path and (d) stress ratio verses axial strain graph of 70% sand + 30% silt specimen at D_r=60%.

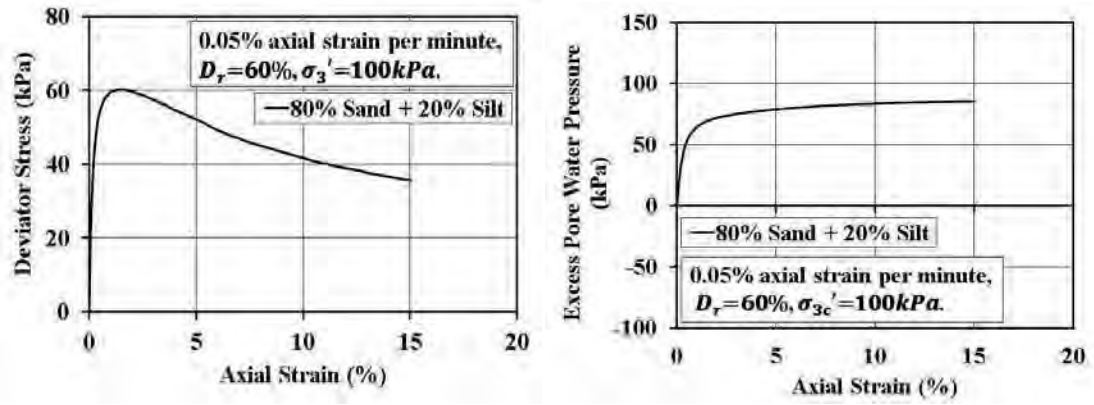

(a)

(b)

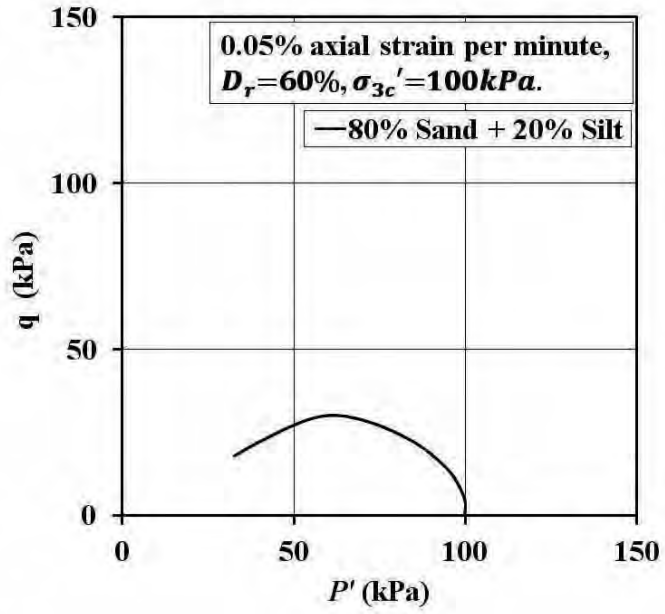

(c)

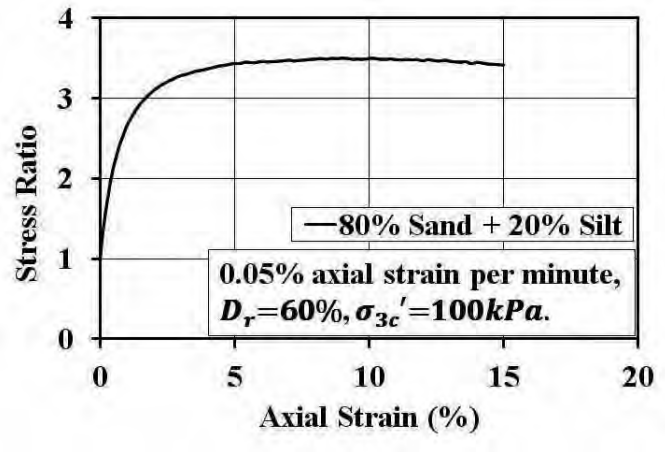

(d)

Figure A. 11. (a) Stress-strain response, (b) excess pore pressure response, (c) effective stress path and (d) stress ratio verses axial strain graph of 80% sand + 20% silt specimen at D_r=60%.

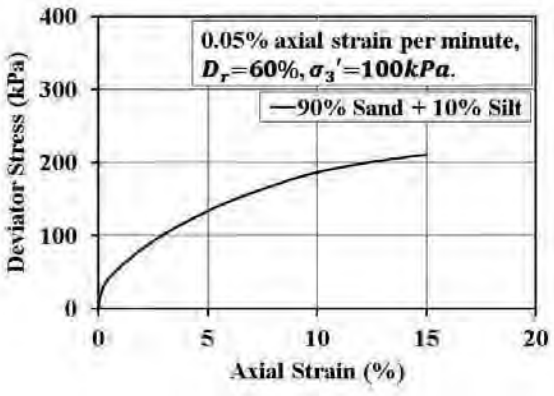

(a)

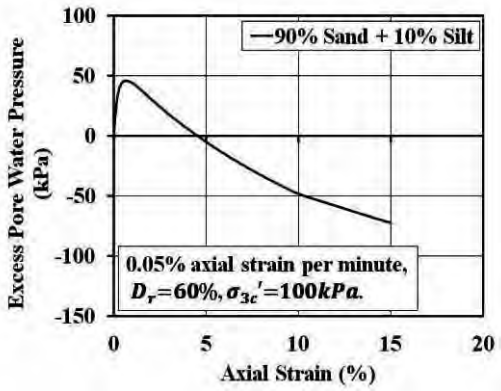

(b)

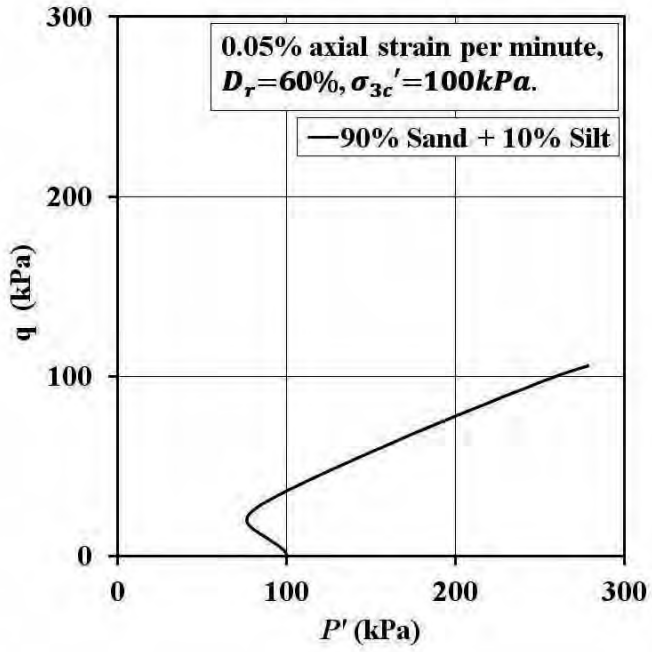

(c)

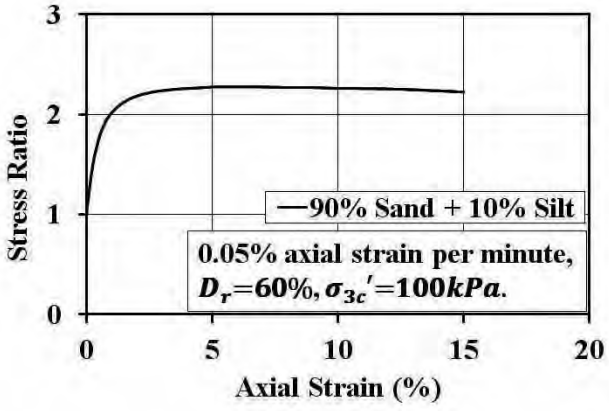

(d)

Figure A. 12. (a) Stress-strain response, (b) excess pore pressure response, (c) effective stress path and (d) stress ratio verses axial strain graph of 90% sand + 10% silt specimen at D_r=60%.

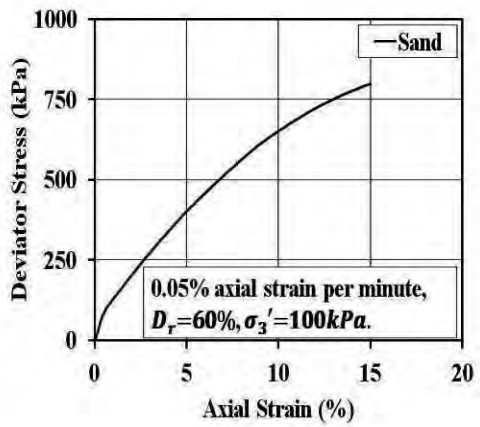

(a)

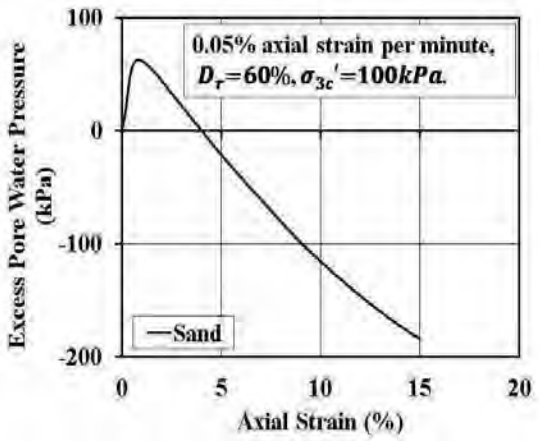

(b)

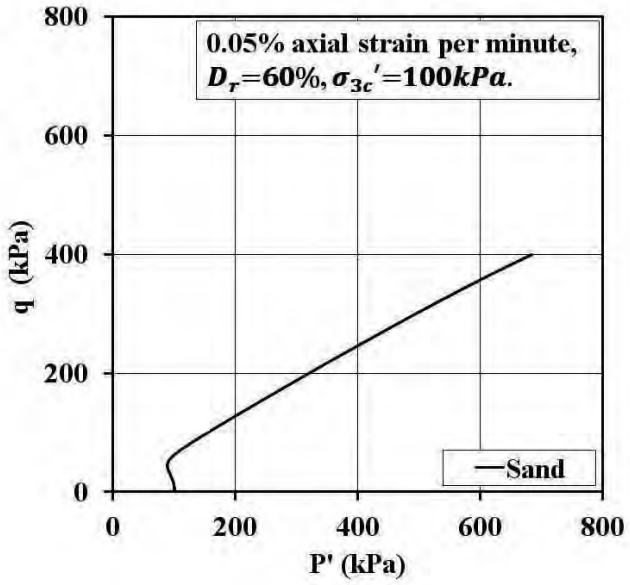

(c)

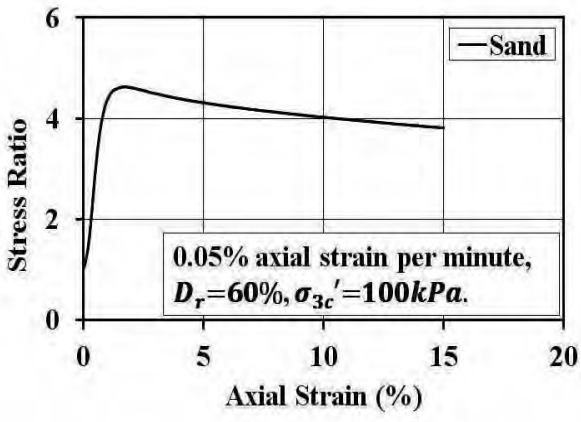

(d)

Figure A. 13. (a) Stress-strain response, (b) excess pore pressure response, (c) effective stress path and (d) stress ratio verses axial strain graph of sand specimen at D_r=60%.

APPENDIX B

CYCLIC TRIAXIAL TESTS RESULT

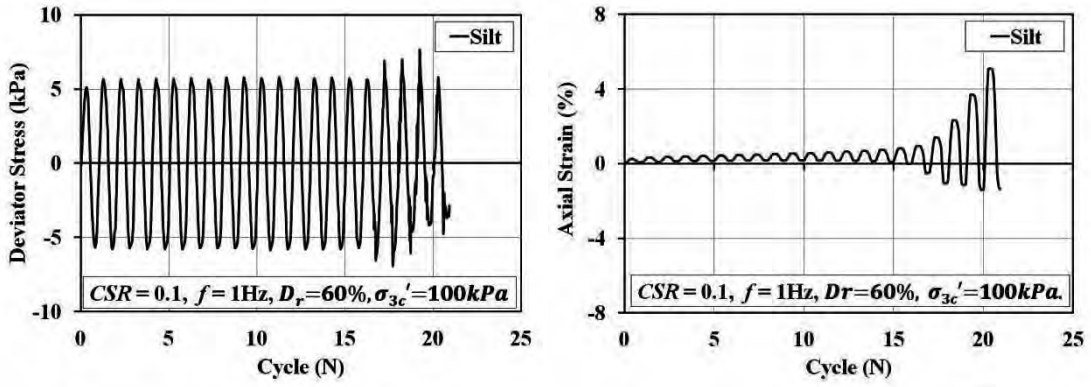

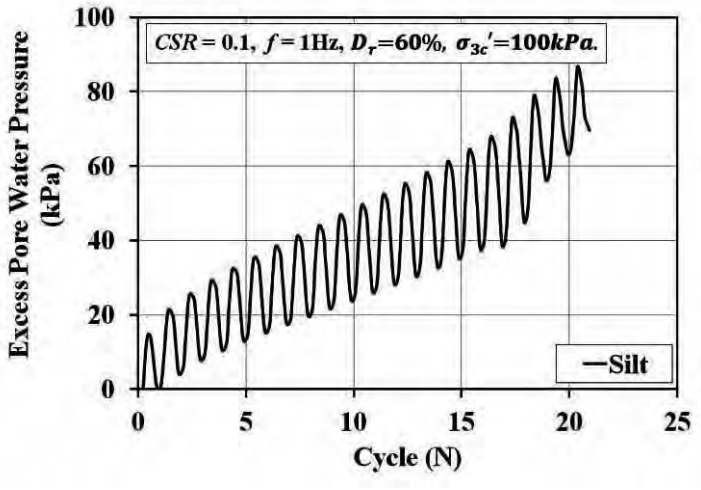

(c)

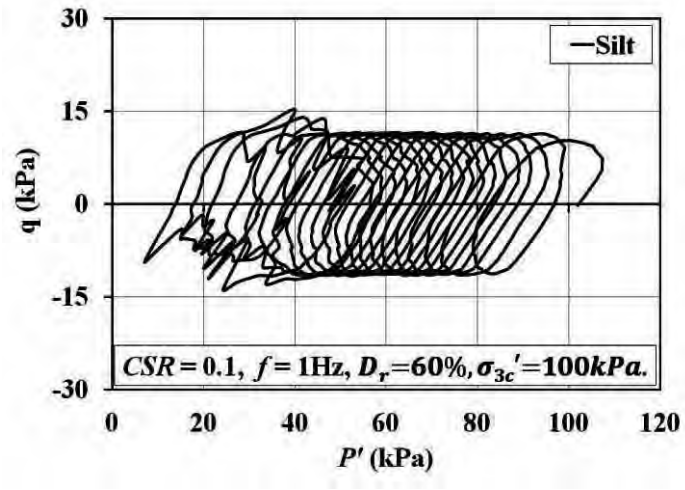

(d)

Figure B. 1. (a) Deviator stress verses cycles, (b) axial strain verses cycles, (c) excess pore water pressure response and (d) effective stress path of silt specimen at D_r=60%, *CSR= 0.1, f* = 1Hz.

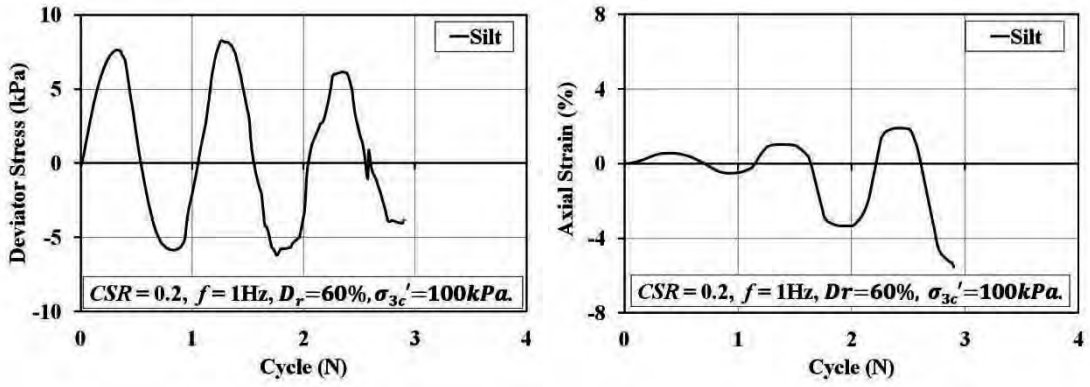

(a) (b)

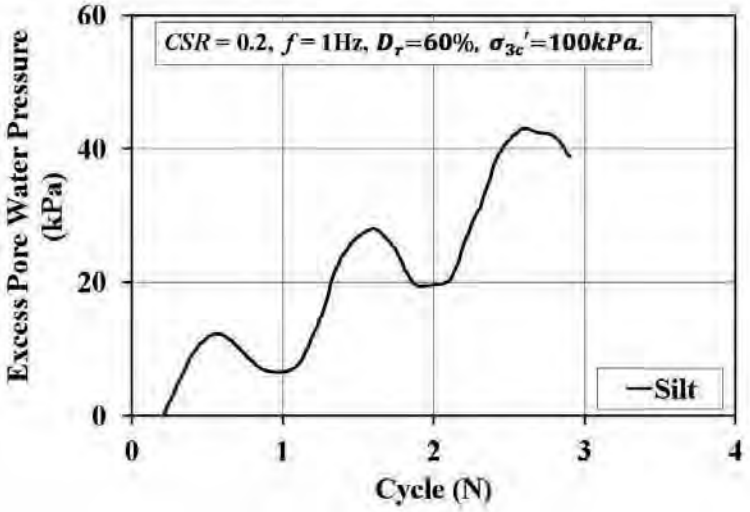

(c)

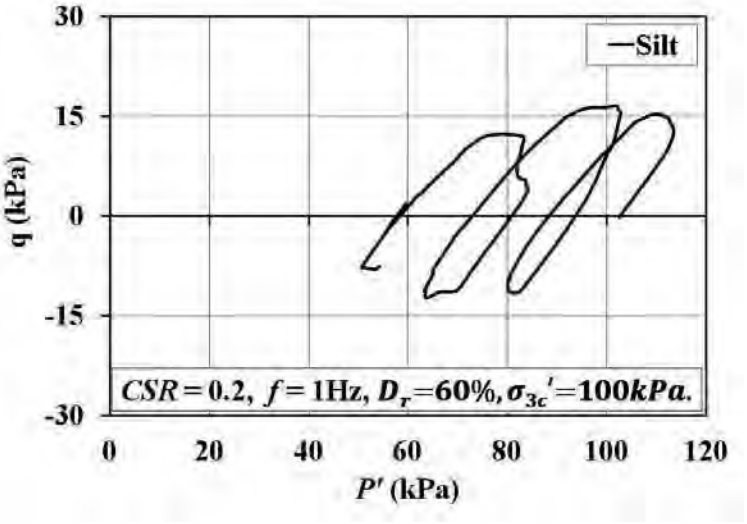

(d)

Figure B. 2. (a) Deviator stress verses cycles, (b) axial strain verses cycles, (c) excess pore water pressure response and (d) effective stress path of silt specimen at D_r=60%, *CSR= 0.2, f* = 1Hz.

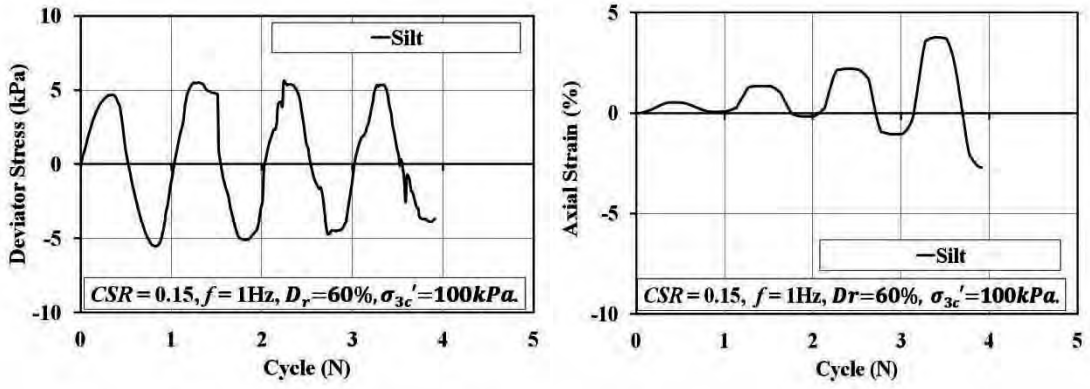

(a)

(b)

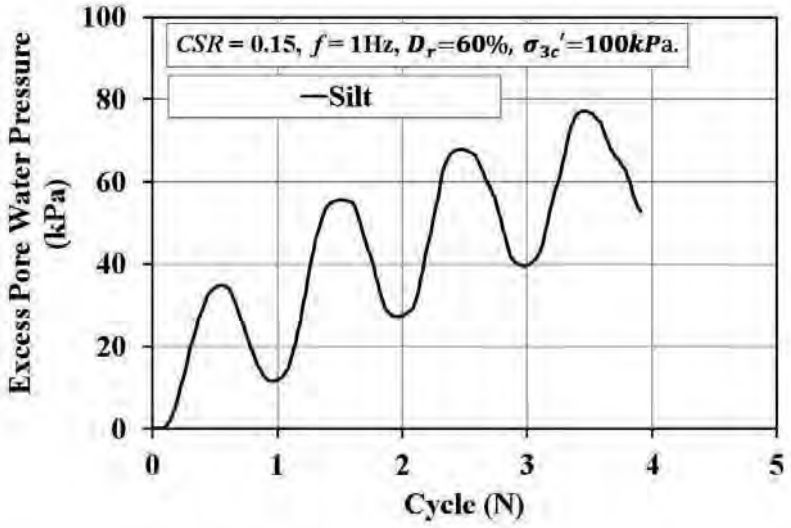

(c)

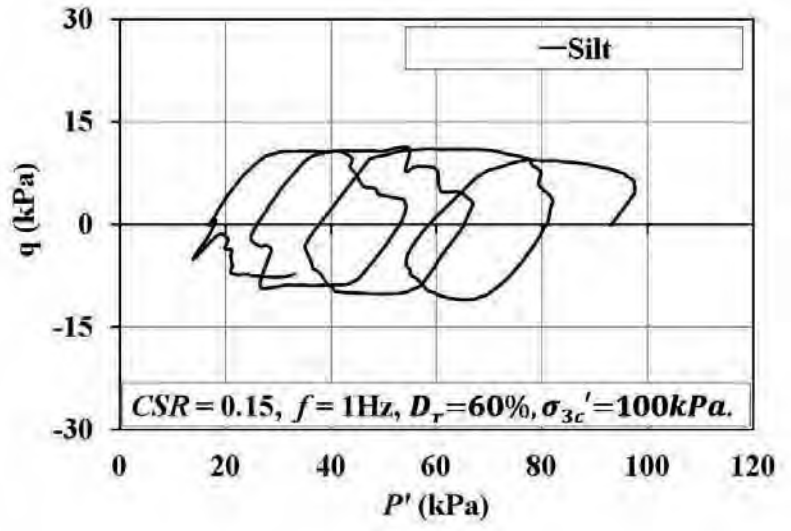

(d)

Figure B. 3. (a) Deviator stress verses cycles, (b) axial strain verses cycles, (c) excess pore water pressure response and (d) effective stress path of silt specimen at D_r=60%, *CSR= 0.15, f =* 1Hz.

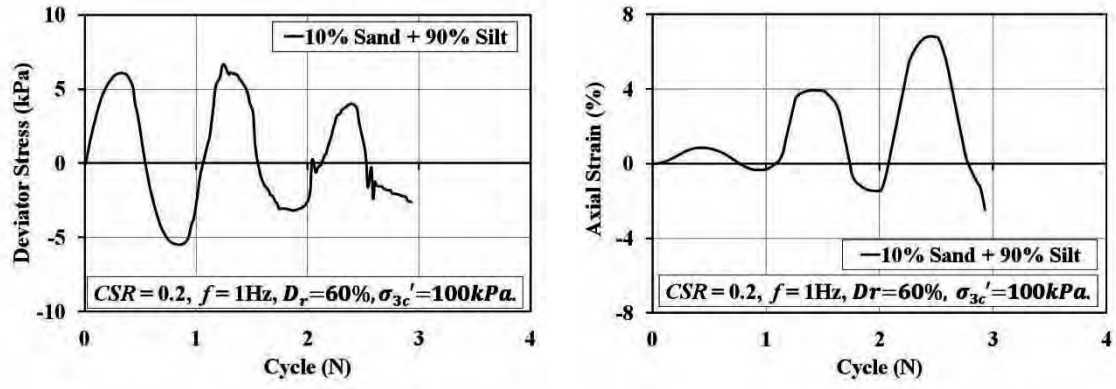

(a) (b)

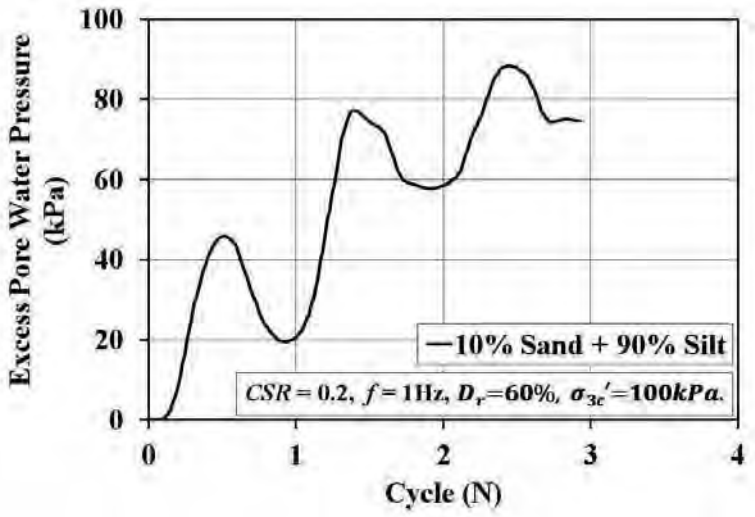

(c)

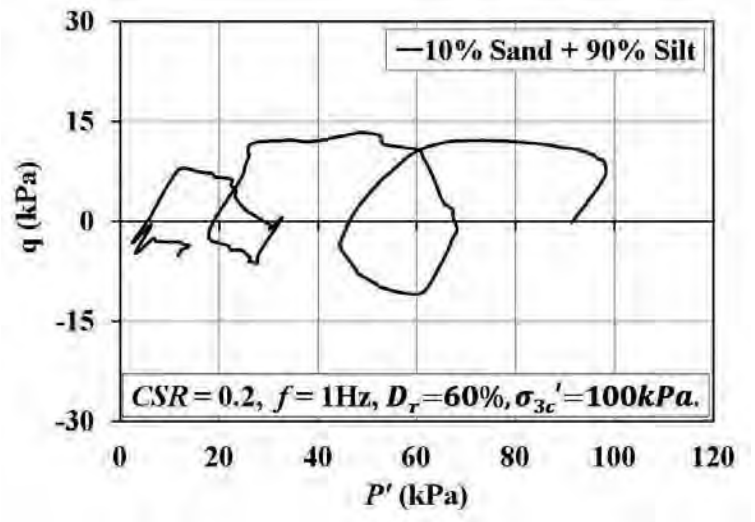

(d)

Figure B. 4. (a) Deviator stress verses cycles, (b) axial strain verses cycles, (c) excess pore water pressure response and (d) effective stress path of 10% sand + 90% silt specimen at D_r=60%, *CSR= 0.2, f* = 1Hz.

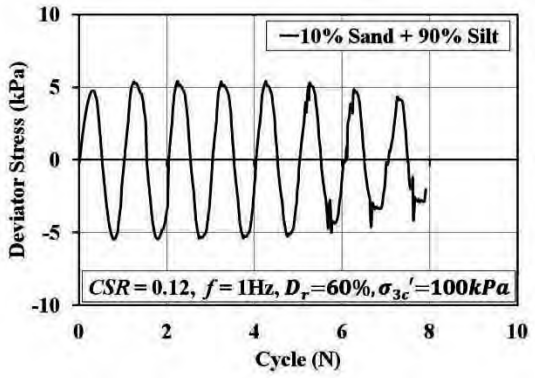

(a)

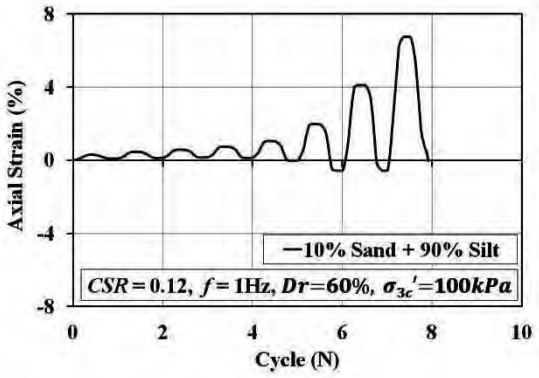

(b)

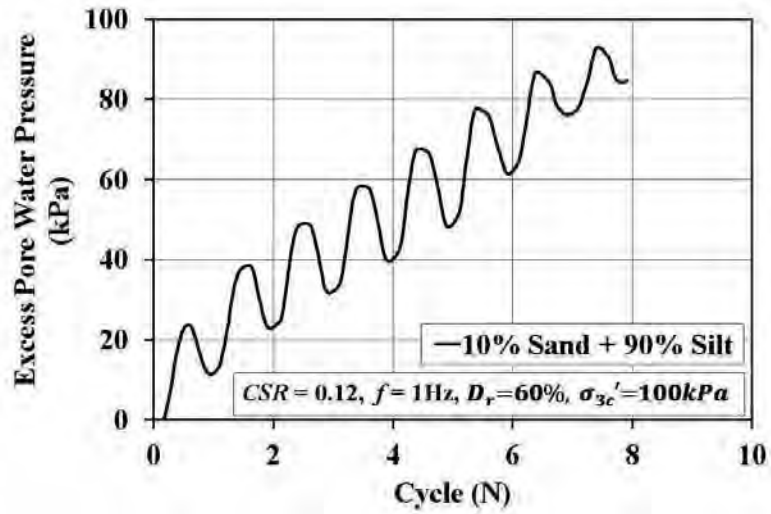

(c)

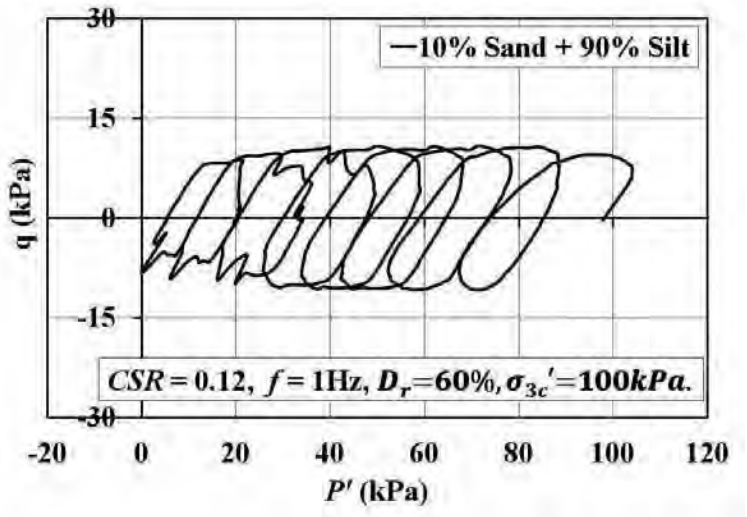

(d)

Figure B. 5. (a) Deviator stress verses cycles, (b) axial strain verses cycles, (c) excess pore water pressure response and (d) effective stress path of 10% sand + 90% silt specimen at D_r=60%, *CSR= 0.12, f* = 1Hz.

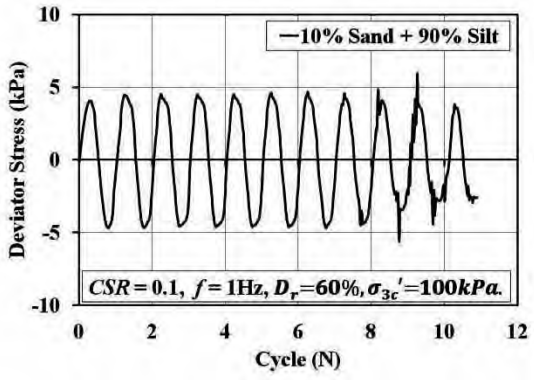

(a)

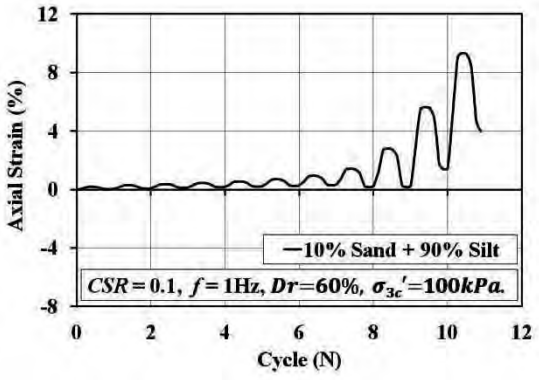

(b)

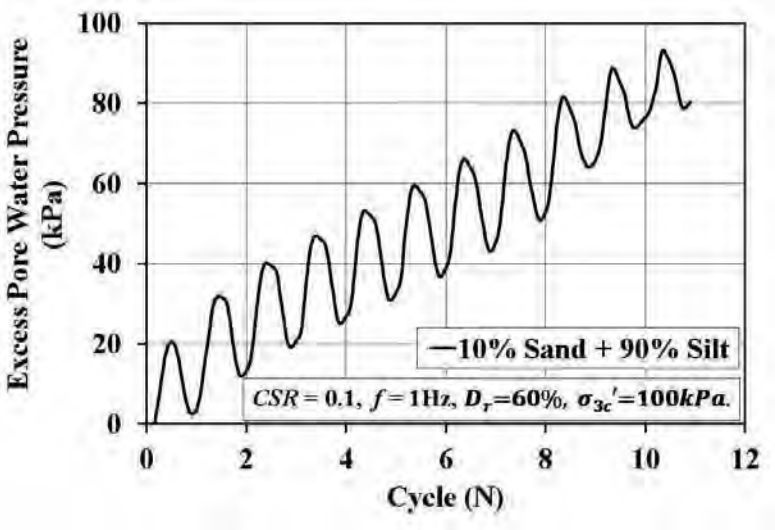

(c)

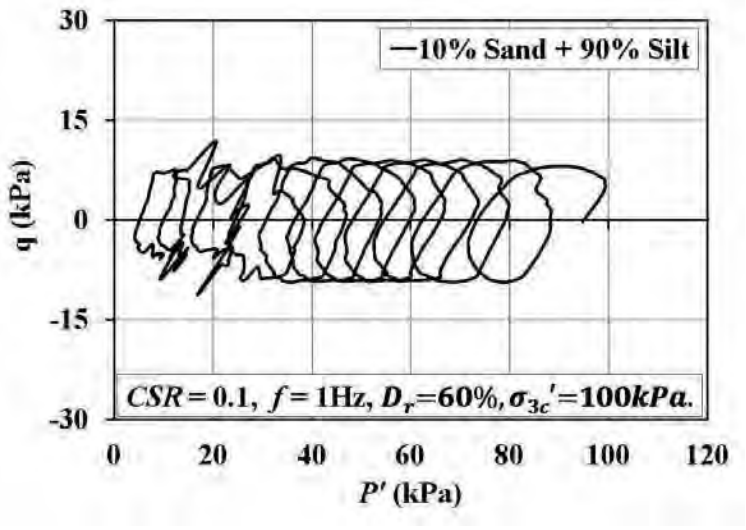

(d)

Figure B. 6. (a) Deviator stress verses cycles, (b) axial strain verses cycles, (c) excess pore water pressure response and (d) effective stress path of 10% sand + 90% silt specimen at D_r=60%, *CSR= 0.1, f* = 1Hz.

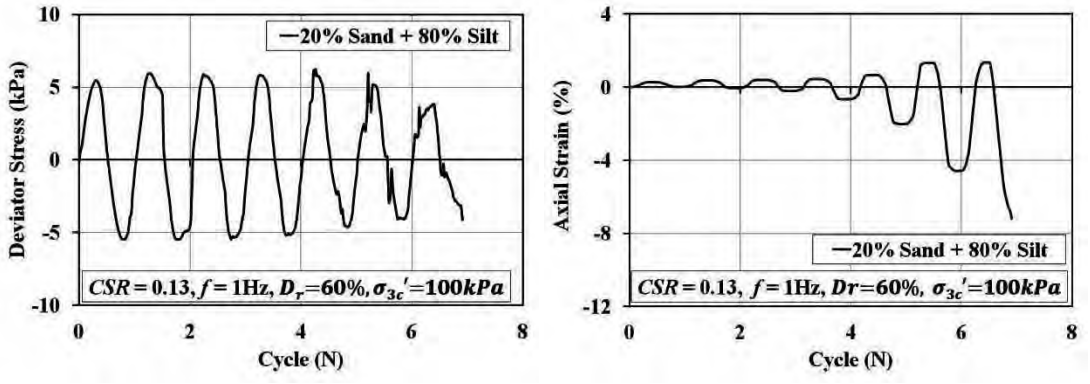

(a)

(b)

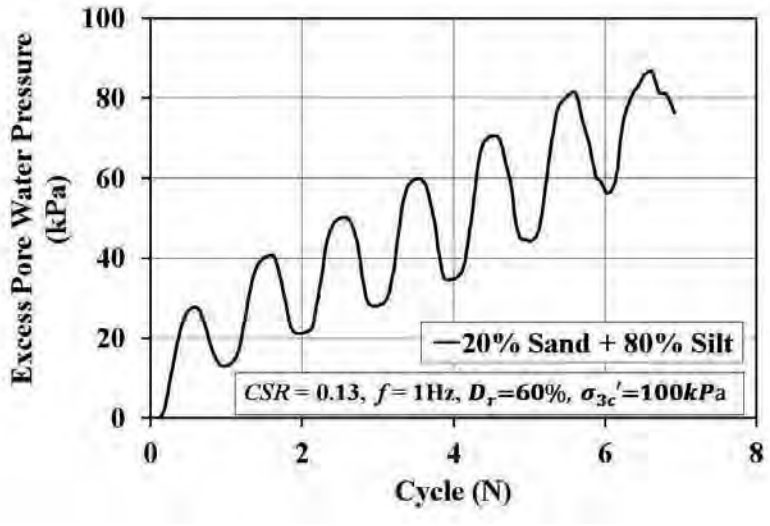

(c)

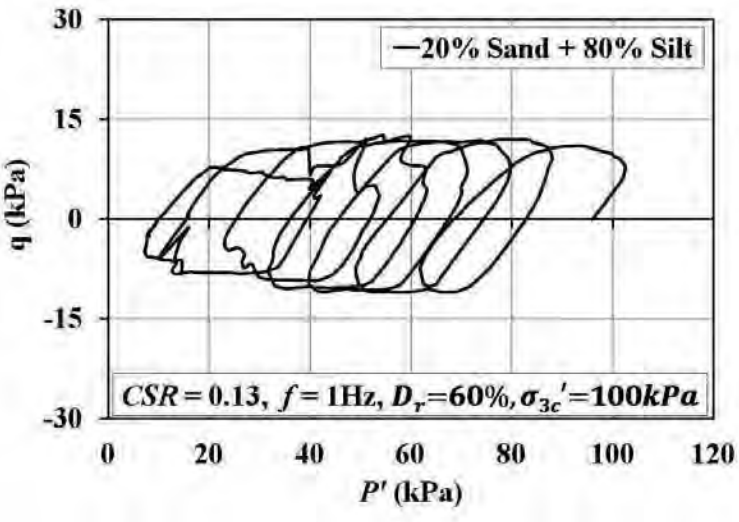

(d)

Figure B. 7. (a) Deviator stress verses cycles, (b) axial strain verses cycles, (c) excess pore water pressure response and (d) effective stress path of 20% sand + 80% silt specimen at D_r=60%, *CSR= 0.13, f* = 1Hz.

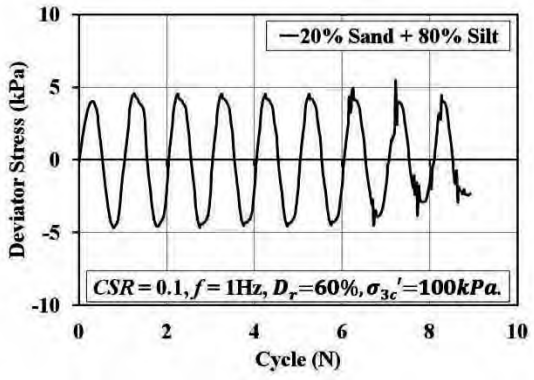

(a)

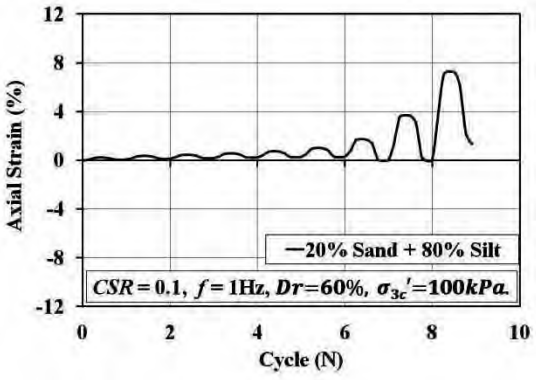

(b)

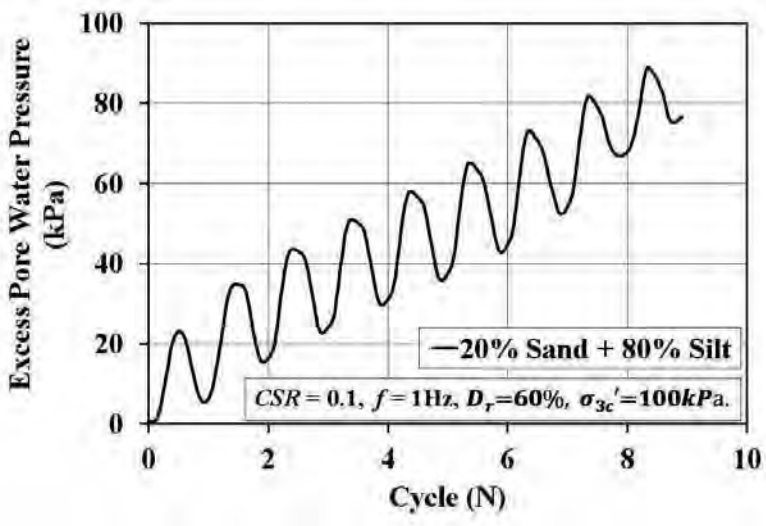

(c)

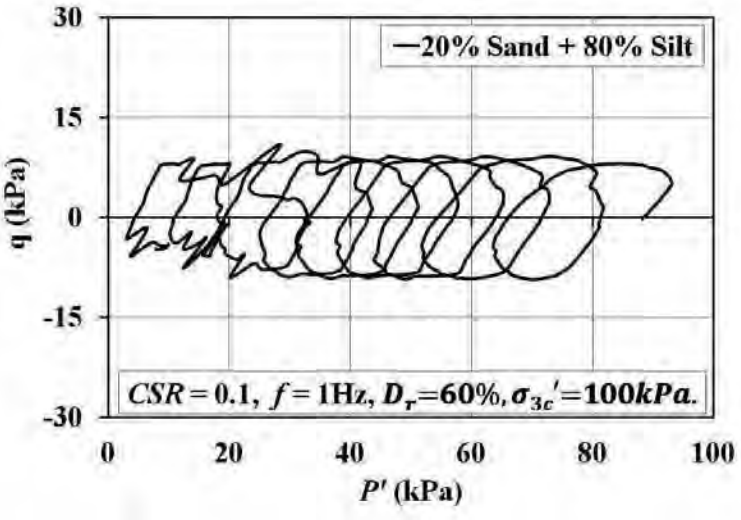

(d)

Figure B. 8. (a) Deviator stress verses cycles, (b) axial strain verses cycles, (c) excess pore water pressure response and (d) effective stress path of 20% sand + 80% silt specimen at D_r=60%, *CSR= 0.1, f* = 1Hz.

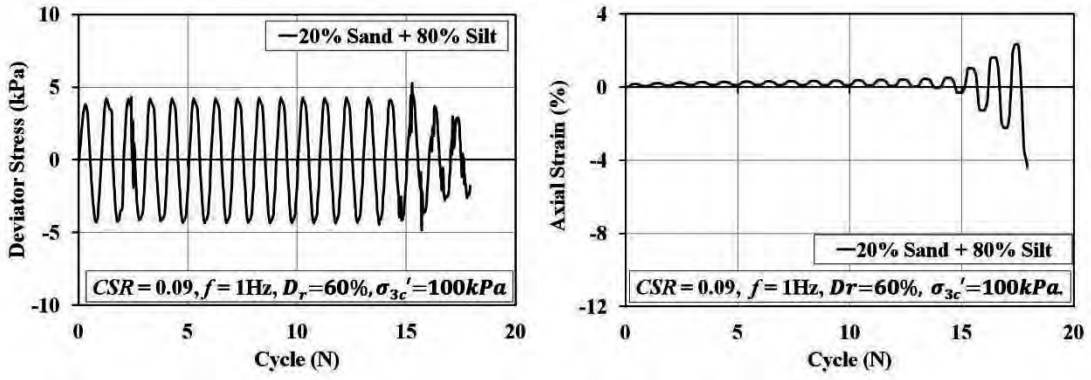

(a) (b)

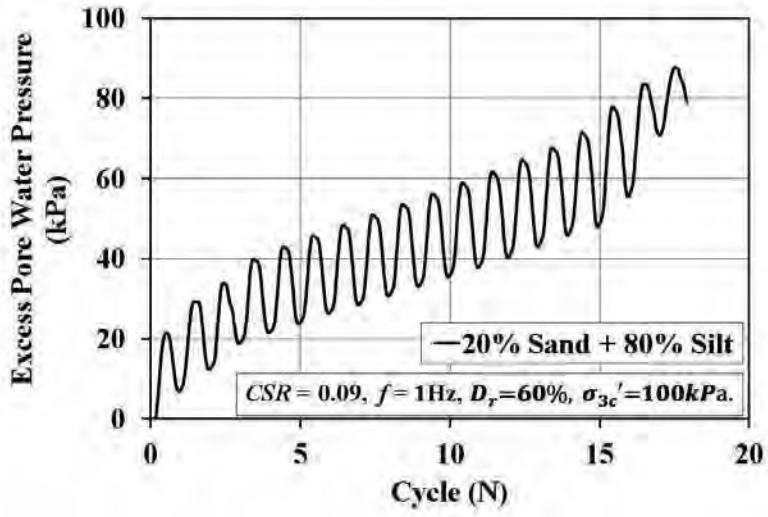

(c)

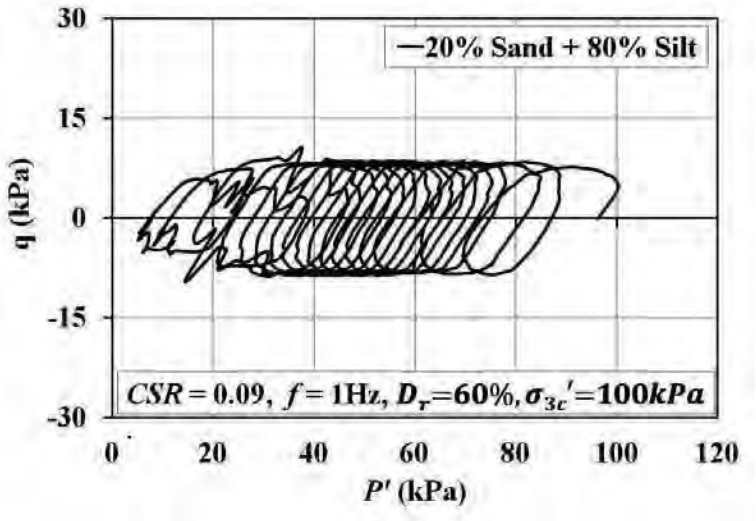

(d)

Figure B. 9. (a) Deviator stress verses cycles, (b) axial strain verses cycles, (c) excess pore water pressure response and (d) effective stress path of 20% sand + 80% silt specimen at D_r=60%, *CSR= 0.09, f* = 1Hz.

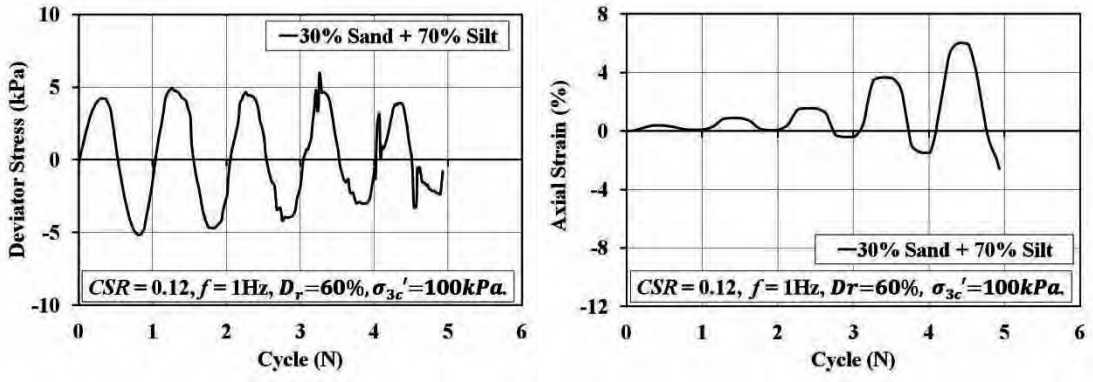

(a)

(b)

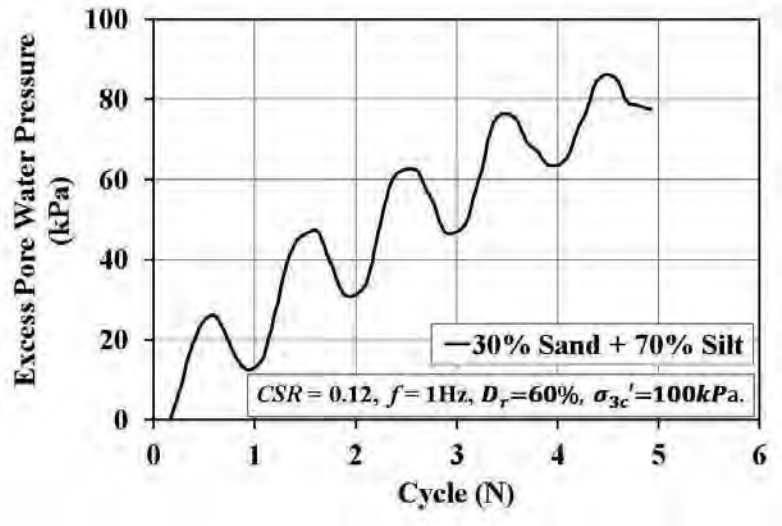

(c)

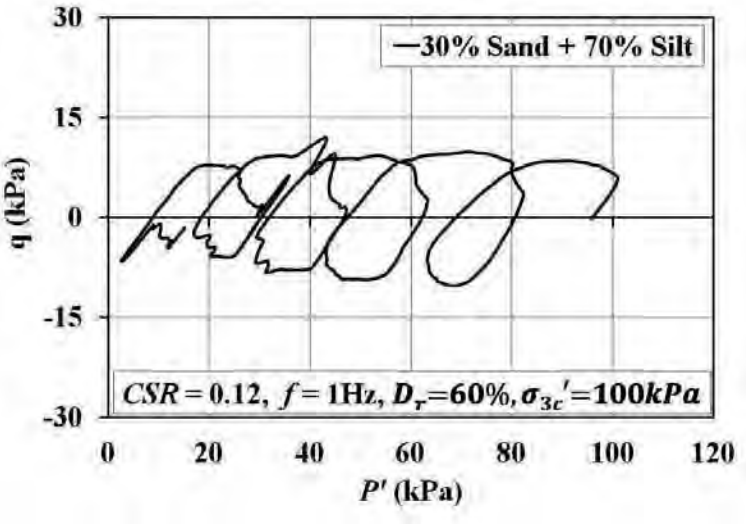

(d)

Figure B. 10. (a) Deviator stress verses cycles, (b) axial strain verses cycles, (c) excess pore water pressure response and (d) effective stress path of 30% sand + 70% silt specimen at D_r=60%, *CSR= 0.12, f* = 1Hz.

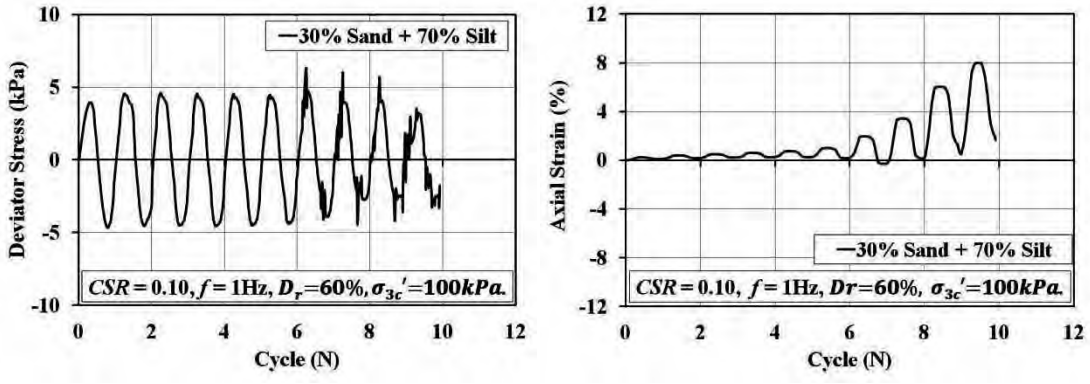

(a)

(b)

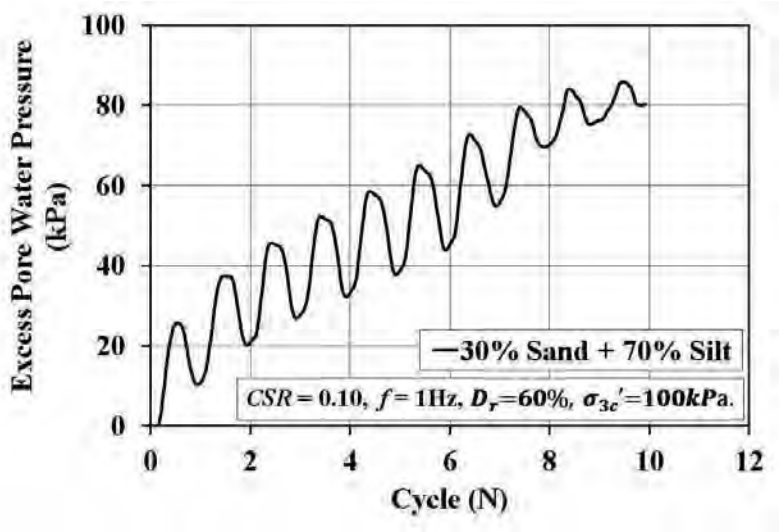

(c)

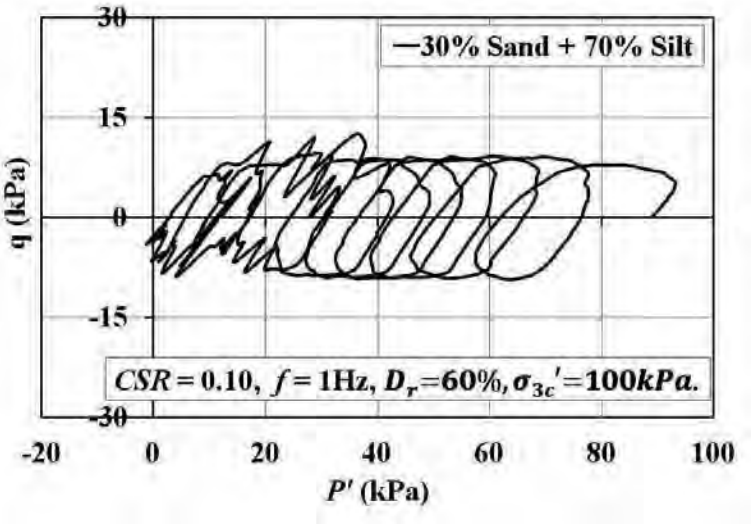

(d)

Figure B. 11. (a) Deviator stress verses cycles, (b) axial strain verses cycles, (c) excess pore water pressure response and (d) effective stress path of 30% sand + 70% silt specimen at D_r=60%, *CSR= 0.10, f* = 1Hz.

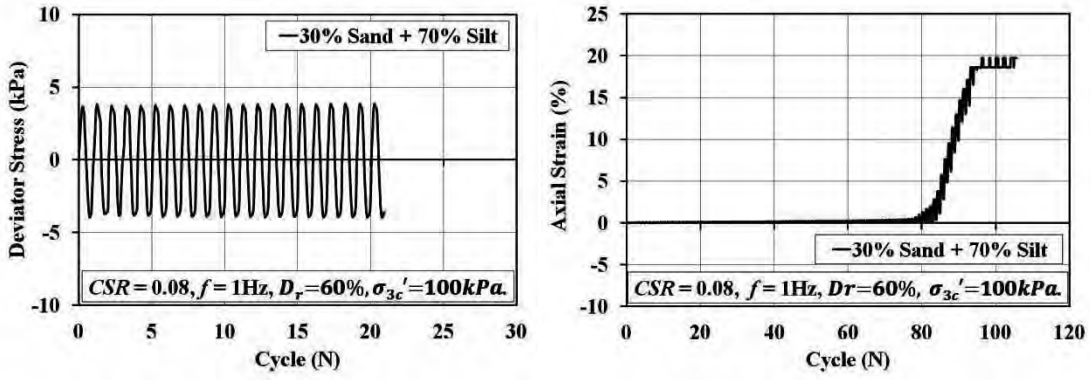

(a) (b)

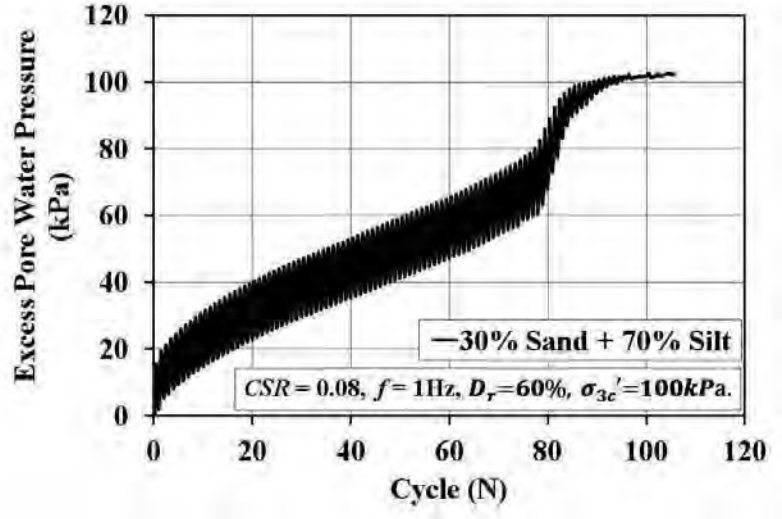

(c)

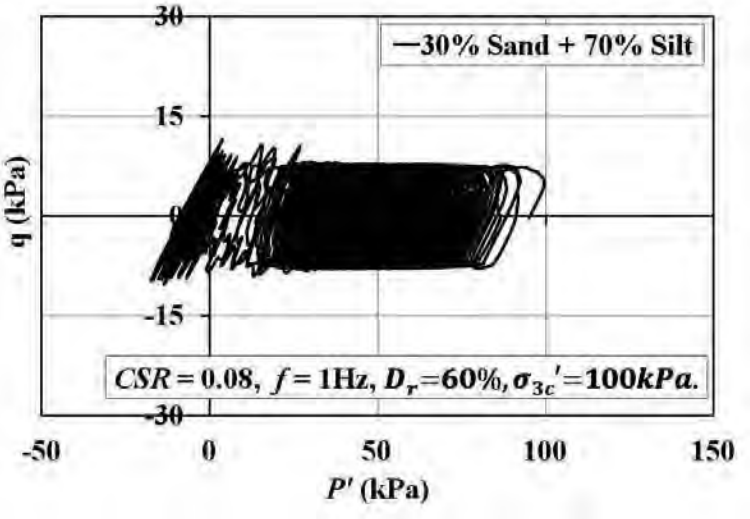

(d)

Figure B. 12. (a) Deviator stress verses cycles, (b) axial strain verses cycles, (c) excess pore water pressure response and (d) effective stress path of 30% sand + 70% silt specimen at D_r=60%, *CSR= 0.08, f* = 1Hz.

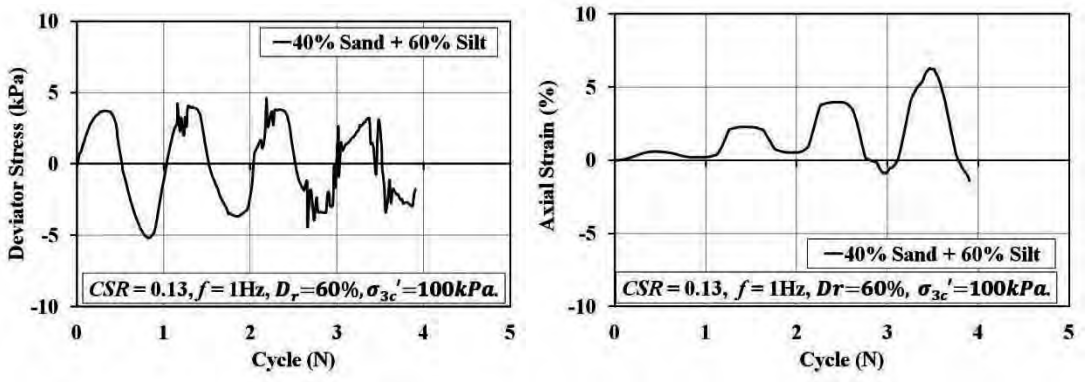

(a)

(b)

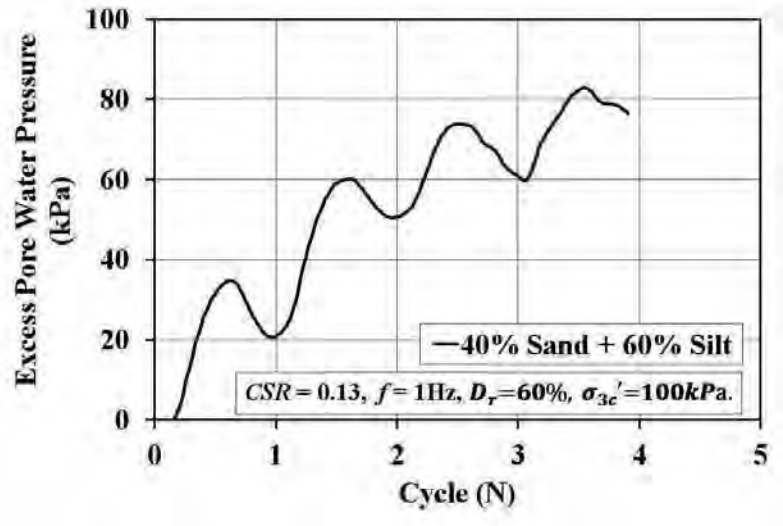

(c)

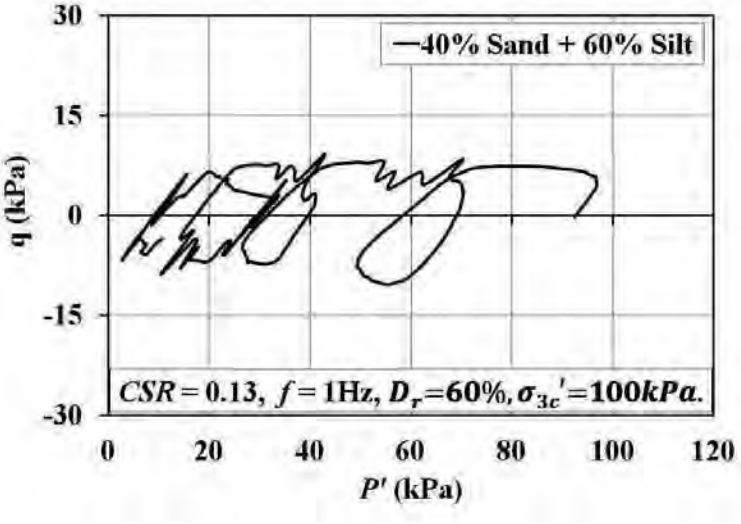

(d)

Figure B. 13. (a) Deviator stress verses cycles, (b) axial strain verses cycles, (c) excess pore water pressure response and (d) effective stress path of 40% sand + 60% silt specimen at D_r=60%, *CSR= 0.13, f* = 1Hz.

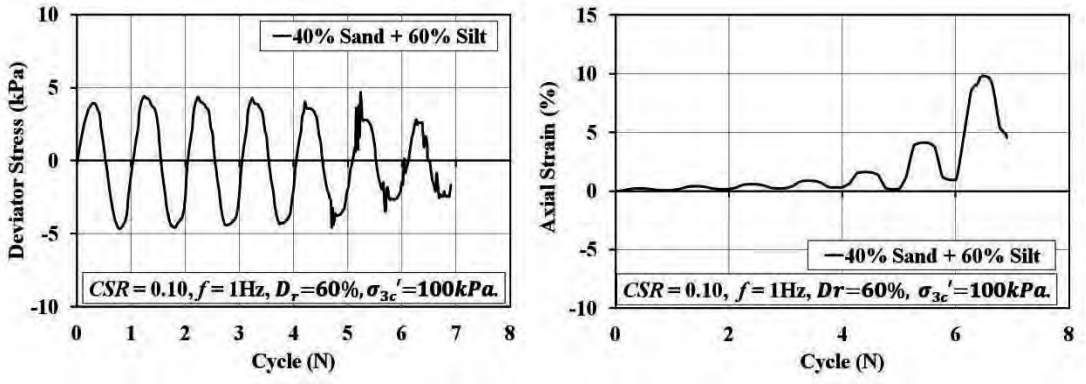

(a)

(b)

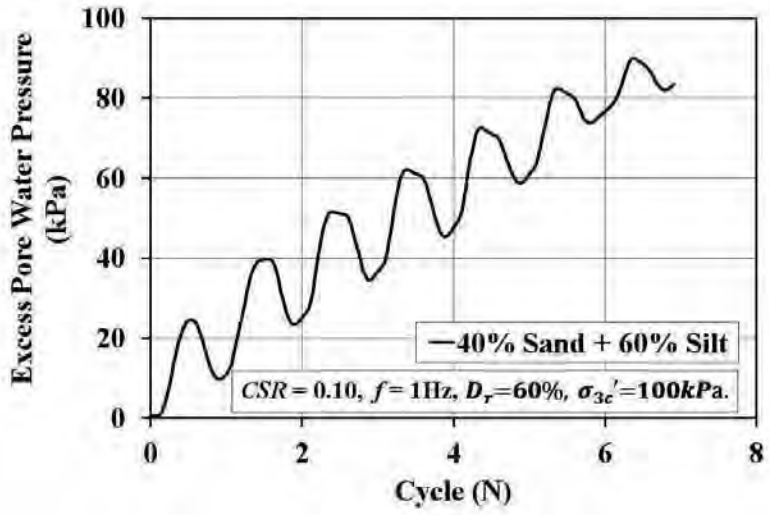

(c)

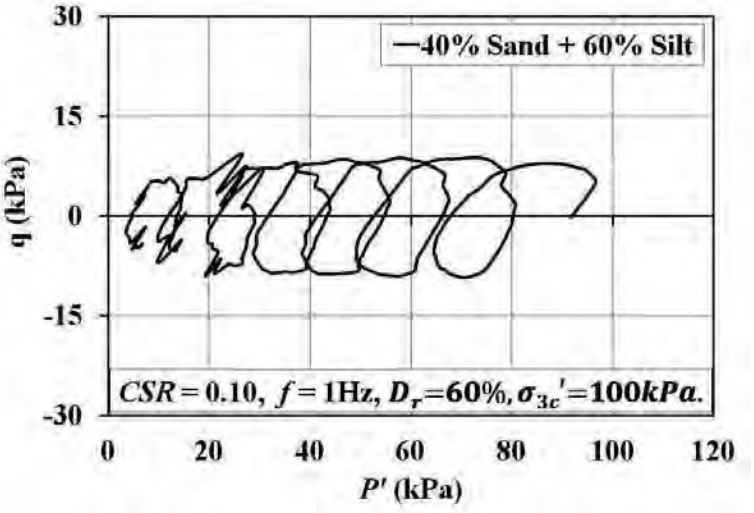

(d)

Figure B. 14. (a) Deviator stress verses cycles, (b) axial strain verses cycles, (c) excess pore water pressure response and (d) effective stress path of 40% sand + 60% silt specimen at D_r=60%, *CSR= 0.10, f* = 1Hz.

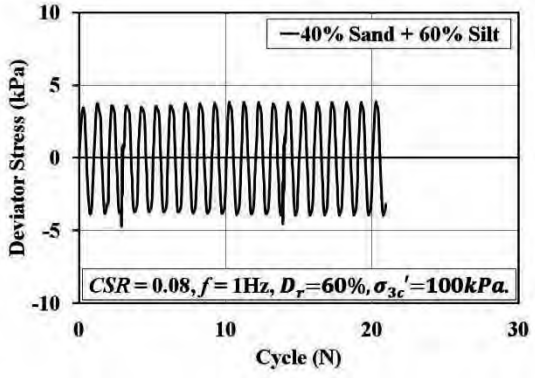

(a)

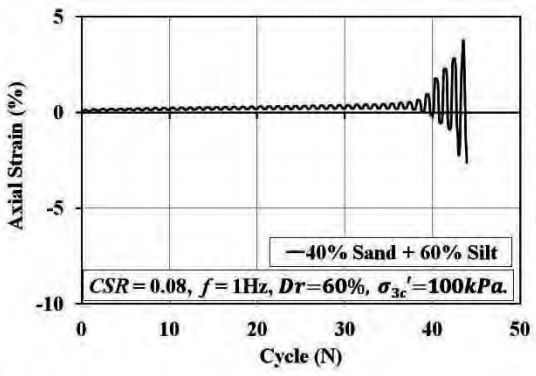

(b)

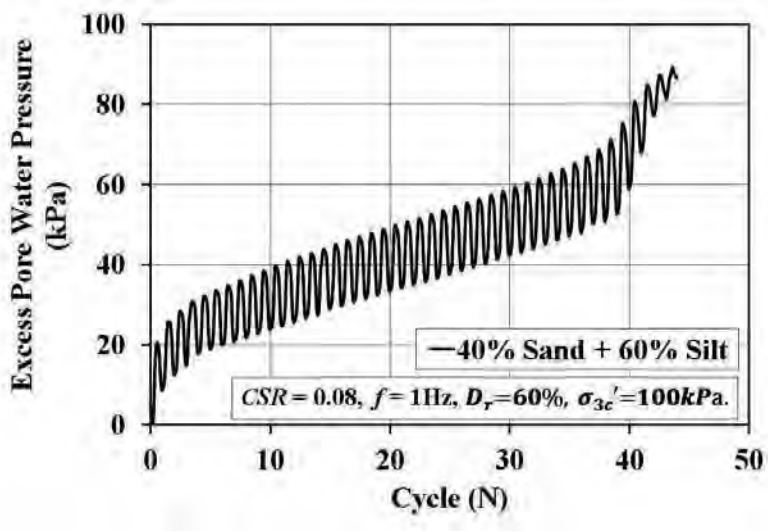

(c)

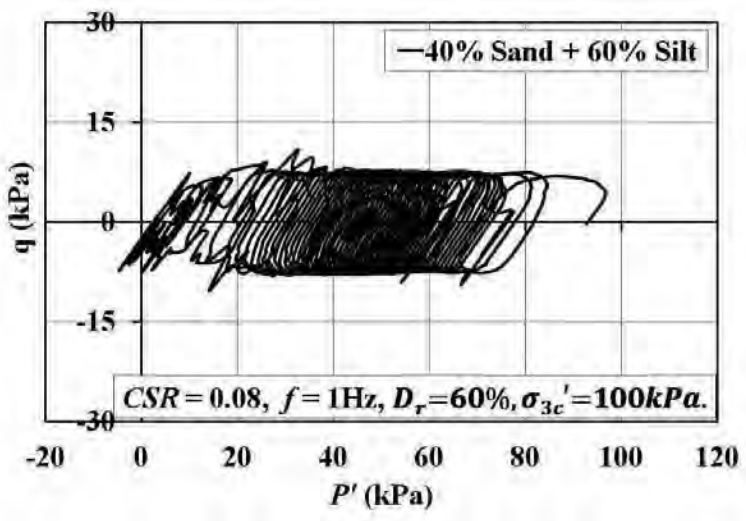

(d)

Figure B. 15. (a) Deviator stress verses cycles, (b) axial strain verses cycles, (c) excess pore water pressure response and (d) effective stress path of 40% sand + 60% silt specimen at D_r=60%, *CSR= 0.08, f* = 1Hz.

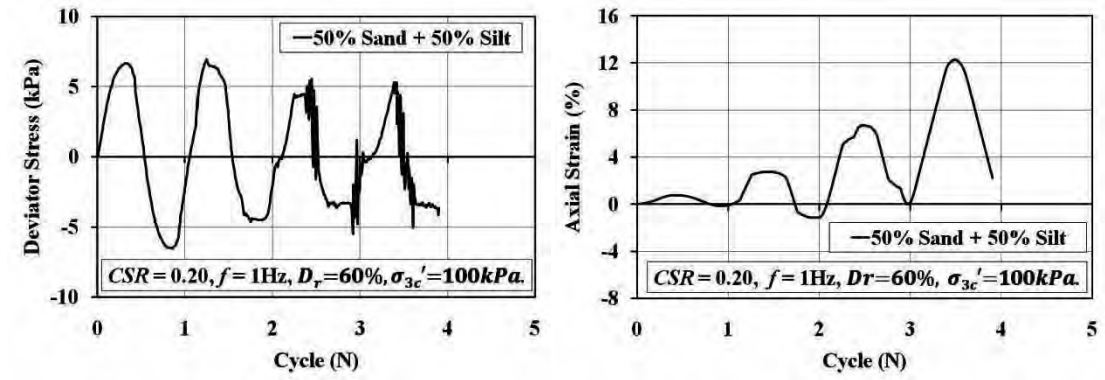

(a) (b)

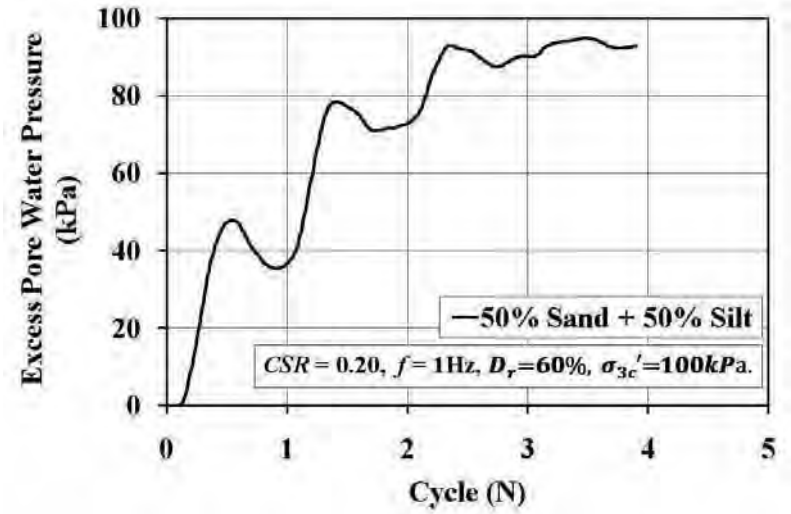

(c)

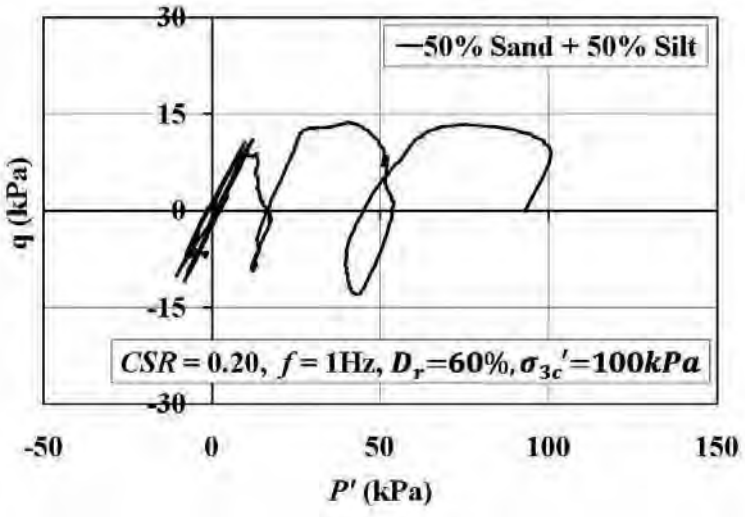

(d)

Figure B. 16. (a) Deviator stress verses cycles, (b) axial strain verses cycles, (c) excess pore water pressure response and (d) effective stress path of 50% sand + 50% silt specimen at D_r=60%, *CSR= 0.20, f* = 1Hz.

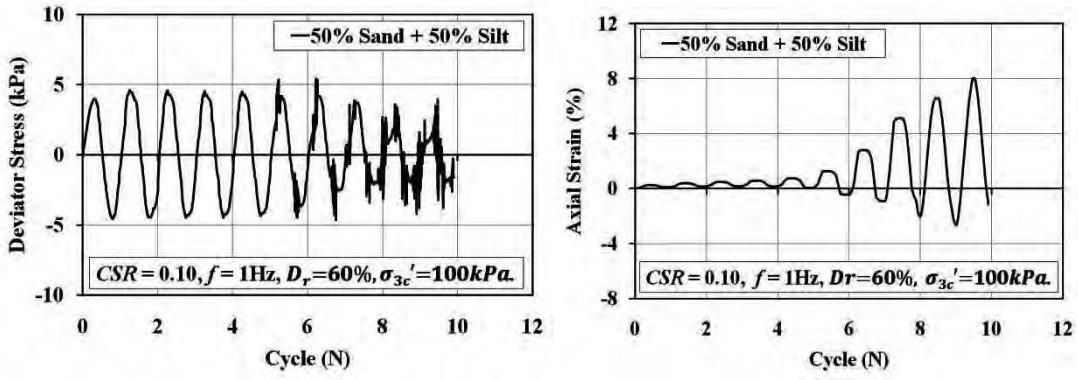

(a) (b)

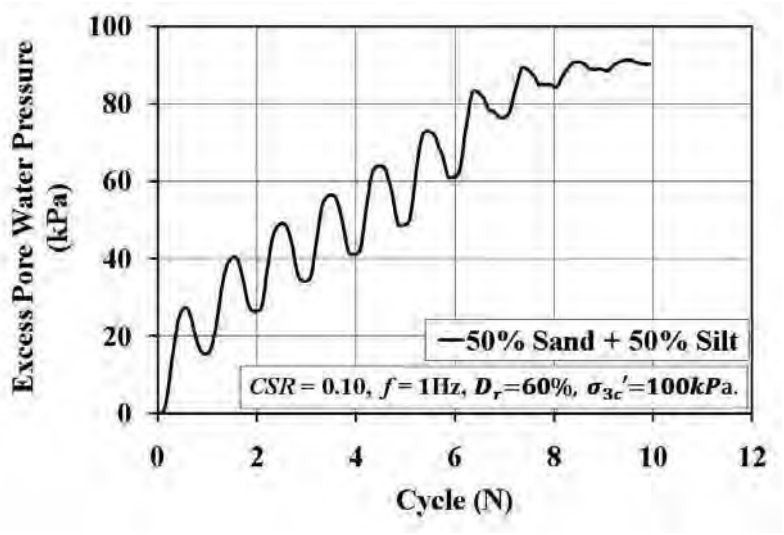

(c)

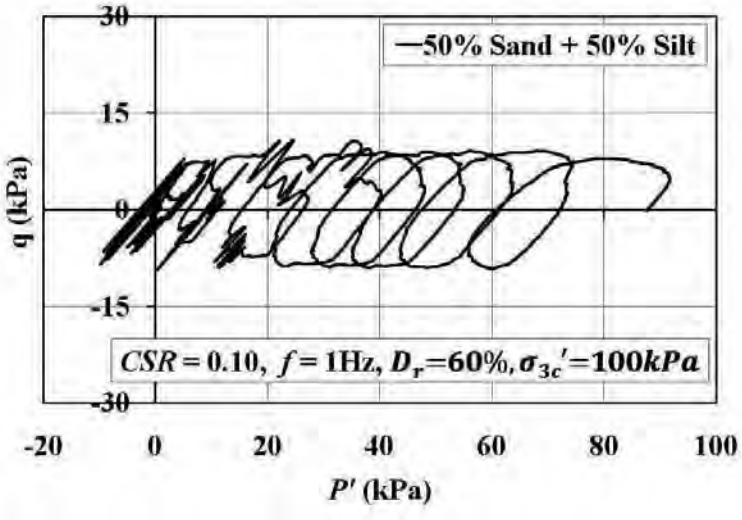

(d)

Figure B. 17. (a) Deviator stress verses cycles, (b) axial strain verses cycles, (c) excess pore water pressure response and (d) effective stress path of 50% sand + 50% silt specimen at D_r=60%, *CSR= 0.10, f* = 1Hz.

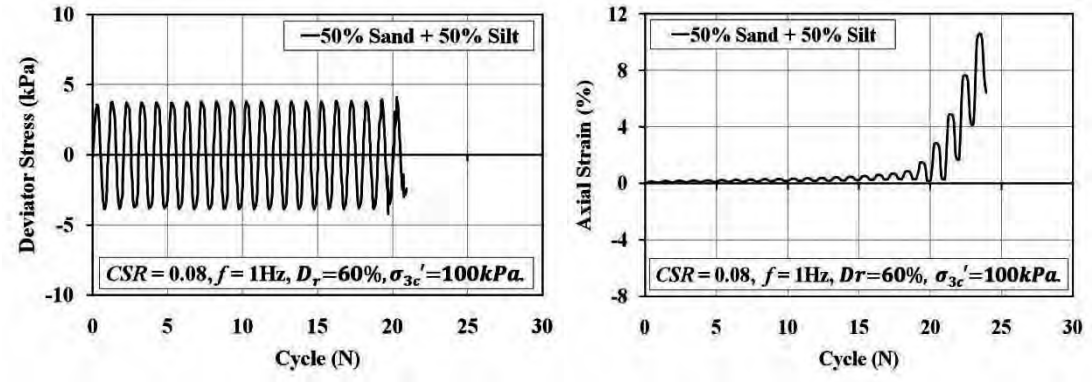

(a) (b)

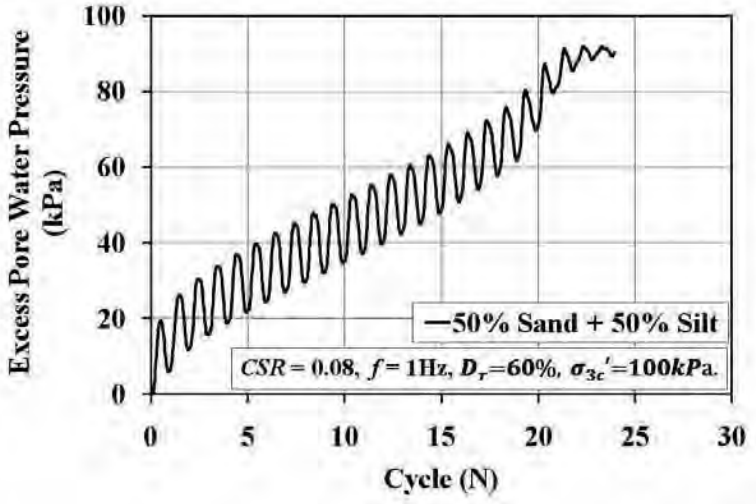

(c)

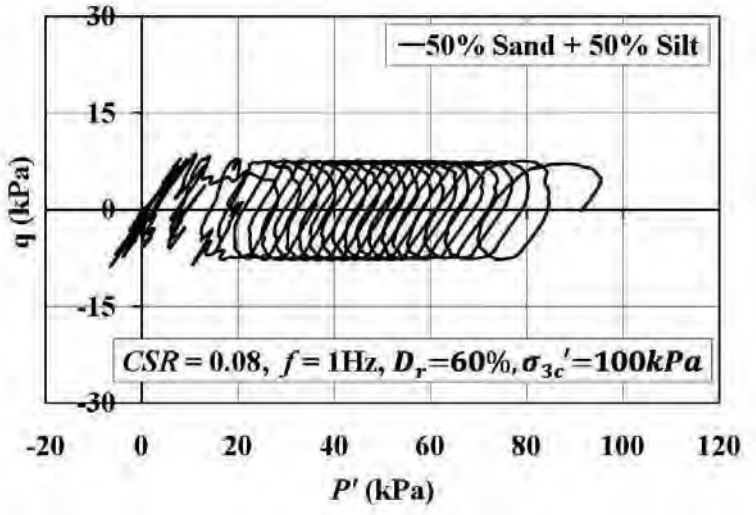

(d)

Figure B. 18. (a) Deviator stress verses cycles, (b) axial strain verses cycles, (c) excess pore water pressure response and (d) effective stress path of 50% sand + 50% silt specimen at D_r=60%, *CSR= 0.08, f* = 1Hz.

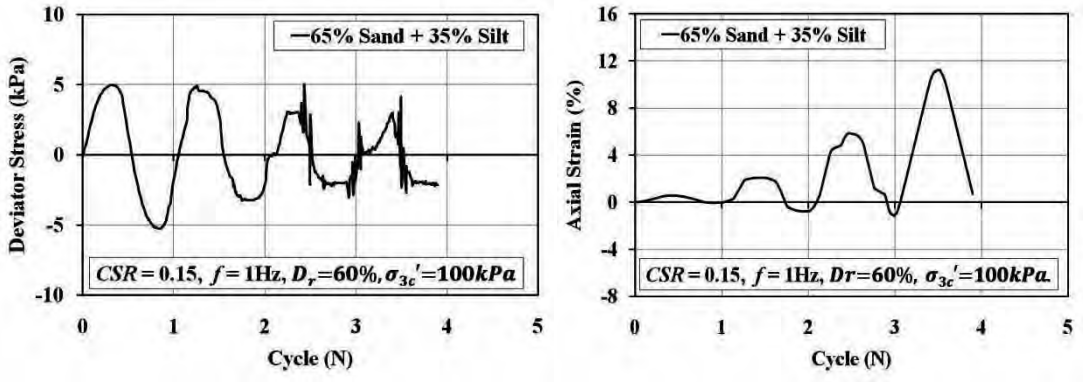

(a) (b)

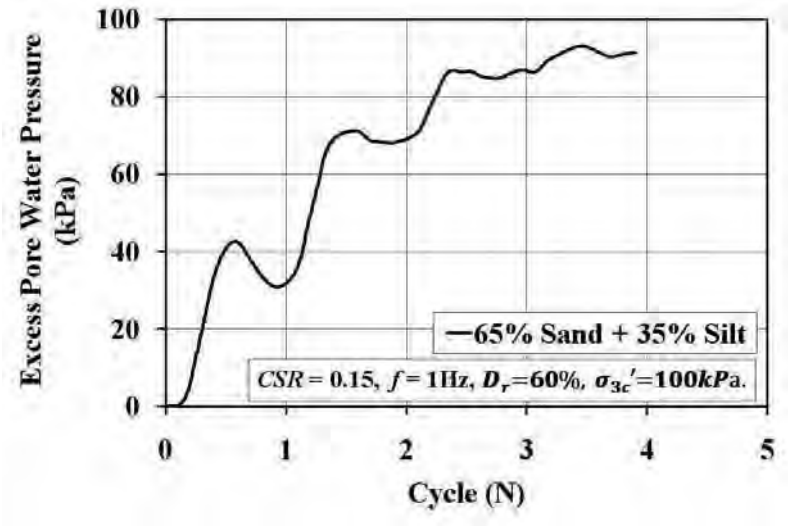

(c)

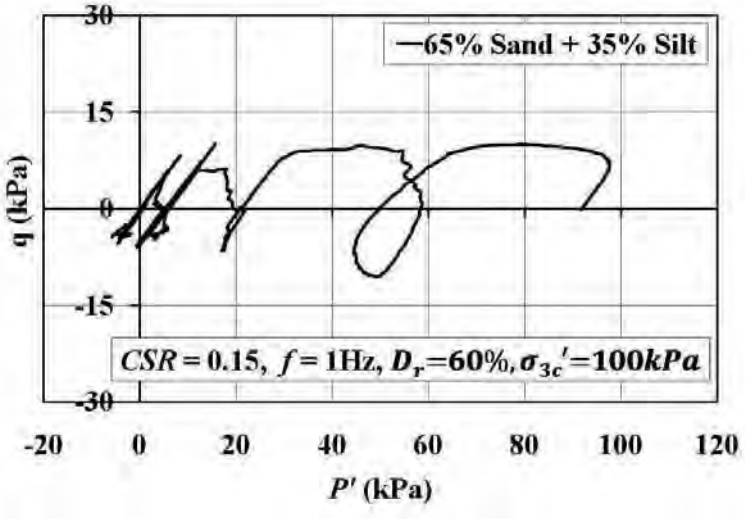

(d)

Figure B. 19. (a) Deviator stress verses cycles, (b) axial strain verses cycles, (c) excess pore water pressure response and (d) effective stress path of 65% sand + 35% silt specimen at D_r=60%, *CSR= 0.15, f* = 1Hz.

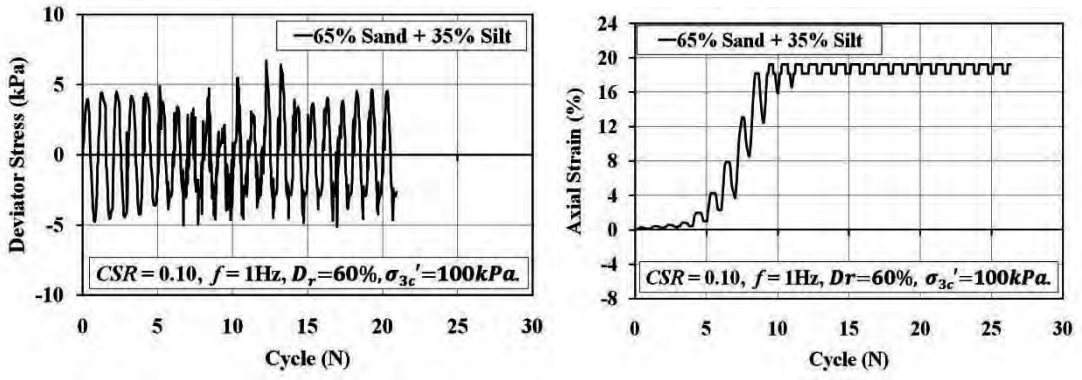

(a)

(b)

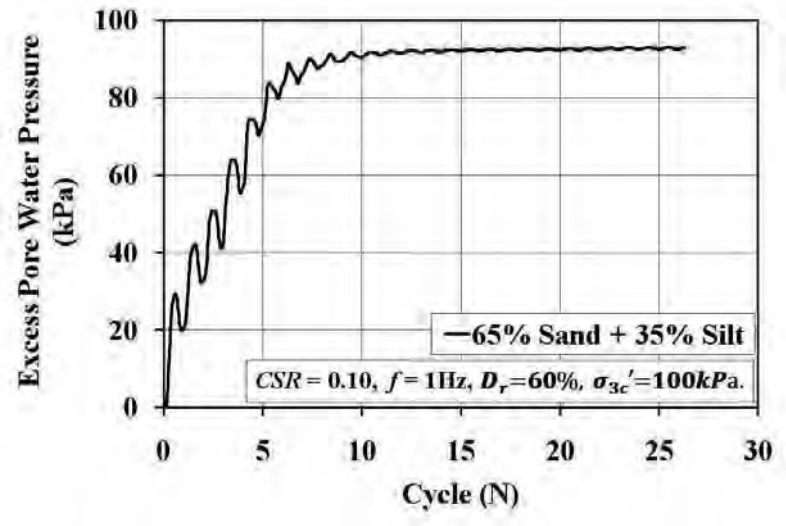

(c)

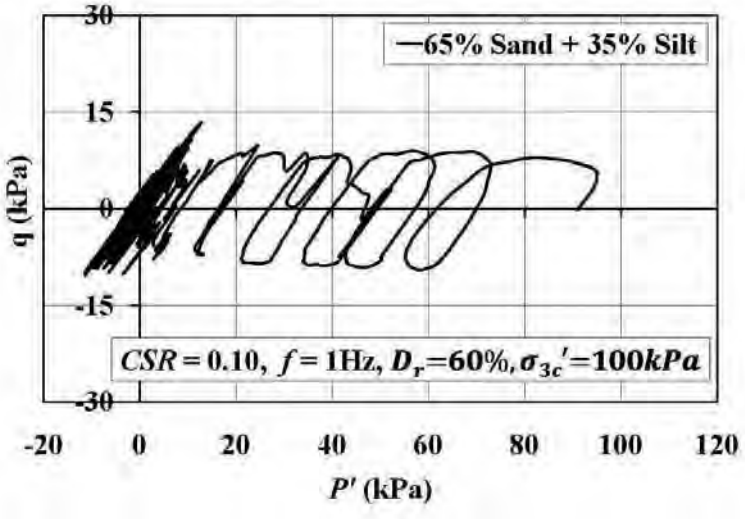

(d)

Figure B. 20. (a) Deviator stress verses cycles, (b) axial strain verses cycles, (c) excess pore water pressure response and (d) effective stress path of 65% sand + 35% silt specimen at D_r=60%, *CSR= 0.10, f* = 1Hz.

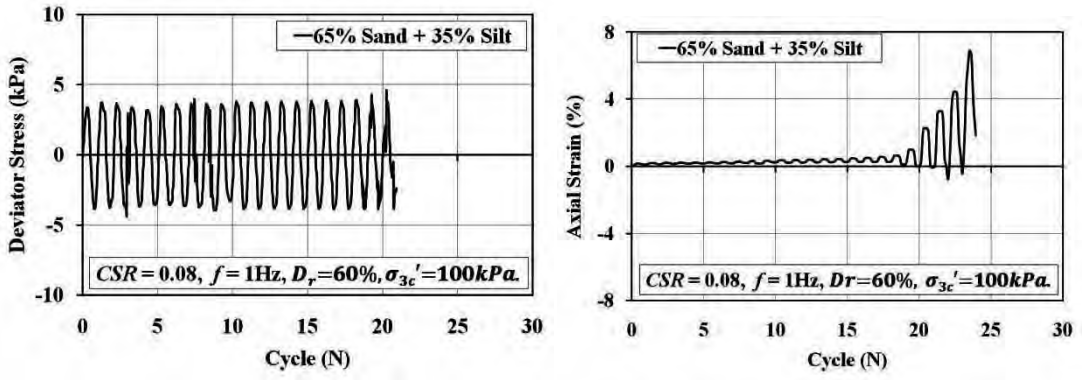

(a)

(b)

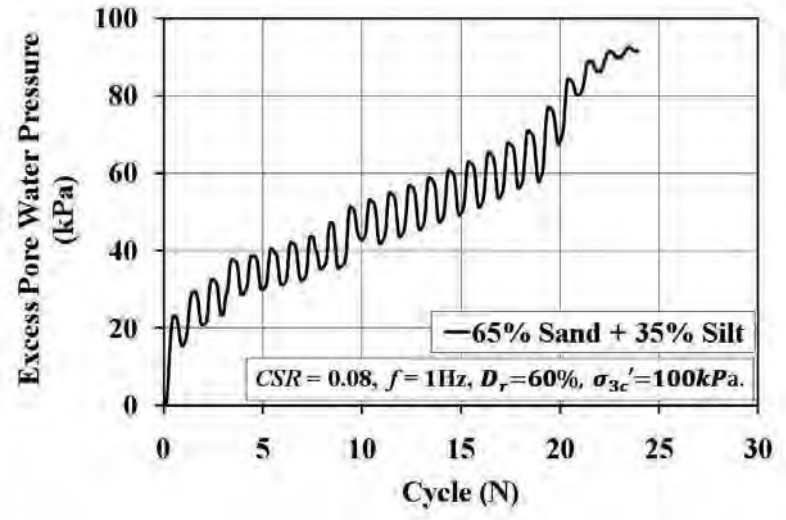

(c)

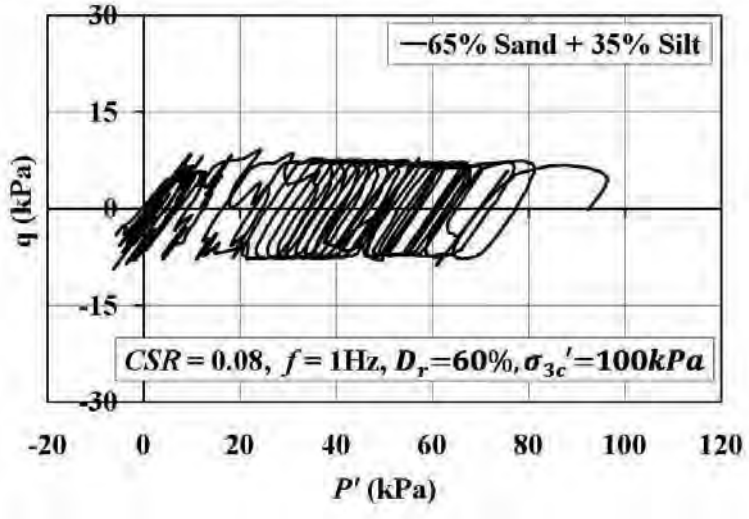

(d)

Figure B. 21. (a) Deviator stress verses cycles, (b) axial strain verses cycles, (c) excess pore water pressure response and (d) effective stress path of 65% sand + 35% silt specimen at D_r=60%, *CSR= 0.08, f* = 1Hz.

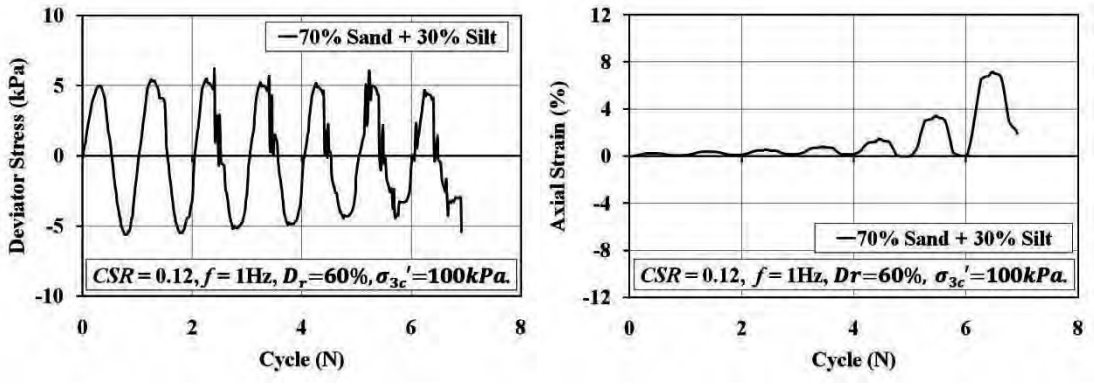

(a)

(b)

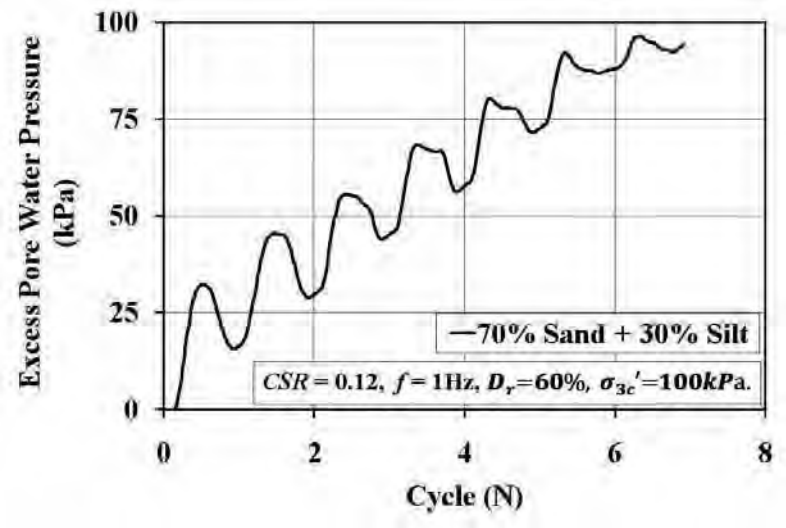

(c)

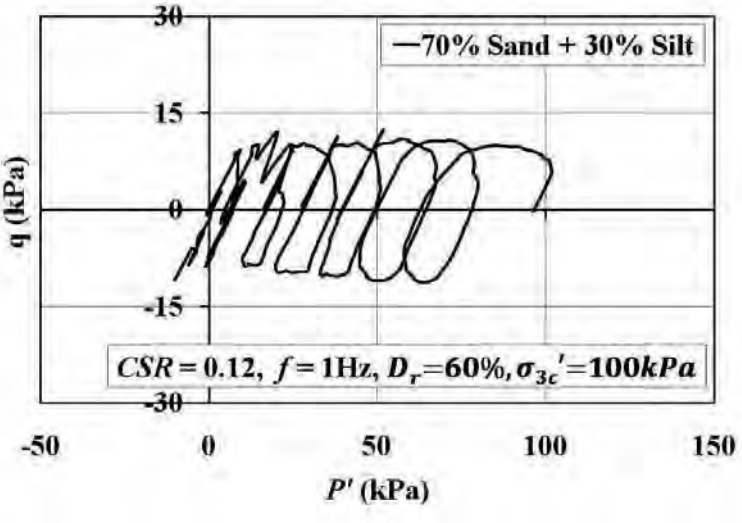

(d)

Figure B. 22. (a) Deviator stress verses cycles, (b) axial strain verses cycles, (c) excess pore water pressure response and (d) effective stress path of 70% sand + 30% silt specimen at D_r=60%, *CSR= 0.12, f* = 1Hz.

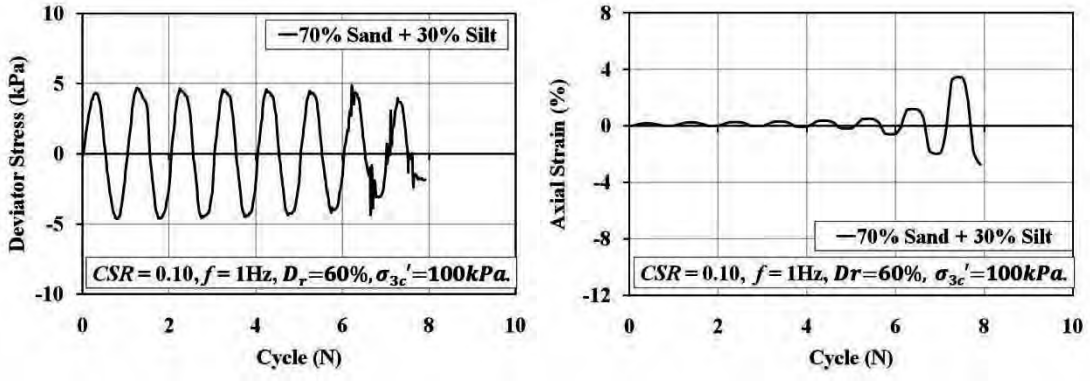

(a) (b)

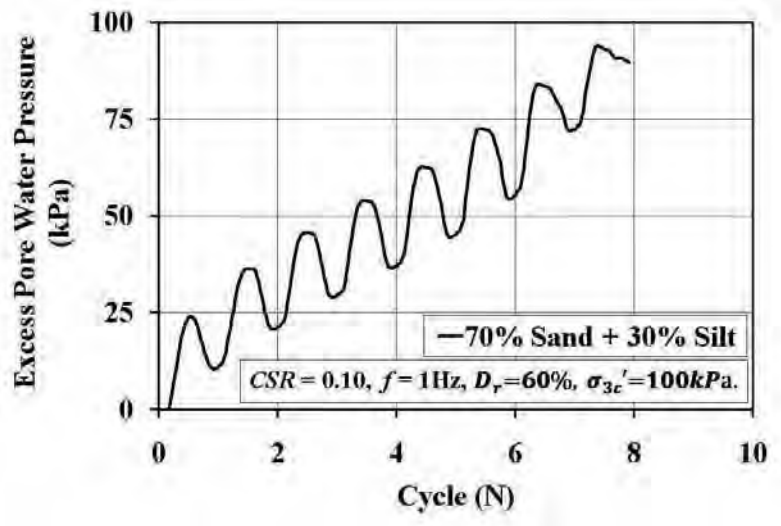

(c)

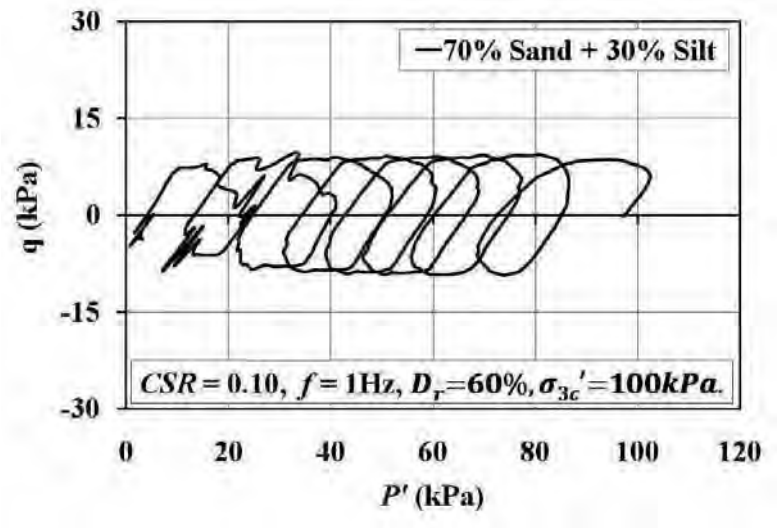

(d)

Figure B. 23. (a) Deviator stress verses cycles, (b) axial strain verses cycles, (c) excess pore water pressure response and (d) effective stress path of 70% sand + 30% silt specimen at D_r=60%, *CSR= 0.10, f* = 1Hz.

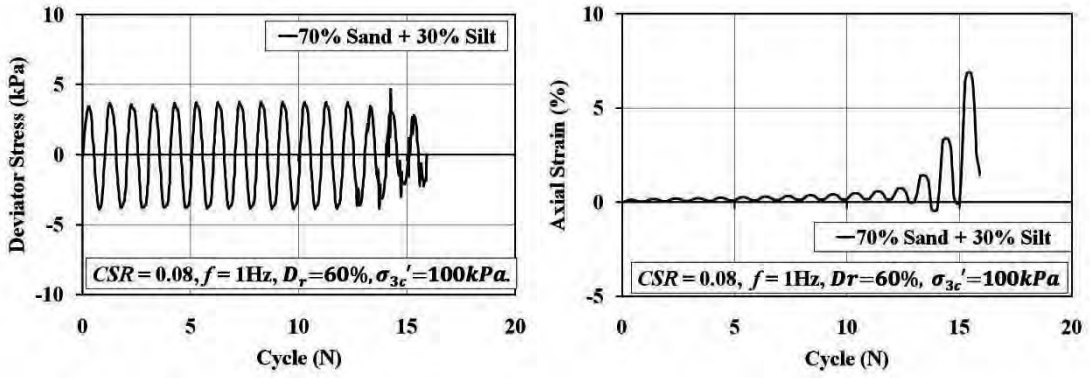

(a) (b)

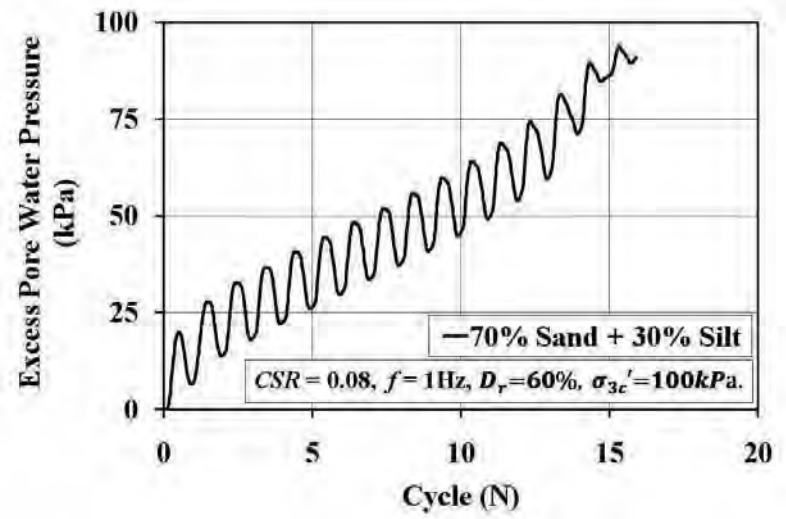

(c)

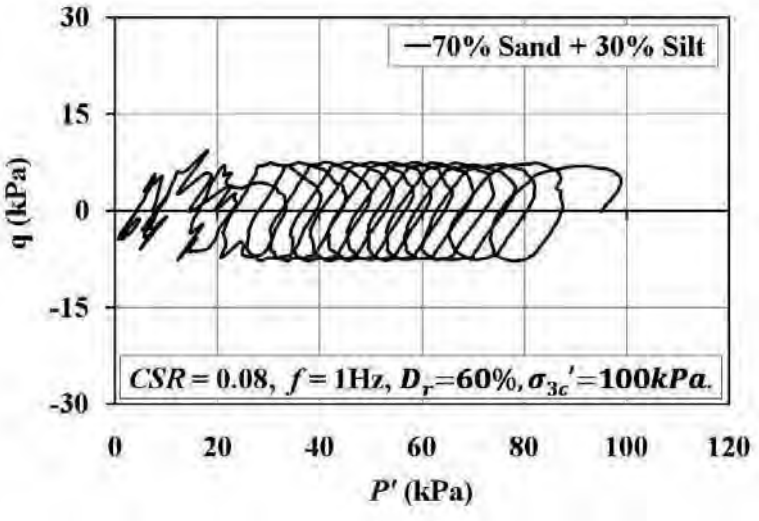

(d)

Figure B. 24. (a) Deviator stress verses cycles, (b) axial strain verses cycles, (c) excess pore water pressure response and (d) effective stress path of 70% sand + 30% silt specimen at D_r=60%, *CSR= 0.08, f* = 1Hz.

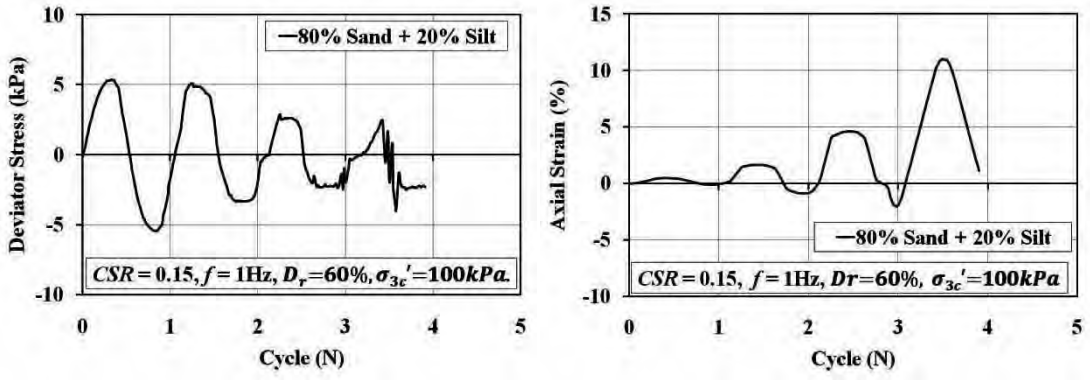

(a)

(b)

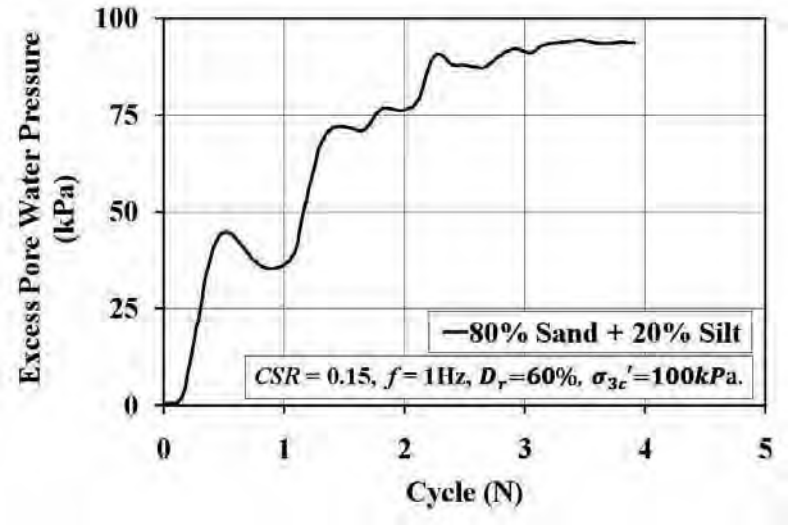

(c)

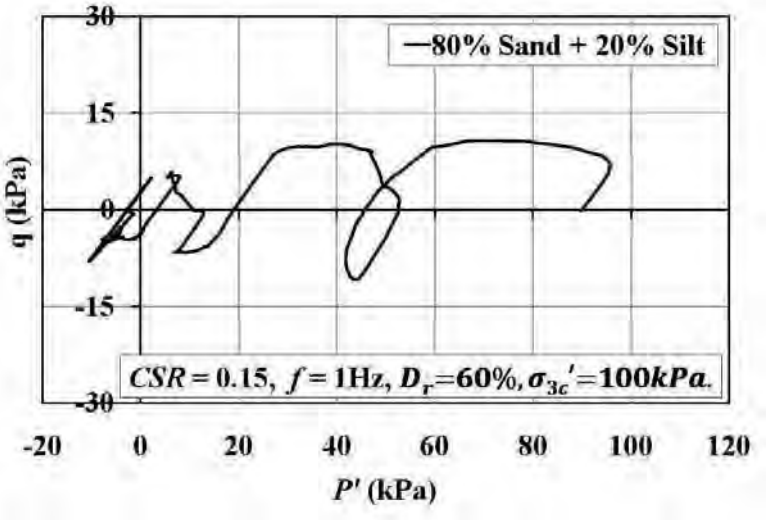

(d)

Figure B. 25. (a) Deviator stress verses cycles, (b) axial strain verses cycles, (c) excess pore water pressure response and (d) effective stress path of 80% sand + 20% silt specimen at D_r=60%, *CSR= 0.15, f* = 1Hz.

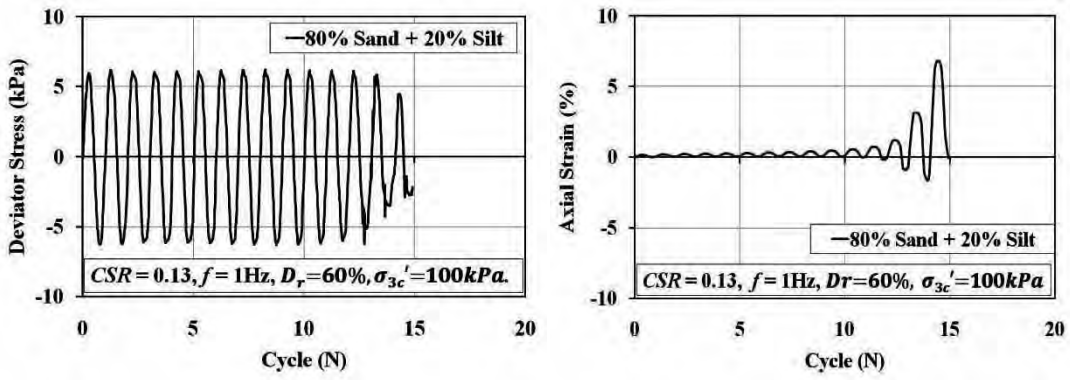

(a) (b)

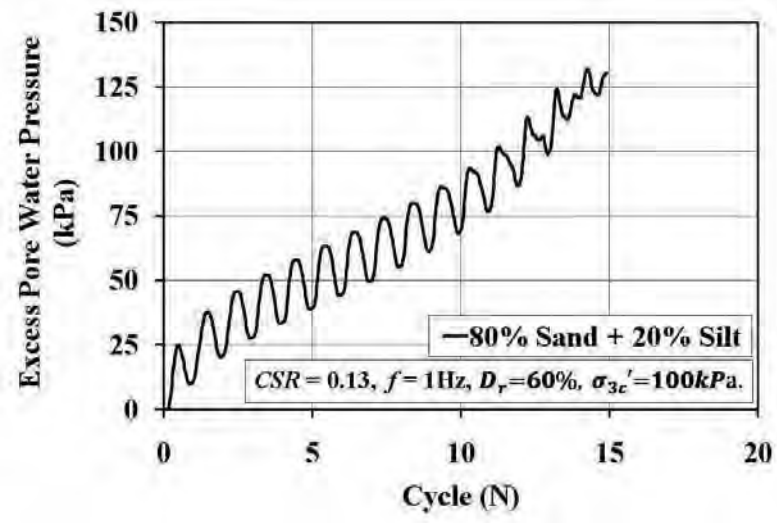

(c)

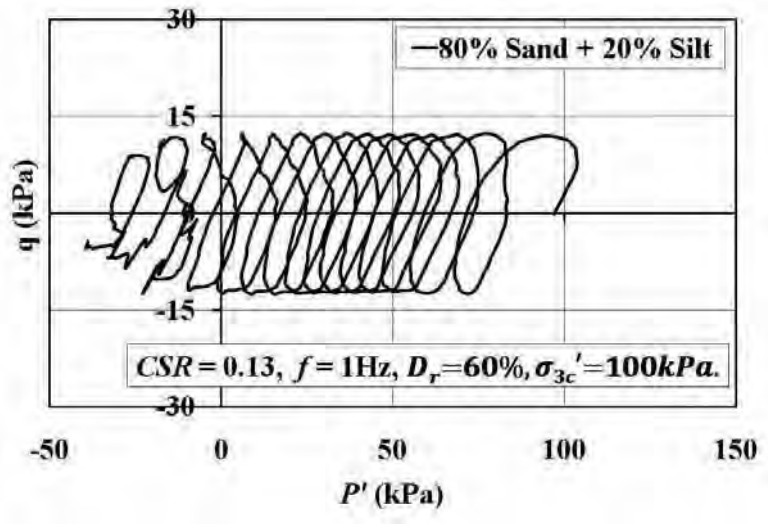

(d)

Figure B. 22. (a) Deviator stress verses cycles, (b) axial strain verses cycles, (c) excess pore water pressure response and (d) effective stress path of 80% sand + 20% silt specimen at D_r=60%, *CSR= 0.13, f* = 1Hz.

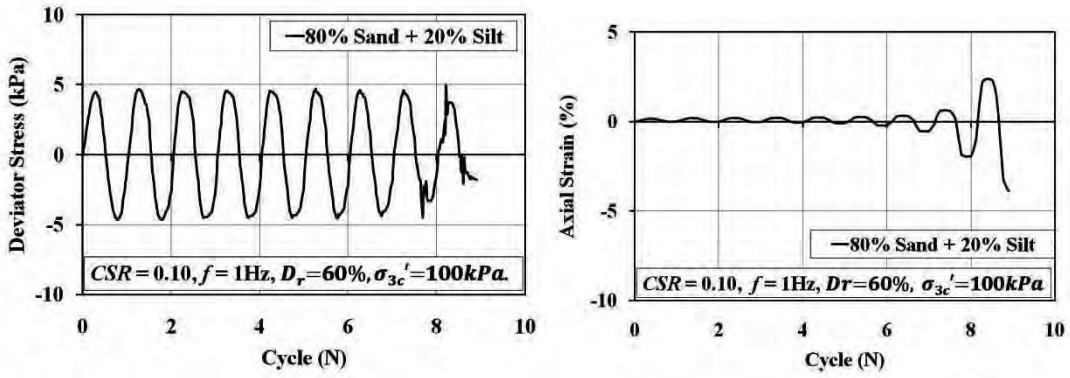

(a)

(b)

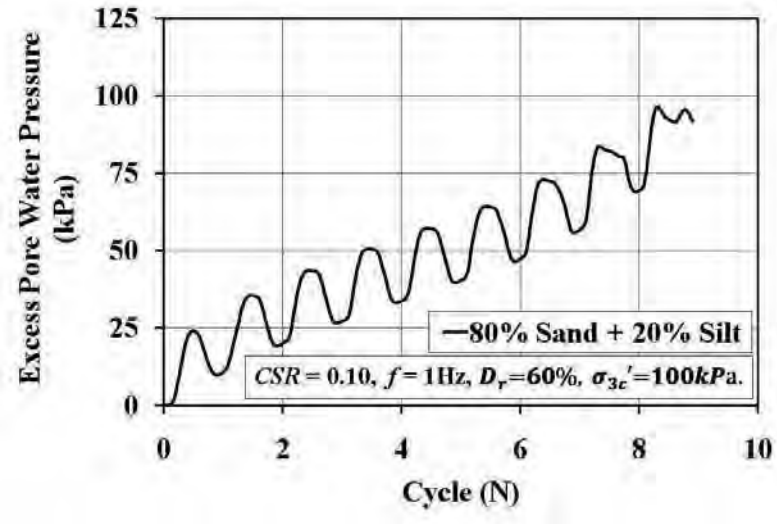

(c)

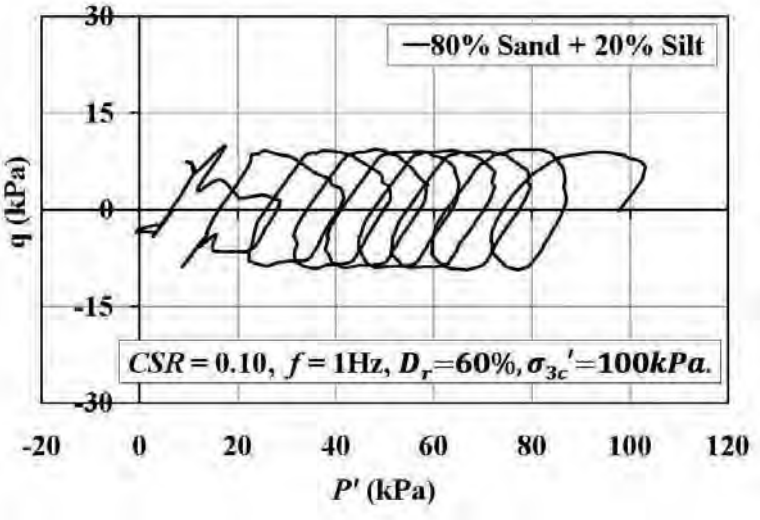

(d)

Figure B. 27. (a) Deviator stress verses cycles, (b) axial strain verses cycles, (c) excess pore water pressure response and (d) effective stress path of 80% sand + 20% silt specimen at D_r=60%, *CSR= 0.10, f* = 1Hz.

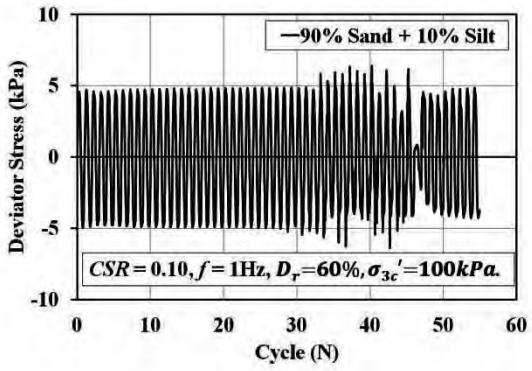

(a)

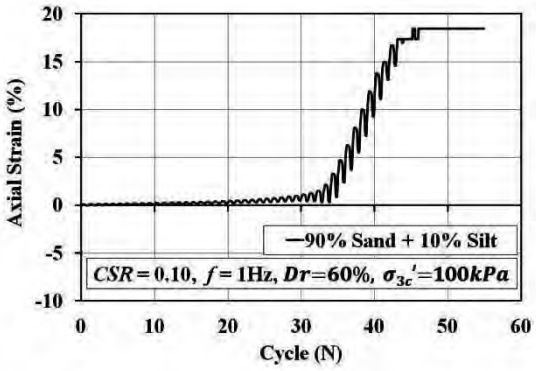

(b)

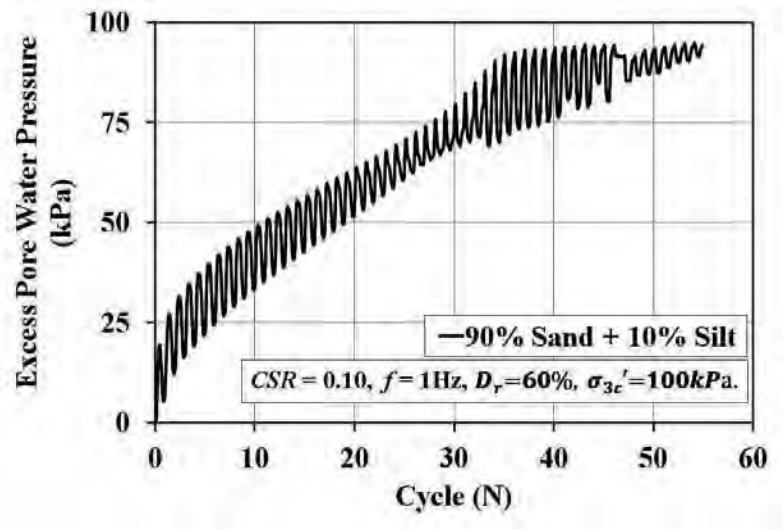

(c)

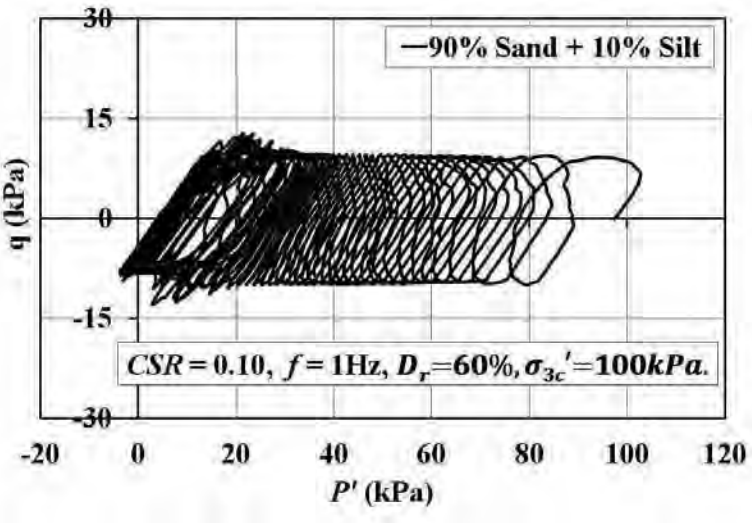

(d)

Figure B. 28. (a) Deviator stress verses cycles, (b) axial strain verses cycles, (c) excess pore water pressure response and (d) effective stress path of 90% sand + 10% silt specimen at D_r=60%, *CSR= 0.1, f* = 1Hz.

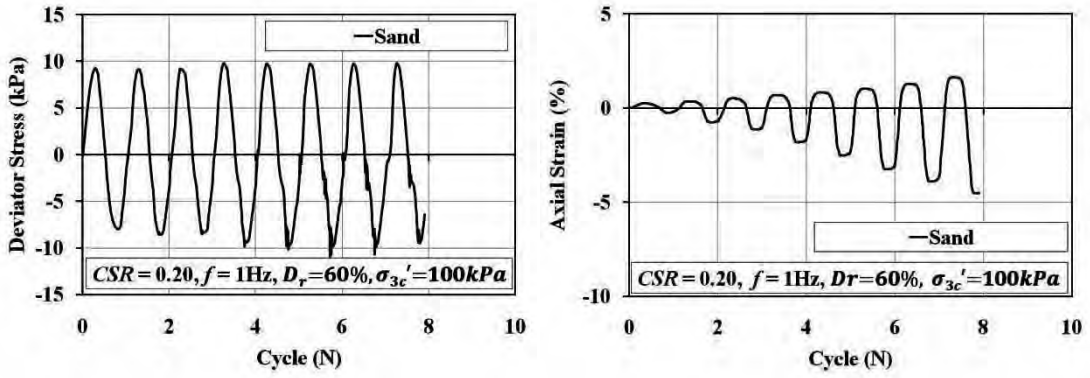

(a)

(b)

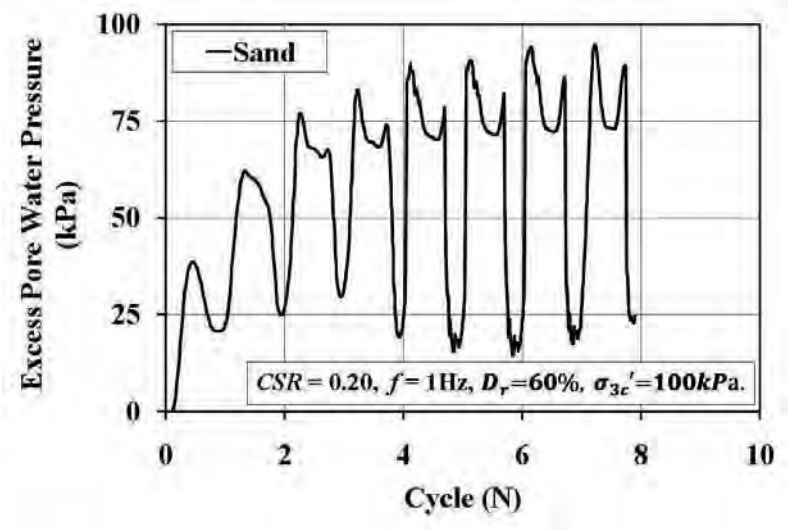

(c)

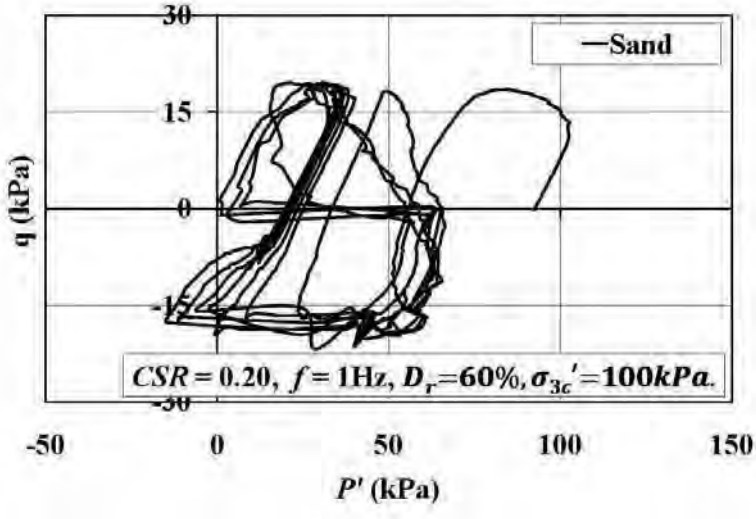

(d)

Figure B. 29. (a) Deviator stress verses cycles, (b) axial strain verses cycles, (c) excess pore water pressure response and (d) effective stress path of sand specimen at D_r=60%, *CSR= 0.2, f* = 1Hz.

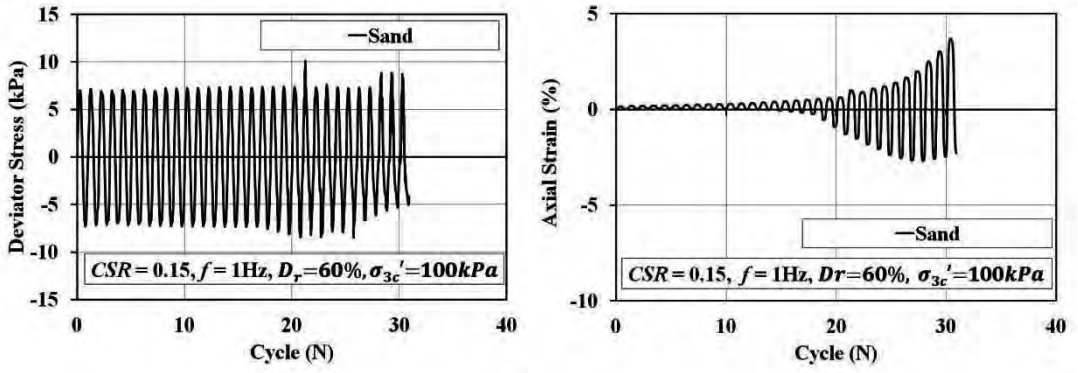

(a) (b)

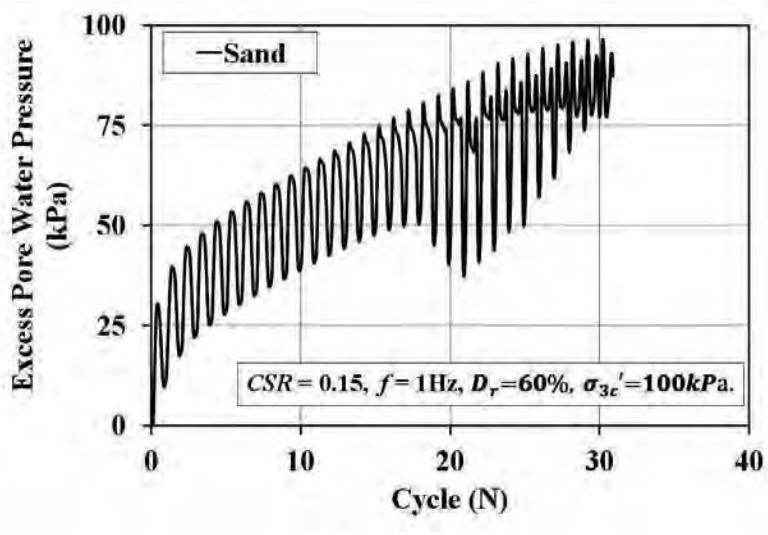

(c)

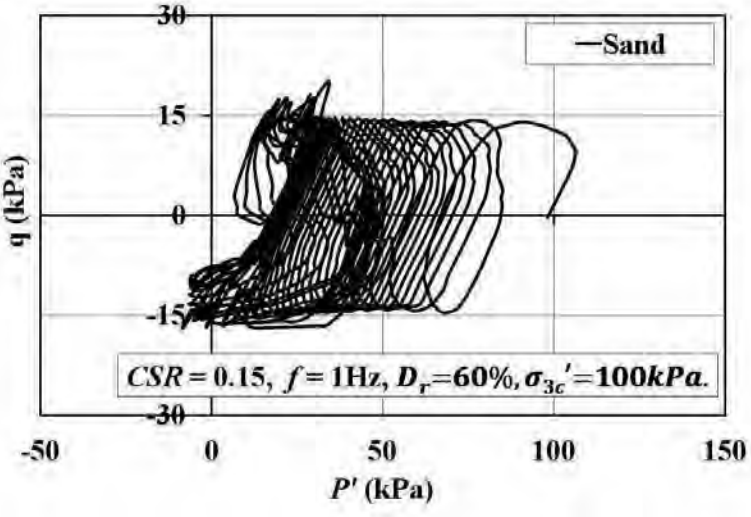

(d)

Figure B. 30. (a) Deviator stress verses cycles, (b) axial strain verses cycles, (c) excess pore water pressure response and (d) effective stress path of sand specimen at D_r=60%, *CSR= 0.15, f* = 1Hz.

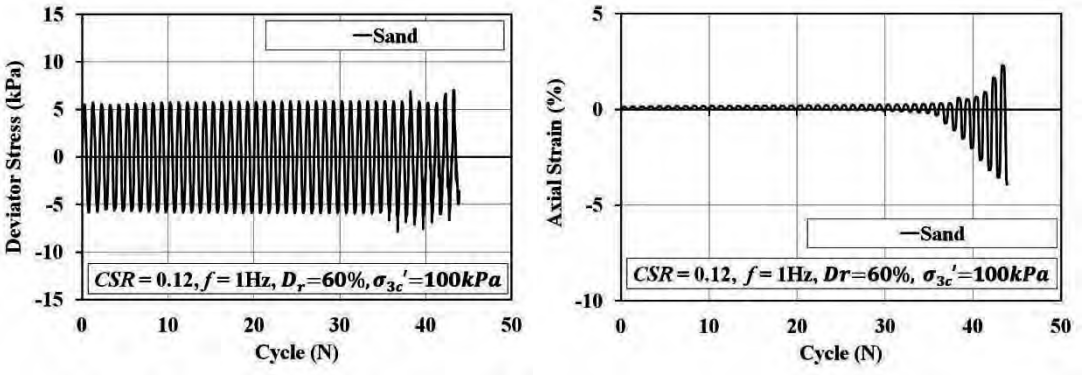

(a) (b)

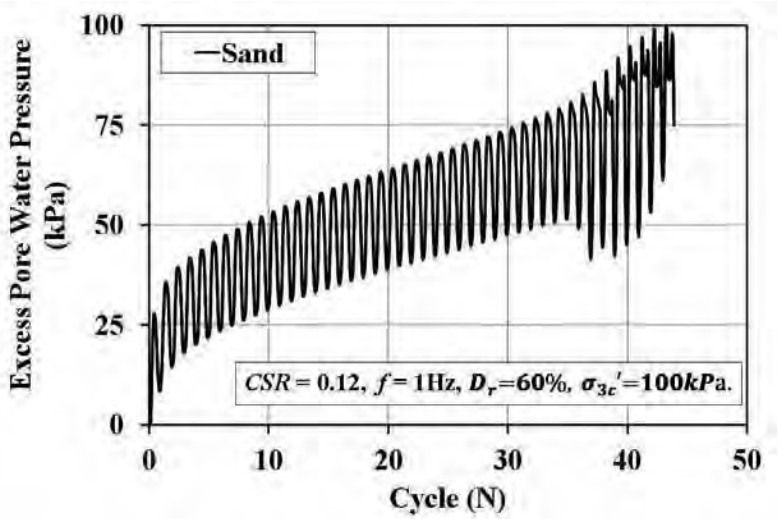

(c)

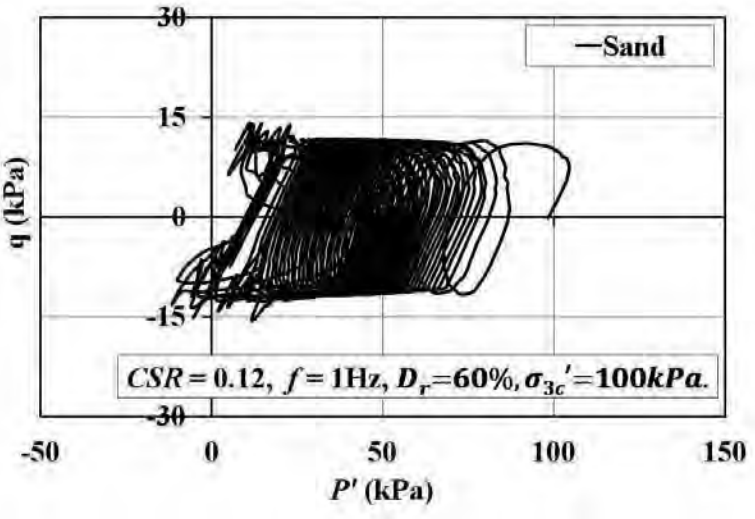

(d)

Figure B. 31. (a) Deviator stress verses cycles, (b) axial strain verses cycles, (c) excess pore water pressure response and (d) effective stress path of sand specimen at D_r=60%, *CSR= 0.12, f* = 1Hz.

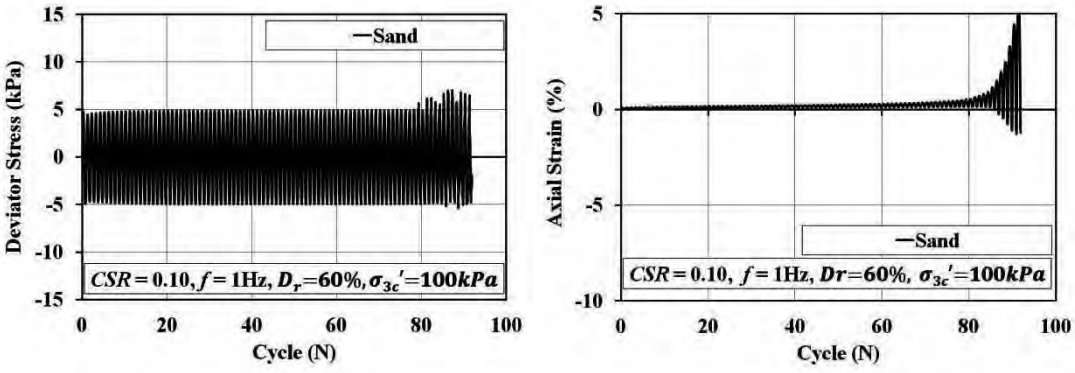

(a) (b)

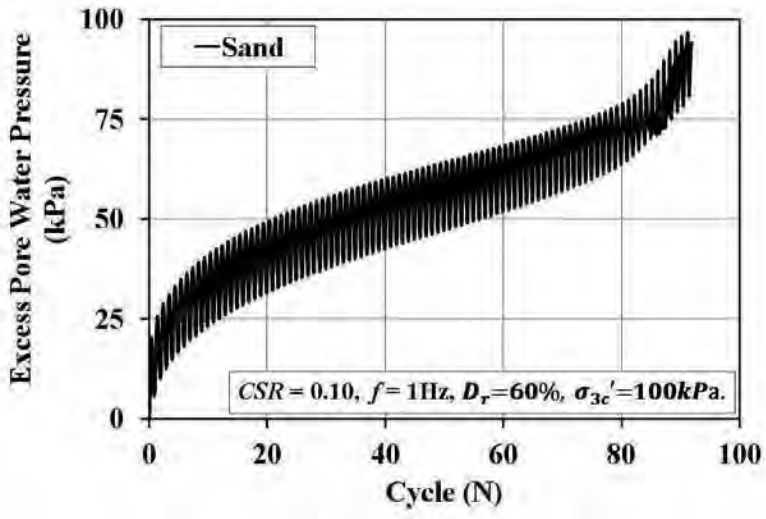

(c)

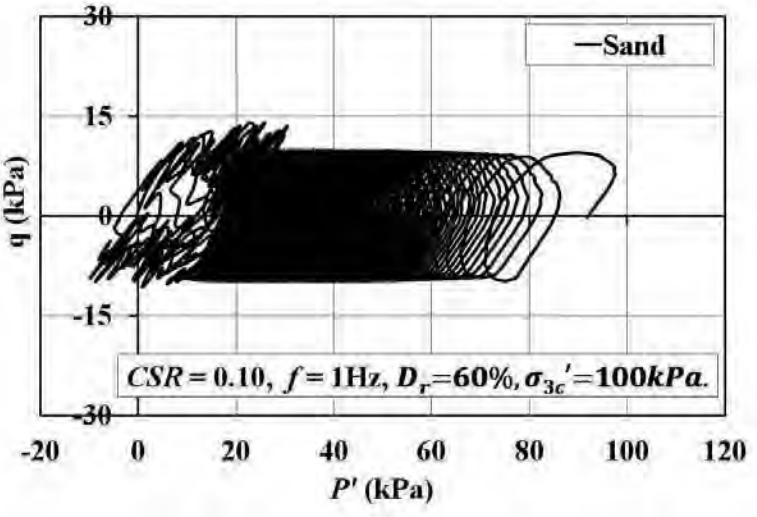

(d)

Figure B. 32. (a) Deviator stress verses cycles, (b) axial strain verses cycles, (c) excess pore water pressure response and (d) effective stress path of sand specimen at D_r=60%, *CSR= 0.10, f* = 1Hz.